DEVELOPMENT OF REAL TIME LEAK DETECTION SYSTEMS FOR STEAM GENERATORS OF SODIUM COOLED FAST REACTORS

By

B. BABU
(Enrollment No: ENGG02200904014)

Indira Gandhi Centre for Atomic Research, Kalpakkam

A thesis submitted to the
Board of Studies in Engineering Sciences

In partial fulfillment of requirements
for the Degree of

DOCTOR OF PHILOSOPHY
of

HOMI BHABHA NATIONAL INSTITUTE

AUGUST, 2016

Homi Bhabha National Institute

Recommendations of the Viva Voce Board

As members of the Viva Voce Board, we certify that we have read the dissertation prepared by **B. Babu** entitled **"Development of real time leak detection systems for steam generators of sodium cooled fast reactors"** and recommend that it may be accepted as fulfilling the dissertation requirement for the Degree of Doctor of Philosophy.

Chairman-**Dr. M.Sai Baba**	Date: 14/9/2017
Guide / Convener-**Dr. B. Purna Chandra Rao**	Date: 14/9/2017
Member 1- **Dr. B.K. Panigrahi**	Date: 14/9/17
Member 2- **Dr. T.Gnanasekharan**	Date: 14/9/17
External Examiner – **Dr. K. Rajanna**	Date: 14/09/2017

Final approval and acceptance of this dissertation is contingent upon the candidate's submission of the final copies of the dissertation to HBNI.

Date: 14/9/2017

Place: Kalpakkam

Dr. B. Purna Chandra Rao

Guide

STATEMENT BY GUIDE

I hereby certify that I have read this dissertation prepared under my guidance and recommend that it may be accepted as fulfilling the dissertation requirement.

_____

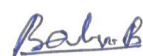Dr. B. Purna Chandra Rao

Guide

Date   : 14/9/2017

Place : Kalpakkam

STATEMENT BY AUTHOR

This dissertation has been submitted in partial fulfillment of requirements for an advanced degree at Homi Bhabha National Institute (HBNI) and is deposited in the library to be made available to borrowers under rules of the HBNI.

Brief quotations from this dissertation are allowable without special permission, provided that accurate acknowledgement of source is made. Requests for permission for extended quotation from or reproduction of this manuscript in whole or in part may be granted by the Competent Authority of HBNI when in his or her judgment the proposed use of the material is in the interests of scholarship. In all other instances, however, permission must be obtained from the author.

(B. Babu)

Date : 14-09-2017

Place : Kalpakkam

DECLARATION

I, hereby declare that the investigation presented in the thesis entitled **"Development of real time leak detection systems for steam generators of sodium cooled fast reactors "** submitted to Homi Bhabha National Institute (HBNI), India, for the award of Doctor of Philosophy in Engineering Sciences, is the record of work carried out by me under the guidance of Prof. B. Purna Chandra Rao, Associate Director, Quality Assurance and Head, Qualirty Assurance Division, Indira Gandhi Centre for Atomic Research, Kalpakkam. The work is original and has not been submitted earlier as a whole or in part for a degree/diploma at this or any other Institution/University.
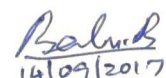
(B. Babu)

Date : 14-09-2017

Place : Kalpakkam

LIST OF PUBLICATIONS ARISING FROM THE THESIS

JOURNALS

1. **B. Babu**, J. I. Sylvia, K.V. Suresh kumar, K. K. Rajan, Development and deployment of miniature MI type sodium leak detector for FBTR, Nuclear Engineering and Design, 2013,Vol. 255,pp. 105-111.

2. **B. Babu**, K.V. Suresh Kumar, G.Srinivasan, Development of a sputter ion pump based SG leak detection system for FBTR, Nuclear Engineering and Design, 2013,Vol. 254, pp. 246-253.

3. **B. Babu**, V. Ramanathan, B. Rajendran, P.V.Ramalingam, B.Raj, Proposed Modernization and Refurbishment of Instrumentation and Control systems of FBTR and Kamini Reactors in India, International Atomic Energy Agency, 2009, Tech Doc No: 1625 pp.95-113.

4. **B.Babu**, M Sai Baba, B.P.C Rao, K.K Rajan, Numerical simulation of miniature Mutual Inductance type leak detector for FBTR, IETE Technical Review, Dec 2016, pp.1-8.

14/09/2017

(B. Babu)

Dedicated to the memory
of
my Parents

ACKNOWLEDGEMENTS

I owe my achievement to my caring and supportive wife Smt.Deepa Babu, my daughter Ms.Priya Babu and my son Mr.B.Akhil who shared all my joy and bitterness during the course of the work. I am thankful to my brother Shri.B.Rajappan Nair for the moral support and inspiration.

(B. Babu)

Date: 14-09-2017

Place: Kalpakkam.

TABLE OF CONTENT

ABSTRACT

Fast Breeder Test Reactor at (FBTR) Kalpakkam demonstrates the sodium cooled fast breeder reactor (FBR) technology to utilize the abundant thorium resource available in India. The shell and tube type once through Steam Generators (SG) are vital for Indian FBRs. The heat generated in the reactor core is extracted by primary sodium and transferred to secondary sodium through an intermediate heat exchanger. The secondary sodium transfers this heat to the feed water in the SG which becomes superheated steam and drives the turbo-alternator.

The SG of FBTR consists of 4 numbers of once through counter flow type heat exchanger modules. Sodium flows on the shell side at ≈ 3 kg/cm^2 and the water / steam flows on tube side at ~ 125 kg/cm^2 (and 200 to 480°C) separated by thin walls of the ferritic steel tubes. Since steam / water is at high pressure, any through wall defect developed in the SG tube can lead to leakage of steam or water into sodium resulting in violent reactions, leading to undesirable consequences. The damage can be extensive depending on the leak size. Therefore, it is essential to detect the leak in the incipient stage for safe and reliable operation. Various methods have been reported for detection of SG leaks in FBRs.

In the open literature, no information is available about any technique for detection of sodium leak in the event of failure of nickel diffuser which is a vital component of the SG leak detection system. As conventional sodium leak detectors cannot be used for detection, development of a non-contact type sodium leak detector is attractive for detecting sodium leak caused by failure of nickel diffuser membrane. The thesis proposes Mutual Inductance type Leak Detector (MILD) for this purpose owing to its various advantages. Leak detection sensitivity has been improved by optimizing the MILD design.

As empirical design of MILD probes and experimental analysis are time consuming, model based approach has been adopted in this research work for designing the probe.

Steam generator leak detection system is required for detection of small leaks and initiation of safety actions. In the event of water/steam leak into sodium in SG, hydrogen is produced due to sodium water reaction. For detection of hydrogen concentration in sodium, a sputter ion pump (SIP) based system is preferred to a QMS based system. SIP based SG leak detection system is reported to be used in some of the fast reactors, but information is not available in open literature regarding the processing of the current signal for initiating safety actions.The thesis discusses the process of development of SIP based system involving modification of the electronic circuit, evaluation and qualification of the output by conducting experiments and formulating safety actions for detection of small leaks.

As response time of the SIP based system is of the order of 3 minutes, due to the large diffusion time involved, development of a diffusion independent system is advantageous for rapid detection of leaks and initiation of safety actions on small leaks. Faster response and ability to detect leaks even in stagnant regions within the SG unit prompted development of an acoustic detector. Its development and the required suitable signal processing techniques are elaborated in the thesis.

The confirmation of the leak signal at all sodium temperatures and identification of the leaking module requires diverse methods and the thesis presents the details of the developed electrochemical hydrogen meter (ECHM) and thermal conductivity detector (TCD).The thesis also discusses the performance of diverse detectors and the future works for further enhancing the performance of the SG leak detection systems.

LIST OF FIGURES

ix

LIST OF TABLES

LIST OF SYMBOLS

m/s	meter per second
V	Volts
ppb	parts per billion
kPa	Kilo pascal
MPa	Mega pascal
g/s	gram /second
kW	Kilo watt
MW	Mega watt
C	Celsius
mA	Milli ampere
mV	Milli volt
eV	electron volt
dB	Decibel
mm	millimeter
ppm	Parts per million
kHz	Kilo hertz
μV	Micro volt
mb	Milli bar
M Ω	Mega ohm
K	Kelvin
C_H	Hydrogen concentration
p_{H_2}	Hydrogen partial pressure
P_{Na}^{H}	Hydrogen partial pressure in sodium
ρ_t	Resistivity at temperature t
ρ_0	Resistivity at temperature t_0
α	Temperature coefficient of resistivity
T_0	Reference temperature
H	Magnetic field intensity
j	Current density
D	Electric flux density
E	Electric field intensity
B	Magnetic flux density
μ	Magnetic permeability
$\in$	Permittivity

LIST OF ABBREVIATIONS

AC	Alternating Current
ADS	Accelerated Driven Systems
ALD	Acoustic Leak Detection
ARNV	Auto Regressive Noise Variance
BCG	Bi-Conjugate Gradient
BWR	Boiling Water Reactor
CDPS	Central Data Processing System
CEA	French Atomic Energy Commission
CG	Conjugate Gradient
DC	Direct Current
DWT	Discrete Wavelet Transform
ECHM	Electrochemical Hydrogen Meter
ECIL	Electronics Corporation of India Ltd
EMF	Electro Motive Force
FBR	Fast Breeder Reactor
FBTR	Fast Breeder Test Reactor
FE	Finite Element
FEMM	Finite Element Magnetic Modeling
FPE	Final Prediction Error
GWD	Giga Watt Day
GWe	Giga Watt Electrical
GWey	Gigawatt-Year of Electric Power
HAD	Hydrogen in Argon Detector
HSD	Hydrogen in Sodium Detector
IAEA	International Atomic Energy Agency
IGCAR	Indira Gandhi Centre for Atomic Research
IR	Insulation Resistance
KAMINI	Kalpakkam Mini Reactor
LED	Light Emitting Diode
LOR	Lowering Of Rod
MDL	Minimum Description Length
MgO	Magnesium Oxide
MILD	Mutual Inductance Leak Detector
MoX	Mixed Oxide
MSM	Mass Spectrometer
MWe	Megawatt Electrical
MWt	Megawatt Thermal
Na	Sodium
NaH	Sodium Hydride
NaOH	Sodium Hydroxide
OD	Outer Diameter
PCB	Printed Circuit Board

PFBR	Prototype Fast Breeder Reactor
PHWR	Pressurised Heavy Water Reactor
PID	Proportional Integral Derivative
PLC	Programmable Logic Controller
PT	Pick-up Transducer
Pu	Plutonium
PuC	Plutonium Carbide
PWR	Pressurised Water Reactor
QMS	Quadrupole Mass Spectrometer
R&D	Research and Development
RMS	Root Mean Squared
SAD	Sodium Aerosol Detection
SG	Steam Generator
SGLDS	Steam Generator Leak Detection System
SGTF	Steam Generator Test Facility
SIP	Sputter Ion Pump
SNR	Signal to Noise Ratio
SOWART	Sodium Water Reaction Test Facility
SS	Stainless Steel
TCD	Thermal Conductivity Detector
TG	Turbo Generator
UC	Uranium Carbide
UHV	Ultra High Vacuum
WDCV	Wavelet Detailed Coefficients Variance
WDET	Wavelet Denoising by Empirical Thresholding

Chapter 1: Introduction

1.1   Fast breeder reactors

Energy is indispensable for the sustenance and even survival of mankind, for all social and economic developments and growth of civilization. Nearly every aspect of development - from reducing poverty, providing safe drinking water, sanitation, adequate food production, education and improving health care - requires reliable access to modern energy service. For a country like India with a population of ~ 1.2 billion and an average annual growth rate of about 8 % (likely to increase further), energy is a central issue. Based on the limited reserves of uranium, in order to sustain the Indian nuclear energy program for long, it is now well established that nuclear energy using the available vast thorium reserves is the only viable alternative that would ensure the energy security of the nation. Nuclear energy is clean, safe and competitive energy source and can replace significant part of fossil fuel based power plants, which contribute largely to green house effects.

India has limited uranium and abundant thorium resources. The uranium resources reasonably assured plus inferred in India is 84,600 tonnes (< 2% of world resource). However, the thorium resource in the country is about 225,000 tonnes (second largest reserve in the world), which has an energy potential of 155,000 GWey. The uranium resource available in the country can feed 10 GWe capacities of pressurised heavy water reactors (PHWR) for ~ 50 years with thermal efficiency of 30 %. Taking cognizance of India's nuclear resource profile, a 'Three Stage Nuclear Power Programme' was formulated for achieving energy independency [1].

Under the first phase of the programme, a series of PHWRs with natural uranium oxide as the fuel have been set up. There are today 18 PHWR units, 2 Boiling Water Reactors and 2 Pressurized Water Reactor (PWR) in operation representing an installed capacity of 6780 MWe,

and 4 PHWRs are under construction. The units in operation and under construction together represent an installed capacity of 9580 MWe.

The once-through open fuel cycle with spent fuel treated as nuclear waste cannot sustain nuclear power development over a long term and so closing the nuclear fuel cycle is the strategy followed by India. Therefore, the plutonium (Pu) produced in PHWRs is reprocessed and can be used as MOX (mixed oxides of uranium and plutonium) fuel in thermal reactors. However, this will not be able to grow the nuclear capacity to desired levels. Hence, in the second stage of the programme, the plutonium will be used in fast breeder reactors (FBR) to grow the nuclear capacity to desired levels. The second stage envisages setting up of FBRs, backed up by reprocessing plants and plutonium based fuel fabrication plants. The third stage envisages exploiting the vast resources of thorium through the route of fast or thermal critical reactors and/or the accelerator driven sub-critical reactors. A beginning of third stage has also been made by commissioning the 30kWt thorium based ^{233}U fuelled research reactor, KAMINI at Kalpakkam.

The need for energy is very large and only nuclear energy through FBRs can meet this demand in the long run. Compared to many other reactor systems, FBRs have a number of advantages. These systems are efficient for handling actinides and long lived fission products in the domain of waste management. The systems can be designated to incinerate high level wastes arising from the reprocessing of spent fuel. This approach minimizes the quantity of waste to be immobilized. Further, FBRs would also provide critical liquid metal technology and high temperature design inputs for the future accelerated driven systems, fusion and high temperature reactor systems. These apart, FBRs can provide electricity at competitive costs over long periods.

Hence, FBRs are considered to be the most preferred and suitable option for providing sustainable and environmentally acceptable energy systems.

1. 2   Fast breeder test reactor

FBTR is a 40MWt, sodium cooled, PuC-UC fuelled fast reactor [2]. Fig.1.1 gives the flow sheet of the reactor. This reactor has successfully operated without any major incidents using the unique carbide fuel which has achieved a burn up of 157 GWD/t an international benchmark. This test reactor has been utilized for fuel development, reactor physics experiments and irradiation of structural materials. This coupled with the extensive R&D efforts in all aspects of FBR technology has laid the foundation for the design and development of a 500 MWe Prototype Fast Breeder Reactor (PFBR). The construction of PFBR was started in 2002 and it is now in an advanced stage of commissioning. PFBR will be the forerunner of a series of FBRs that are to follow soon.
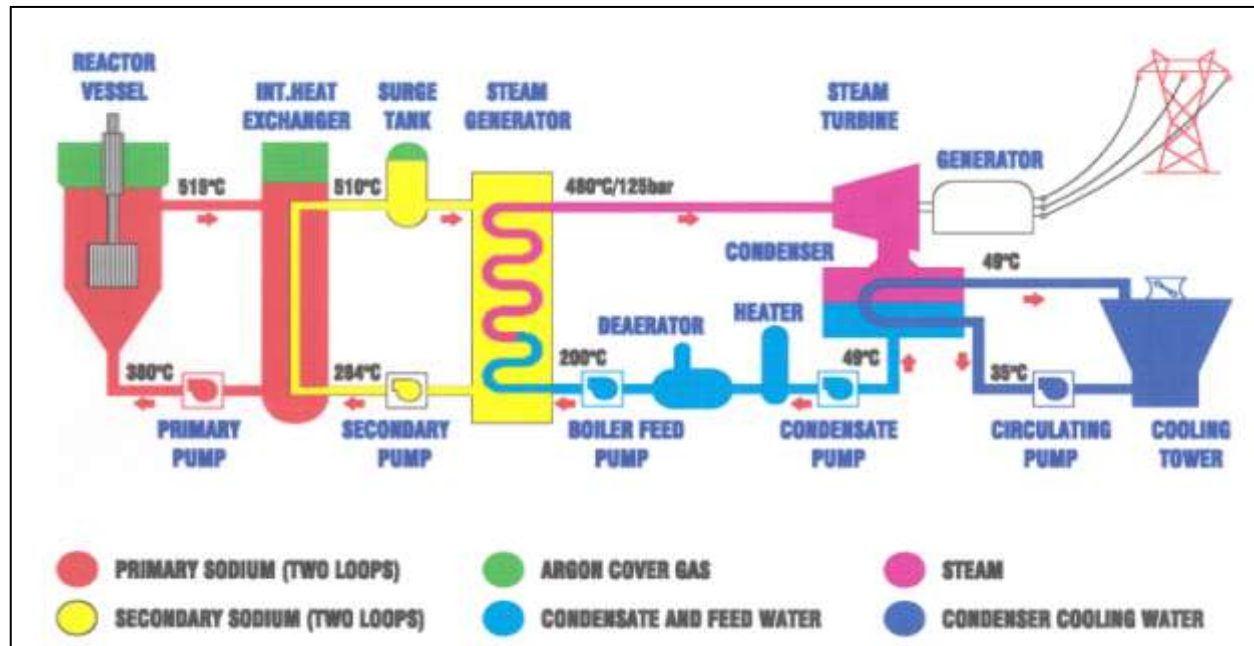
Fig. 1.1: Schematic flow diagram of FBTR

Heat generated in FBTR is removed by two parallel hydraulically coupled primary sodium loops, and transferred to the corresponding secondary sodium loops. Each secondary sodium loop is

provided with two once-through Steam Generator (SG) modules. The steam from SG in both the loops is fed to a common steam water circuit comprising a Turbo Generator (TG) and a 100% Dump condenser. Usually the turbine is in operation. In the case of its non-availability, reactor operation can be continued by dumping the steam in the Dump condenser. Stainless steel (SS316) is the material of construction for reactor vessel, primary and secondary sodium circuits whereas ferritic steel is the material used for SG. Table 1.1 gives the main characteristics.

Table 1.1: FBTR main characteristics

Reactor coolant	Sodium
Primary circuit concept	Loop
Thermal power	40 MWt
Electrical power	13.2 MWe
Fuel	70% PUC 30% UC [MARK I core]
Core height	320 mm
Sodium inlet temperature	380^oC
Sodium outlet temperature	515^oC
Sodium inventory	150 t
Steam conditions at turbine inlet	490^oC at 125 kg/cm^2
Control rods	Boron carbide
Neutron flux	3×10^{15} n·cm^{-2}·s^{-1}

1.3   FBTR steam generator

The function of SG is to transfer heat from secondary sodium system to feed water to generate superheated steam. Sodium flows on the shell side at ≈ 3 kg/cm^2 and the water flows on tube side at ~ 125 kg/cm^2 and temperature 200 to 480^oC separated by thin walls of the ferritic steel tubes [3]. The SG consists of four numbers of liquid sodium heated once through counter current flow type heat exchanger modules each of 12.5 MWt rating made from 2.25 Cr-1Mo stabilized steel fitted with economizer, evaporator and superheater combined into a single unit as shown in

Fig.1.2. Each module consists of a shell of diameter 177.7/193.7 mm, 90 m long, triple S-bent in which seven tubes of diameter 25.7/33.7 mm are arranged in a uniform triangular pitch. The once-through type SG is selected to limit the water inventory available for reaction with sodium, if any, in case of a tube failure. Table 1.2 gives the SG features.
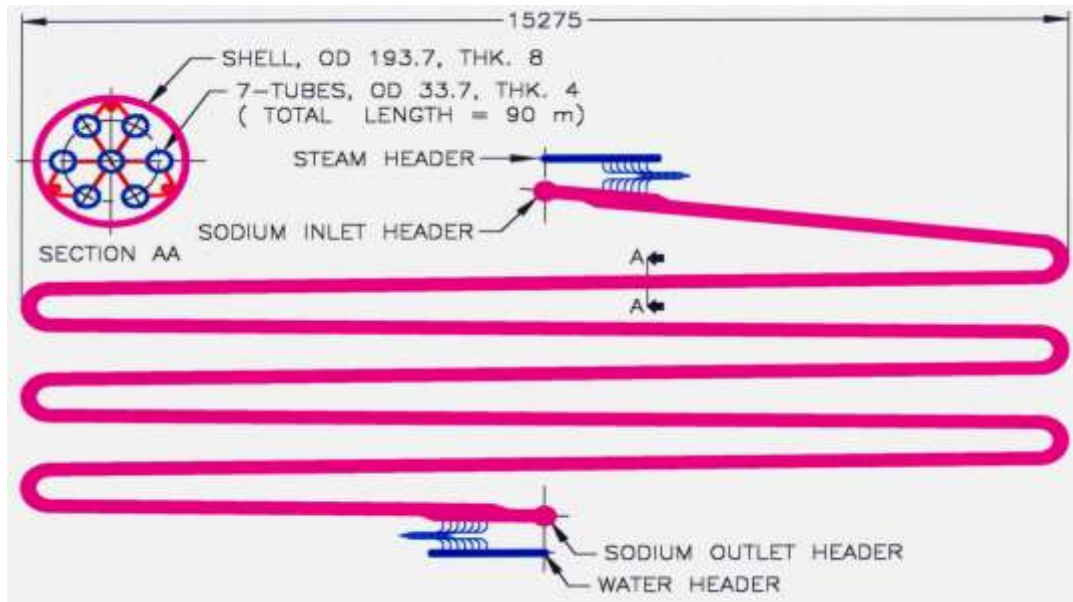
Fig. 1.2: FBTR steam generator

Table 1.2: FBTR SG features

No of modules	4
Rating of module	12.5 MWt
Material of construction	2.25 Cr-1Mo stabilized steel
Dimensions of shell	$\varnothing$ 177.7/193.7 mm,
Length of Module	90m
No of tubes in each module	7
Dimensions of tube	$\varnothing$ 25.7/33.7 mm
Sodium pressure in shell	~3 kg/cm^2
Sodium temperature in shell	200 to 480°C
Water pressure in tube	~ 125 kg/cm^2

The feed water gets converted into superheated steam in SG. Since water/steam is at high pressure, during a leak, water will enter into sodium causing violent reaction leading to severe damage to the SG. The damage can be extensive depending on the leak size. It is therefore essential to detect any leak at the incipient stage itself and remedial measures be taken at the earliest. This is accomplished by detecting H_2, the inevitable product of the sodium water reaction, in sodium and in the cover gas.

1.4   Need for SG leak detection

In case of a breach in tube integrity, water leaks into sodium resulting in the following exothermic reactions:

$$Na + H_2O \longrightarrow NaOH + 1/2\ H_2 \qquad\qquad (1.1)$$
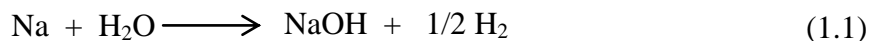
(Water = -35.2 kcal/g.mole, Steam = -45.7 kcal/g.mole)

This is the primary reaction which occurs within a few milliseconds and considered as total. The leaked water gets completely reacted in presence of excess sodium. The evolved hydrogen is either dissolved in liquid sodium or goes to the cover gas in the expansion tank. The following secondary reactions occur slowly in a manner depending upon temperature, ratio of reactants and other conditions.

$$2Na + H_2 \rightleftharpoons 2NaH \qquad\qquad (1.2)$$

(Endothermic)

(Forward reaction = -13.7 kcal/g.mole)

The dissociation half life time of NaOH in liquid sodium is 1s at $320\,^{o}C$ and 0.2s at $500\,^{o}C$ [4]. At temperatures above $410\,^{o}C$, the following reactions take place:

$$[NaOH]_{Na} + \text{excess Na} \longrightarrow [O_2]_{Na} + [H]_{Na} \qquad (1.3)$$

$$2Na + 2NaOH \longrightarrow 2Na_2O + H_2 \qquad (1.4)$$
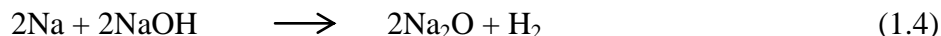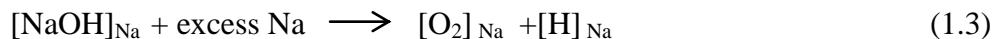
(NaH decomposes at 350 ^oC, NaOH decomposes at 310 ^oC)

However, the following reaction occurs under the condition of excess sodium and temperatures higher than 320 ^oC.

$$2Na + H_2O \longrightarrow Na_2O + H_2 \text{ (-31.8 Kcal/g.mol)} \qquad (1.5)$$
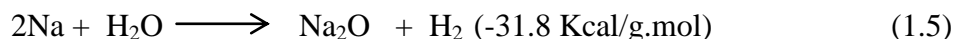
Reaction process is affected by temperature, ratio of water to sodium and other conditions in the reaction zone. The sodium water interaction is rather a complicated, multistage process where successive reactions with sodium hydroxide and hydrogen formation followed by their interaction with sodium take place. The final concentration of water sodium interaction products is determined by the thermodynamic equilibrium conditions and the time of reaching the equilibrium by kinetics of the reactions proceeding [5]. Hence, it is difficult to predict which reactions would occur inside the SG under leaking conditions.

In case of a small water/steam leak into sodium through a pinhole crack in the tube, sodium water reaction gives rise to high-temperature reaction products of corrosive nature. These reaction products cause a combined corrosion /erosion effect in the pinhole and subsequent enlargement in size of the hole. This phenomenon is called 'self wastage'. The development of a crater in the tube takes significant time as compared to time taken for the enlargement of leak. At this stage, leaking water/steam in the form of a jet stream causes damage to adjacent tubes on which the reaction products impinge. This is called 'adjacent tube wastage'. With this much increased leak rate, the jet stream of reaction products effect extensive damage to the surrounding tubes within a short time [6]. Sodium-water reaction produces hydrogen and heat,

thus causing pressure build up in the SG and temperature rise in the vicinity. Pressure build up in the SG is so rapid that sodium is displaced by hydrogen produced in the reaction zone [7].

1.5   SG leak detection techniques

The leak of water / steam into sodium is generally classified as micro, small, intermediate and large leaks as given in Table 1.3 [8]. In case of a micro leak, only self-wastage occurs. The micro leak by itself is not alarming and the leak rate is known as non-damaging leak rate. A further development can enhance the leak rate. As a consequence of the self-wastage, a micro leak generally develops into a small leak, if not detected early.

The leaks with rate in the range of 10 g/s to 2 kg/s are classified as the intermediate leaks. In case of a large leak, the tube wall is completely perforated allowing large-scale water leakage. This leads to a sudden increase in the pressure and temperature in the vicinity due to sodium-water reaction.

Table 1.3: Classification of leaks with leak rate

Types	Leak rate
micro leak	< 50 mg/s
small leak	50 mg/s to 10 g/s
intermediate leaks	10 g/s to 2 kg/s
large leak	> 2 kg/s

Various types of leak detection techniques are being employed for detection of leaks in sodium heated fast reactor steam generators worldwide [9].

Different leak detection methods are found suitable for different leak situations. All physical and chemical events resulting from a leakage can be utilized to produce a quantitative signal for detection of a leak. They can be broadly classified as:

(a) Increase in H_2 and NaOH content in the sodium stream due to Na/H_2O reaction.

(b) Increase in hydrogen concentration in the cover gas

(c) Increase in pressure arising from the H_2 produced in the reaction (ensuing H_2)

(d) Noise frequency spectrum due to the reaction flame characteristic of the leak of different

nature.

These are described in the following sections:

1.5.1 Measurement of hydrogen concentration in sodium

Small leaks are detected using hydrogen in sodium detectors at normal operating temperatures. Hydrogen is highly diffusive through metals owing to its small atomic size. If a metallic membrane with high permeability for H_2 separates sodium from a gas space, hydrogen in sodium can diffuse through the metal and build up in the gas space to an equilibrium pressure. The relationship between this pressure, P_{H_2}, and concentration of hydrogen in sodium, C_H (Na) in ppm is given by Sievert's Law [10]:

$$\sqrt{P_{H_2}} = \frac{C_H}{K} \tag{1.6}$$

where K is the Sievert's constant for the system and it is almost independent of temperature. In a dynamic hydrogen meter the hydrogen pressure in the gas space is maintained low by using vacuum pumps. The hydrogen flux, F, through the membrane is related to hydrogen concentration in sodium as given below:

$$F = \left(\frac{A}{d}\right)\left[(P_{Na}^H)^{\frac{1}{2}} - (P_1^H)^{\frac{1}{2}}\right]D_0 \times e^{\frac{-E_0}{RT}} \tag{1.7}$$

where,

    A   - Area of the membrane cm^2

    d   - Membrane thickness cm

    P_{Na}^H - Hydrogen pressure in sodium

    P_1^H - Partial pressure of hydrogen in vacuum side

D_0 - Diffusion constant for membrane material

R - Gas constant

T - Temperature of the membrane K

E_0 - Activation energy for diffusion J/mole

Nickel is usually used as the membrane material in the hydrogen meters because of its large diffusion constant and material strength, compatibility with sodium and small activation energy. The hydrogen flux can be measured by many methods. It can be correlated to the ion current of the ion pump. This flux is highly dependent on the temperature of the membrane and so the temperature of the probe has to be controlled within $\pm 1^o$C. These meters are calibrated in situ by operating them in the equilibrium mode. Two types of meters are used to detect the presence of H_2: (i) quadrupole mass spectrometer (QMS) which detects the partial pressure of H_2 in the system and (ii) sputter ion pump (SIP) which detects the total pressure.

The QMS can be used for measurement of the hydrogen partial pressure on the chamber side. The QMS meters are fast responding and highly sensitive. They are simple and easy to operate. They have been reliably operated in fast reactor in the ranges as low as 0.02 to 1ppm of hydrogen in sodium [11].

Hydrogen concentration in sodium is measured in a sampling line taken at the outlet of steam generator. Sodium drawn from the sampling line is heated to a temperature of 450^oC and allowed to pass through a set of thin walled nickel tubes. These nickel tubes act as the diffuser and permeate hydrogen into a vacuum chamber. The vacuum pump connected to the system pumps out the hydrogen diffusing through the membrane. A QMS tuned to hydrogen is used for measuring the hydrogen pressure. The hydrogen-in-sodium detectors (HSD), in majority of the fast reactors utilize similar setups.

Some reactors do not use mass spectrometers, but instead utilize the calibrated sputter ion pump (SIP) to detect hydrogen pressure. The advantage of this system is that fast response can be achieved by choosing a small volume with little flow resistance. However, high dependence of this measurement sensitivity on nickel membrane is often a disadvantage.

A change of $1^{o}C$ in the nominal membrane temperature can cause an error of as much as 1%. Similarly the membrane surface "poisoning" affects the measurement strongly. Hence, the detection systems are to be calibrated frequently by injecting known amount of hydrogen.

The principal drawback of this leak detection of measuring hydrogen in sodium is that the reaction product namely, hydrogen has to travel from the leak to the location of the nickel membrane. Because of this reason this cannot be employed in the stagnant sodium regions. During full power operation, when the sodium flow is highest, the hydrogen transportation time is typically about 50 seconds and it can only be higher during lower power operations. Further, the time taken for hydrogen to diffuse through the nickel membrane needs to be added. The thickness of the membrane is about 300 microns and is usually maintained at around $450^{o}C$. This response time, which depends on the thickness of nickel tubes and the operating temperature, is in the range of 30 seconds. Although such a slow response detector is undesirable for controlling events associated with catastrophic consequences, these are regularly employed for detection of initial stages of leak.

1.5.2 *Measurement of hydrogen partial pressure in cover gas*

The hydrogen in argon detectors are used during start up and shutdown, at which the sodium temperatures are low (~$200^{o}C$). Intermediate size leaks are detected by rise in secondary sodium circuit cover gas pressure. Large leaks are detected by sodium leak detectors placed downstream

of the rupture discs. Cover gas space of the SG or a capacity downstream of the SG can be monitored for pick up of hydrogen.

This is useful during start up and low power operation since the sodium temperature is normally low under these conditions and there is a possibility that hydrogen evolved by the sodium/water reaction is carried by sodium in gaseous form and can escape into the cover gas. Relatively large quantity of hydrogen is available in the cover gas as compared to the fraction that is dissolved in the sodium detection by a HSD.

In this, a coil of nickel tube is inserted into the cover gas to be monitored. A carrier gas, normally argon, sweeps the hydrogen diffused through the wall of the nickel coil. The carrier gas passes through two chambers of the thermal conductivity detector (TCD) block before entering the nickel coil and the gas coming from the Ni coil is passed through the other two chambers of the TCD block. Each chamber of the TCD houses a heated filament and these filaments form a Wheatstone bridge. When there is no hydrogen present in the cover gas, the bridge is balanced to give null output. The balance is offset when the carrier gas picks up hydrogen.

1.5.3 *Electrochemical hydrogen meters*

Using an electrochemical meter that works on principles of concentration cell is an alternate method to measure the hydrogen pressures. The measurement of hydrogen level in sodium by electrochemical cell is by using a solid $CaH_2/CaCl_2$ electrolyte and LiH reference electrode. These cells develop electromotive force depending on the hydrogen concentration. The EMF (E) can be calculated from the following (Nernst's) equation:

$$E = \frac{RT}{2F \times \ln\left(\frac{PH_2Li}{PH_2Na}\right)} \tag{1.8}$$

where,

$PH_2\,Li$ - H_2 partial pressure in Li/LiH reference electrode.

PH_2Na - H_2 partial pressure in sodium
F   - Faraday constant
T   - Temperature
R   - Gas constant

The EMF is proportional to the hydrogen potential difference across the electrolyte. The change in the meter signal is proportional to the ratio of initial and final hydrogen concentrations. This cell can detect small changes. For example a change of 4ppb in 100ppb level can be detected. This feature makes it suitable for detecting leaks at low power operation. Of course, the transportation time remains as a problem here also because the reaction products should reach the cell to generate output signal. This instrument is not suitable for measuring hydrogen in the cover gas. The solid electrolyte $CaCl_2$ has a high seebeck coefficient and any thermal gradient present in the sensor portion will give error in voltage output [12, 13].

1.5.4 Leaks causing rise in the cover gas pressure

The cover gas pressure in the tank downstream of the SG increases because of the hydrogen released from sodium-water reaction. This pressure increase is rather fast and is measurable in case of intermediate and large leaks. This pressure signal can be suitably utilized to initiate safety action. Such a system is effective as the pressure build up is relatively high compared to the normal cover gas pressure. This detection method is independent of the operating conditions of the SG and is suitable for use both during start up and normal operation. As it does not necessitate any type of control of parameters like temperature, flow etc., it is a more reliable method of the leak detection. This is utilized for detection of leak in the intermediate range [12].

1.5.5 Acoustic detectors

The small leaks are detected by hydrogen detectors and steam generator is drained on sodium and water side to minimize the risk of propagation by wastage effect. The large leaks, necessitating instantaneous safety signal, are detected by instrumented rupture discs [14]. The

intermediate leaks have the dangerous potential of inflicting damage to tubes other than the one with the primary leak, if the leak goes undetected for more than a few seconds which is insufficient for the hydrogen detectors to respond. An acoustic detection system with good sensitivity and reasonably quick response is attractive for detection of intermediate leaks.

Using the liquid sodium experimental devices signal processing techniques and physical properties of the sodium-water reaction has been studied in Korea, since early 1990s [15, 16]. Studies on Super Phenix reactor showed that the acoustic noise produced by a steam leak into sodium was similar to that of acoustic noise produced by the injection of argon through a small orifice [17].

IAEA organized a coordinated research program entitled 'Acoustic Signal Processing for the Detection of Sodium Boiling'. In this program, several countries submitted their research results based on the sodium-water reaction and background noise data [18, 19]. The major emphasis of this program was the detectable leak size and signal processing techniques. They concluded that a minimum detectable leak size with a high reliability is about 1g/s, and, in the case of less than this value, it is possible to detect the leak, if the physical phenomena are well-defined.

There are two methods in the acoustic technique. One is the passive method, which detects leak by receiving sounds generated due to sodium-water reaction and other is the active method using ultrasonic waves. Even though the passive method has difficulty in separating the acoustic signal from the background noise, this method has been implemented in several reactors and is widely preferred for research due to simple installation and maintenance [20, 21].

Acoustic detectors measure the sound generated by the leaking water/steam as well as the products of the sodium/water reaction. The acoustic signals arising from these different

processes differ from each other in their frequency so that they can be easily separated and analyzed.

The instruments used for acoustic leak detection system comprise of wave guides, pick-up transducers (PT), amplifiers, signal conditioners and analyzing instruments. The waveguides carry the sound waves generated by sodium–water reaction to the PTs. Waveguides are cylindrical SS rods welded to the SG shell to provide acoustic path. The PTs are piezoelectric sensors designed to operate even at high temperatures of the order of $750^{o}C$ and with response range of 0-500g. The analyzer instruments isolate the signal generated by the leak from the noise generated by other processes on the basis of frequency.

Signals from these instruments are processed by microprocessor based logic device which utilizes the already stored calibrated 'finger print' of the 'non-leak' and 'leak' patterns. This leads to the decision of alarm or trip. Thus acoustic detectors are very effective in case of fast developing leaks. Acoustic detectors can also be utilized for approximately locating the leaks by taking into account the different speeds of the sound waves along the shell; the wave guide and the liquid sodium. Development and evaluation of acoustic detectors is still an open area for research.

Acoustic leak detector which has good sensitivity for leak above 1 g/s and shorter response time (<10seconds) can act complimentary to a hydrogen detection system. Hence, acoustic leak detection devices are installed at various locations on the outer shell of the SG. There are stagnant sodium zones near top and bottom tube sheet thermal baffles and hydrogen in sodium detectors will not be very effective for detection of leaks in these zones. On the contrary, acoustic leak detectors are useful for these stagnant zones. Another important area envisaged for acoustic leak detector is providing protection against rapidly escalating leaks.

1.5.6 Rupture discs

Rupture discs provided in the sodium circuit of the SG respond in a few milliseconds to the pressure rise caused by the leak with rates greater than 1 kg/s. The sodium leak detectors make contact between two probe electrodes in the event of gushing sodium on rupture of the disc and detect a large leak in the steam generators. The leak detectors initiate the isolation of the faulty SG unit and other safety actions ensue. Rupture discs along with sodium leak detectors located at the storage and expansion tank (with a lower burst pressure) detect intermediate leaks. This is used in almost all the SGs under operation. The principle, attractive features and advantages of different detection techniques are given in Table 1.4.

1.6 Detection of Small leaks

As seen above, the size of the leak bears an inverse dependence on the time necessary for detection, processing of the leak signal and corrective action. In all situations, the intermediate and large leak conditions should be prevented. This requires development and use of high performance detection methods to tackle micro and small leak situations. Among the known techniques, detection of hydrogen partial pressure in sodium and in Argon cover gas are the most promising methods for detecting leak (in the micro and small leak range) in fast reactor steam generator systems.

Table 1.4: SG leak detection techniques

Leak detection technique	Principle	Features	Advantages
Measurement of hydrogen concentration in sodium	Diffusion through nickel diffuser- measurement by quadrupole mass spectrometer	Diffuser temperature control ±1°C, ultra high vacuum system required ,transit time 3minutes, leak in UHV system, Random failure of QMS analyser filament and interruption in UHV system for replacement of filament	Detects small leaks, can detect partial pressure of H_2 when kept tuned
Measurement of hydrogen concentration in sodium	Diffusion through nickel diffuser-measurement by Sputter ion pump	Diffuser temperature control ±1°C, Hydrogen transit time 3minutes, Processing circuit to extract current signal required	Detects small leaks and no interruption in vacuum system as no filament is used
Measurement of hydrogen concentration in sodium	Electrochemical principle by hydrogen meters	Hydrogen transit time 3minutes Any thermal gradient in the sensor will give error in voltage output	Detects small leaks and no vacuum system required
Hydrogen in cover gas argon	Hydrogen in argon detector- measurement by thermal conductivity detector	Suitable for sodium temp <250°C, uses thin nickel membrane in the form of tubes, Does not respond when sodium temp>250°C, TCD block temperature to be precisely maintained	Detects small leaks when sodium temperature is <250°C
Acoustic detection	Measurement of sound generated by leaked water/steam and reaction product	As SNR is of order of -10dB to -16dB special signal processing techniques required	Detects small leaks, rapid response and no transport delay
Increase in cover gas pressure	Pressure switch actuation	Fast detection independent of reactor condition	Suitable for leaks > 10g/s
Rupture discs	Rupture due to high pressure	Pressure increase due to sodium water reaction	Suitable for leaks >2kg/sec

1.7. State-of-the-art leak detection

 Monitors developed so far for detecting hydrogen in sodium are based either on high diffusivity of hydrogen through metals or on electrochemical cell based on a hydride ion conducting solid electrolyte.

1.7.1 Phenix reactor, France

Phenix reactor is of 563 MWt (250 MWe) having 3 independent secondary circuits ensuring heat transfer from the intermediate heat exchanger in the SG by circulating sodium. Each SG comprises of an evaporator, a super heater and a reheater unit consisting of 12 numbers of vertical banks of large S-shaped water/steam tubes. No cover gas space is provided. The evaporator is made of 2 ¼ Cr-1Mo steel and the super heater and reheater modules are made of 321 H material respectively.

The leak detection is accomplished by hydrogen in sodium detection (HSD) and hydrogen in argon detection (HAD) systems. The HSD system consists of a nickel diffusion membrane detector fitted with a 200 lps capacity ion pump. The sampling lines from each evaporator are grouped into one and sent to a detector. Similarly, the sampling lines of superheater and reheater also are grouped and sent to their respective detectors. Sodium temperature is maintained above 400°C. It is reported that the HSD system is capable of measuring the hydrogen concentration of upto 5 ppb. The HAD system also is a vacuum system based diffusion meter fitted with a mass spectrometer to detect hydrogen partial pressure [22].

1.7.2 Super phenix reactor, France

The 1300 MWe super phenix reactor [23] has one SG in each secondary sodium loop. The SG consists of once through type evaporator and super heater with helical tubes made of Ni 33-Cr 21-Ti Al Mn steel. The free level of sodium in SG is provided with Argon cover gas. The HSD

and HAD are similar to the Phenix reactor except that the sample of sodium is accurately maintained at 460°C. The resolution of hydrogen concentration measurement in HSD is reported to be 2ppb. Rupture discs are provided in the SG inlet and outlet heaters for detection of large leaks [24, 25].

1.7.3 BN-350 reactor, Russia

The secondary sodium circuits of 750MWt fast reactor contain 5 loops. The SG for each loop is made up of two evaporator and two super heaters, the evaporators are of bayonet type with gas space. The super heaters also are of the same type without gas space. Both evaporator and super heaters are made of 2 ¼ Cr-1 Mo steel. The sample drawn from the two evaporator outlets are connected together and sent to one detector. There is a similar arrangement for the super heaters too. For small leaks, HSD and HAD with vacuum system nickel membrane based diffusion technique is used with sputter ion pump. No MSM is used. For detection of intermediate and large leaks, use of expansion tank pressure monitoring and rupture discs in expansion tank was reported [26]. In BN-350 two large sodium leaks occurred as a result of defect formation in steam generator tubes. After sodium water reaction occurrence, the operation of the steam generator safety system as well as sodium and water draining took place. Loss of tightness of an evaporator tube sodium water reaction in the inter tubular space was found to be due to a leak [27].

1.7.4 BN-600 reactor, Russia

The 600 MWe fast reactors are with shell and straight tubes module type SG, consisting of evaporators made of 2 ¼ Cr-1 Mo steel and super heaters and reheater made of 18 Cr- 9Ni steel. Only HSD system is used for hydrogen detection. The detectors are similar to those in BN-350 [26, 28].

1.7.5 Monju reactor, Japan

The 280 MWe rated reactor contains 3 secondary circuits. The SG is of helical coil design with gas space consisting of an evaporator and a separate super heater for each loop. The material of the evaporator tube is 2 ¼ Cr-1Mo steel whereas super heater is made of austenitic stainless steel. The HSD is a nickel detector-ion pump system with the membrane maintained at 500°C. They are located at the outlet of each SG and on the return line to pump tank. A special feature is that the vacuum systems have two separate chambers. Left side chamber is called dynamic chamber, and is composed of Ni membrane, ion pump, ultra high vacuum gauge and their connecting vacuum piping. Right side chamber is called as static chamber and is composed of Ni membrane same as that of dynamic chamber and a Schultz gauge for measuring the static equilibrium pressure. To conduct the evacuation of static chamber, both chambers are connected with each other by opening two vacuum stop valves. Sodium is heated up to 500°C through an economizer which have an electric heater immersed in the sodium. Sodium flow is separated by a distributor which changes the direction at the inlet of Ni membrane. It is cooled down by an economizer before routing it back to the main loop through electromagnetic flow meter. Outer diameter at the location of the economizer is 34 mm, total length is 1.5 m [29].

1.7.6 Prototype fast reactor (PFR), UK

The PFR has 3 secondary sodium circuits. There is one SG for each secondary circuit, comprising of one evaporator, one superheater and one reheater made of 9 Cr-1 Mo steel. The SGs are of U shape with cover gas. The sample of sodium in the HSD system is drawn from the outlet of the evaporator unit feeding four detectors in parallel. The detectors are made of nickel membrane and measurement of hydrogen partial pressure is based on thermal conductivity detector. The detector is maintained at 450°C. The performance of this meter was reported not to

be satisfactory and it was required to calibrate and standardize the thermal conductivity meter once in 2 days. The HAD system consisted of two nickel membrane detectors for cover gas space of evaporator, super heater and reheater. The detector temperature was maintained at 550 $^{\circ}$C. Besides this, the cover gas pressure also was monitored. The acoustic sensors, electrochemical oxygen and hydrogen meters were tried on experimental basis in the installation [30].

1.7.7 SNR 300 reactor, Germany

 The 327 MWe reactors are provided with 3 secondary loops [31]. The SGs are made up of once through evaporator and separate super heater, with straight tubes in first and second loops and helical tube in third loop without cover gas space. The tubes are made of stabilized 2 ¼ Cr-1 Mo steel. The HSD contains detectors based on nickel tube and ion pump combination without mass spectrometer. This is located in the main return line. A sketch of the detector is given in Fig.1.3. The nickel membrane, consisting of 4 cylindrical fingers, is fed with sodium by a small electromagnetic pump with a flow rate up to 1 m^3/h. Membrane material is Ni 201 a LCNi 99. The thickness of the fingers is 1 mm and the surface volume 65.6 cm^3. A controlled membrane temperature of 500°C is maintained, independently from the loop temperature, by an electrical heater system combined with a tube in tube heat exchanger.

Sodium flow is controlled by a permanent magnetic flow meter. The ion pump has a pumping speed of approximately 3.5 1ps for hydrogen and operates normally in a pressure range from 1×10^{-11} to 5×10^{-11} kg/cm^2. This corresponds to a lower sensitivity level of $< 2 \times 10^{-3}$ ppm. The static mode response time from 0 - 63 % is in the order of approximately 100s and the dynamic mode response time which is the normal mode is negligible.

The membrane is maintained at 500°C and sputter ion current is processed for hydrogen detection and estimation. For intermediate leak, the pressure in the expansion tank is monitored. Rupture discs are provided at the inlet and outlet of each module.
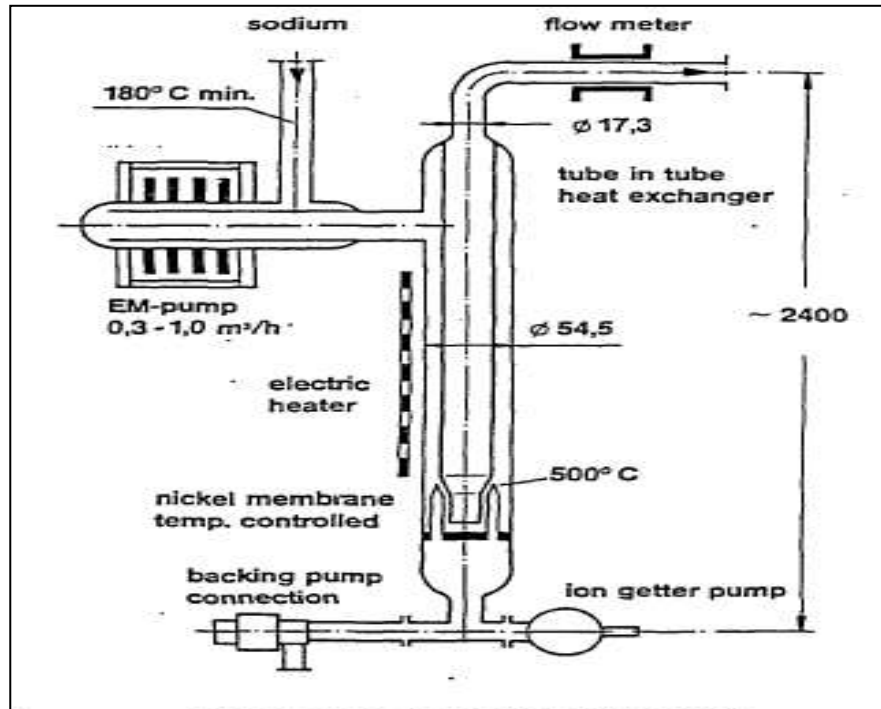
Fig. 1.3: Hydrogen Detector of SNR-300 [31]

The two detectors in the main pipe have to serve for two functions:Measurement of the absolute hydrogen content to control the hydrogen diffusion from the water side and the effectivity of cold trap operation

- Direct signalization of the concentration gradient which is used to adjust different alarm levels

- Though at an early stage of development, it was decided to explore the possibility of in-situ calibration of detectors due to the following reasons:

- Complex design of the detectors with special attention to the needed sensitivity and accuracy of the signals

- Aging effects of pumps

- Replacement of ion pumps

- Minimize charging of cold trap by additional impurities [31].

1.7.8 Clinch river breeder reactor plant, USA

The 380MWe rated reactor is provided with 3 secondary circuits. The SG for each secondary unit is made of 2 evaporators and 1 separate super heater [28]. Both evaporator and super heaters are made of 2 ¼ Cr-1 Mo steel. The HSD is made of nickel membrane detector. The ion pumps are located at the outlet of each module and at the common return line. Ion pump current is used as the signal for leak detection. No MSM is used in this installation. The HAD is placed at the vent line of each module. Electrochemical oxygen meter is located at the common return line for the purpose of gross monitoring.

1.7.9 Experimental breeder reactor (EBR-II), USA

This is a 62.5 MWt experimental reactor. The SG is once through type with double walled straight tube construction. There are two SGs each one of which contains four evaporators and one super heater. Both evaporators and super heaters are made of 2 ¼ Cr-1 Mo steel. One nickel membrane based HSD is located at the outlet of each unit and two such detectors are installed on the common return line. The detector temperature is maintained at 480°C. Electrochemical oxygen sensor is also used [28]. The list of FBR SGs and the hydrogen leak detectors is shown in Table 1.5

Table 1.5: List of FBR SGs and the hydrogen leak detectors

Reactor,	Reactor features	SG features	Detector- HSD	Detector- HAD
Phenix, France	250MWe, three secondary circuits, Each has one SG with evaporator, super heater and reheater	No cover gas space, evaporator of 2 ¼- 1 Mo	HSD by nickel diffuser, 200lps ion pump, sodium temp. 400 °C ,smallest H_2 detection of 5 ppb,	HAD, vacuum system based diffuser meter fitted with mass spectrometer
Super Phenix, France	1300MWe, one SG in secondary loop	No cover gas space, evaporator of 2 ¼- 1 Mo	HSD similar to Phenix except that sampled sodium is accurately controlled at 460 °C	HAD similar to Phenix
BN-350 Russia	750 MWe , secondary circuit contains 5 loops, SG for each loop made up of 2 evaporators and 2 superheaters	Both evaporator and superheater of 2 ¼ Cr- 1Mo, sample drawn from two evaporator outlets are connected together and sent to one detector	HSD with nickel diffuser and ion pump. No MSM used. Magnetic Discharge Pump having a vaccum connection to a hydrogen permeable membrane	HAD with vacuum system based nickel diffuser , For intermediate and large leaks expansion tank pressure monitoring and rupture disc in expansion tank used
BN-600, Russia	600MWe, with shell and straight tubes module type SG	Evaporator of 2 ¼ Cr-1 Mo , superheater and reheater of 18 Cr-9Ni	Only HSD used , detector similar to BN-350	
PFR, UK	250MWe, 3 secondary circuits, one SG for each secondary, each SG has one evaporator, one super heater and one reheater	Evaporator of 2 ¼ Cr- 1 Mo, superheater of 9 Cr- 1 Mo, SG of U shape with cover gas space	HSD system draws sampled sodium from evaporator unit feeding to 4 detectors in parallel, Nickel membrane and H_2 p/p by thermal conductivity detector, temp at 450 °C, performance not good as calibration required every two days	HAD with two nickel membrane detectors for cover gas space of evaporator, super heater and reheater. Temp. at 550 °C, cover gas pressure also monitored. Acoustic sensors, electrochemical oxygen and hydrogen meters tried on experimental basis, no information available

CRBRP, USA	380MWe, 3 secondary circuits, each SG has 2 evaporators and 1 separate super heater	Both evaporator and super heater of 1 ¼ Cr- 1 Mo	HSD with nickel membrane and ion pumps located at outlet of each module and at the common return line, No MSM used.	HAD placed at the vent line of each module. Electrochemical oxygen meter located at the common return line for gross monitoring
SNR 300, Germany	327 MWe, 3 secondary loops, SG of once through evaporator and separate superheater	Straight tubes in first and second loops and helical tube in 3 rd loop without covergas space	HSD with nickel tube and ion pump without MSM, Membrane at 500 °C, For intermediate leak, pressure in expansion tank monitored, Rupture discs at outlet and inlet of each module	
Monju, Japan	280 MWe , 3 secondary circuits	Evaporator of 2 ¼ Cr-1Mo, super heater of austenitic, SG of helical coil design with gas space consisting of an evaporator and a separate super heater for each loop.	HSD with nickel detector-ion pump , membrane at 500 °C, located at the outlet of each SG and on the return line to pump tank	
EBR _II, USA	62.5 MWt , SG is once through type of double walled straight tube, 2 SGs each of 4 evaporators and one super heater	Both evaporators and super heater of 2 ¼ Cr- 1 Mo.	One nickel membrane based HSD at outlet of each unit and two such detectors on the common return line, detector temperature at 480 °C. Electrochemical oxygen sensor developed by Westinghouse also used	
FBTR, India	40MWt, 13 MWe loop type , SG consists of 4 nos of once through counter flow type heat exchanger modules each of 12.5 MWt rating	SG modules of 2 ¼ Cr- 1Mo stabilized steel economizer, evaporator and super heater combined into a single unit	Nickel diffuser and ion pump, detector temperature at 450 °C	HAD based on thermal conductivity detector, pressure switch for cover gas pressure increase, rupture disc for large leak.

1.8 Main incidents and related experience feedback

1.8.1 Operation of the steam generators (sodium-water reactions)

Every steam generator of the first generation reactors experienced sodium-water reactions. They

are summarized in Table 1.6 [22].

Table 1.6: Sodium-water experiences of first generation steam generators

Reactor	No of leaks due to sodium water reaction
PHENIX	5
PFR	40
BOR 60	1
BN350	3 after 1980
BN600	12

Even if these sodium-water reactions happened in different SG designs, they are mainly of three

types.

- **Manufacturing problems**

Several sodium-water reactions occurred during or shortly after sodium filling, due to

manufacturing defects, in particular in the Russian reactors. A crack was revealed at PFR in a

sheet metal/plate weld during filling in 1976.

- **Fatigue cracks**

A poor design or unsuitable operational modes caused thermal shocks and mechanical fatigue.

Fatigue cracks then caused sodium-water reactions. This was the case for the first 4 reactions, for

example, occurring at Phénix where unwanted cold water got into the reheater during start-ups,

generating fatigue cracks.

- **Corrosion**

Corrosion phenomena could lead to an open crack and a sodium-water reaction. This was the

case for PFR, for example, when repeated corrosion occurred at the tube/plate joints. This was

also the case for the fifth sodium-water reaction at Phénix. In each case, the flow of the

pressurized jet of steam, upon reaction with the sodium created a blowtorch whose tip could, within a few minutes, pierce through the neighbouring steam tubes, and even the SG shell.

The initial sodium-water reaction, in some cases, resulted in significant damage due to the relatively long detection response time and the SG emptying and inerting time.

- The 1st sodium-water reaction at Phénix: 30kg of water reacted. The improvements made reduced the injections to be limited to between 1 and 4 kg for the next 4 reactions.

- The reaction occurred in February 1987 at PFR, in the common part of the tube bundle of superheater No. 2, by cracking of a tube resulting from vibration of the bundle. 39 tubes around the initial tube were pierced by pressurization. The related pressure build-up of the secondary sodium led to the burst rupture disk failure.

- Major sodium-water reactions occurred at BN350 and BN600, the most significant of which was in January 1981 with 40 kg of injected water.

1.8.2 Feedback from experience

The lessons learned from these incidents for future reactors are as follows:

In terms of protection:

- Reliable and faster hydrogen detection is essential.

- Automatic shutdown accompanied by a rapid depressurization on the steam side.

- Design of a casing around the self-supporting SG, capable of withstanding the most violent sodium-water reaction.

- Rupture disk to limit the potential pressure increase.

Effective prevention implies several requirements:

- An improved design from the thermo-mechanical point of view to avoid fatigue cracks

- Appropriate materials.

- High quality manufacturing (testing of absolutely each weld, no weld beads, etc.).

- Care when operating (prevention of spurious thermal shocks, good conservation of the circuit during draining periods, etc.).

Understanding the reasons for these incidents and enforcement of related prevention rules enabled sodium-water reaction to be avoided at Superphénix and on BN600 from 1992 onwards.

1.9   Performance requirement of a leak detection system

The performance features of a leak detection system arise from the following considerations:

- The response time of leak detection should be as small as possible. However, in the case of micro and small leaks the total time from initiation of the leak to the detection is of the order of 100 seconds. A control over this is very difficult and in any case, it cannot be improved very much because the inherent delay arises from the steam generator operation itself [14, 32].

- The sensitivity of leak detection system has two aspects (i) the smallest water leak it can detect and (ii) the change in the signal strength as the leak rate changes. In case of the hydrogen in sodium detectors, the smallest leak is derived from the smallest rise in hydrogen concentration it can detect. The system should be able to discern leak of different size quantitatively. Thus, as the leak gets enhanced with time, the detector should yield a reliable voltage signal to assess the situation [33].

- Reliability of the system is an important aspect and it should be such that the spurious trip rate is limited to once in 2 years. This reduces the non-availability of the system to better than 10^{-3}.

- It is essential to ensure compactness along with high performance specifications such as short response time, high output stability and good resolution. Such performance

reliability is achieved by improving the stability and reproducibility of the detector instrumentation. The reliability can be increased with multiple detectors and redundant methods. The leak detector system consists of vital components such as nickel diffuser and ion pumps. The availability is affected by failure of vital components such as nickel diffuser and hence it has to be detected at the earliest [27].

- Reliable calibration methods establish the relationship between meter output and the concentration of hydrogen in sodium ensuring the performance of the leak detection system at different measurement conditions.

- The genuineness of SG leak signal is of paramount importance as it may result in spurious reactor trips or false alarms. The overall availability can be improved by minimizing the downtime taken for system calibration and spurious actuation. The leak detection systems developed for SGs of FBTR, meeting the above requirements are discussed in this thesis.

1.10 Motivation and objectives

1.10.1 Motivation

The integrity of nickel diffuser in the steam generator leak detection system is important as its failure can result in sodium leak into ultra high vacuum system. The conventional spark plug and wire type sodium leak detectors cannot be used for detection of sodium leak as they interfere with the vacuum system. In the open literature, no information is available about any technique for the detection of sodium leak in the event of failure of nickel diffuser used for the SG small leak detection systems. Hence, it is required to develop and deploy a non-contact type and miniature size sodium leak detector based on mutual inductance for detection of sodium leak from failure of a nickel diffuser. As empirical design of the mutual inductance probes and experimental

analysis are time consuming, a model based approach is a good possibility.

It is found from literature that random failure of a QMS filament causes spurious reactor trips based on a SG leak signal. The intervention in the vacuum system for replacement of a QMS ion source filament and subsequent calibration is time consuming and result in significant reactor downtime. An alternate detection system using a sputter ion pump (SIP) ionization current, which is already in the circuit, in place of a QMS is worth exploring, as the ionization current is a function of the total gas molecules in the UHV chamber. Implementation of this concept, however, requires development of a technique to extract the SIP current signal with adequate protection against high voltage and converting it into a 0-10V DC signal suitable for connecting to monitoring and safety systems. In several instances, SG and reactor trips were reported due to spikes in the leak signal [34]. It is beneficial to focus research on noise detection and rejection techniques for eliminating spurious spikes and ensuring genuineness of the leak signals.

It is found from the literature that no confirmatory test for verifying the genuineness of the signal on actuation of SG leak signal is possible. For such situations, triplication using multiple systems and initiation of SG or reactor trip based on redundancy logic appears as a possible option for ensuring genuineness of a signal.

Problems in ultrahigh vacuum reduce the availability of a QMS system and detailed research investigations may throw some new light. Detectors using diverse principles such as electrochemical hydrogen sensor can be explored for leak detection. Response of hydrogen in sodium detection system is slow when sodium temperature is less than 250°C. In view of this; a system that can detect hydrogen in cover gas Argon using a thermal conductivity sensor appears a very good alternative as they work at lower sodium temperatures.

Response time of the SG leak detection systems is high of the order of 3 minutes as diffusion depends on temperature and likely large distance between the leak location and sensor. Acoustic techniques can give much more rapid response than that of hydrogen detection as transport delays are not involved and velocity of sound. In acoustic detector based systems, the acoustic noise generated when the steam/water leaks into sodium, is usually of the order of -10dB to -16dB. In an operating SG, sodium flow, water/steam flow, and boiling noise along with the noise from adjacent machinery contribute to background noise. Hence, from the normal RMS of the time signals, it is very difficult to judge the initiation of a leak. Development and use of special signal processing techniques may be useful to detect leak with reasonable signal to noise ratio (SNR). It is beneficial to focus research in the area of development of signal processing techniques. Systematic research in this direction is attractive.

The initiation of SG leak signal for reactor trip can be due to the leak in any of the SG modules in each loop and identification of the leaky module is not possible in the QMS or SIP based system. Installing several acoustic sensors is a possible option for identification of the defective module. Systematic research in this direction is attractive.

1.10.2 Objectives

The objectives of the thesis include the following:

a) To develop a non-contact type sodium leak detector for early identification of the failure of nickel diffuser in the SG leak detection system and deploy it at site.

b) To develop an alternate system using sputter ion pump, in place of a quadrupole mass spectrometer, for detection of small leaks in steam generator at incipient stages and to explore multiple systems for improving the reliability of SG leak detection system.

c) To study the performance of detectors by conducting experiments for reliable detection

of leaks.

d) To develop diverse detectors such as electrochemical hydrogen detectors and hydrogen

in argon detectors.

e) To demonstrate the complementarity and coherency of the overall detection approach.

Chapter 2: Development of miniature mutual inductance type leak detector

2.1. Preamble

A non-contact type sodium leak detector is useful for detecting sodium leak caused by failure of nickel diffuser membrane. For application in sodium, Mutual inductance type leak detector (MILD) is attractive and advantageous. Optimization of MILD is important as detection sensitivity can be improved by optimization of excitation current and frequency. The process of optimization ensures high detection sensitivity and low temperature sensitivity of the probe. Empirical design of probes and experimental analysis are time consuming. Hence, model based approach for designing the probe is adopted in this research work. This chapter discusses the process of development of MILD.

2.2. Identification of requirements

Various sodium leak detection systems are already employed in FBTR. Wire type leak detectors, made of ϕ1.5 mm nickel wire, are used to detect sodium leak from pipelines [35]. Spark plug type leak detectors are being used to detect sodium leak from sodium capacities, bellow-seal valves and the primary sodium double envelope [35]. From the experience, the spark-plug type leak detectors are not reliable as they may not detect sodium leak in time, if the electrode is not properly wetted by the leaking sodium. Further, the metal-to-ceramic sealing is a weak part and has potential to fail in the highly corrosive and high temperature sodium environment. With these conductivity based detectors, sodium leak of the order of 100 g/h can be detected in about 2 h. Sodium Aerosol Detection (SAD) system serves to detect minute quantity of sodium leak from the primary pipelines and from the steam generator casing. It can sense 1 mg of sodium per m^3

(1 nanograms/cm^3) of carrier gas instantaneously. All these methods require direct contact with sodium and therefore require an opening in vacuum circuit for introducing the sensors, which will affect UHV in the circuit. Hence, an alternate method that uses mutual inductance type leak detector that does not require direct contact of sodium with the sensor, is conceived in this work.

2.3.   Mutual inductance type leak detector proposed

MILD consists of a primary coil and a secondary coil wound around a stainless steel bobbin as shown in Fig. 2.1.
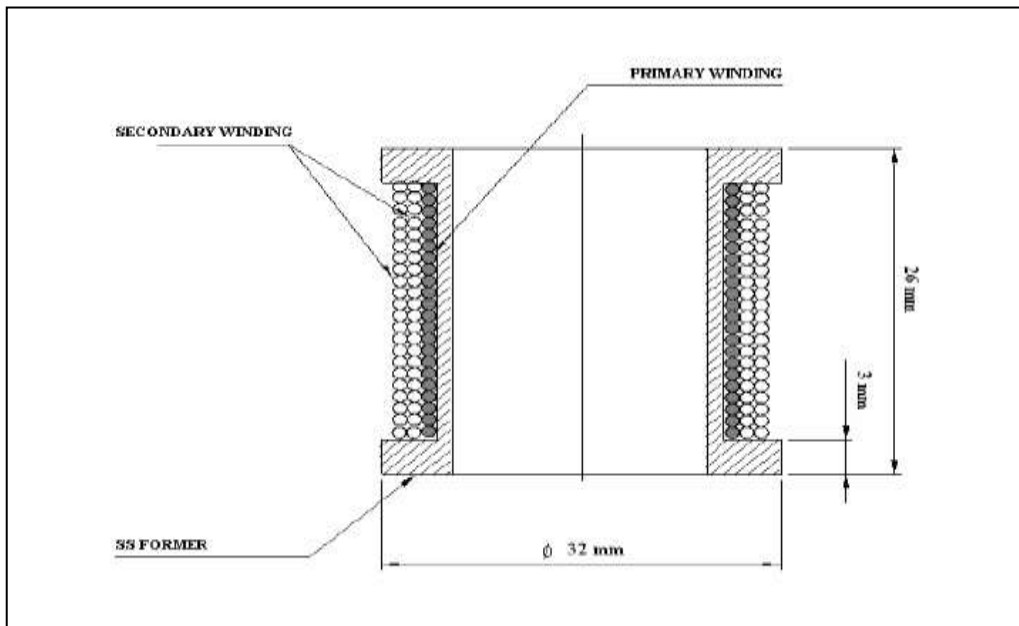
Fig.2.1: Block diagram of Mutual inductance level detector

It works on the principle of decrease in mutual inductance between these two coils when sodium is present around them, as shown in Fig. 2.2. The primary coil is excited with AC constant current of 100 mA. An emf will be induced in the secondary coil. Presence of sodium in the vicinity of the probe leads to reduction in the mutual inductance of the probe, which in turn, reduces the secondary voltage. The reduction in the secondary e.m.f indicates sodium leak. Response time of the MILD is of the order of a few seconds and the minimum detectable sodium

leak is related to the pocket volume. Overall response time is a function of the distance of the pocket from the leak location and the size of the leak.
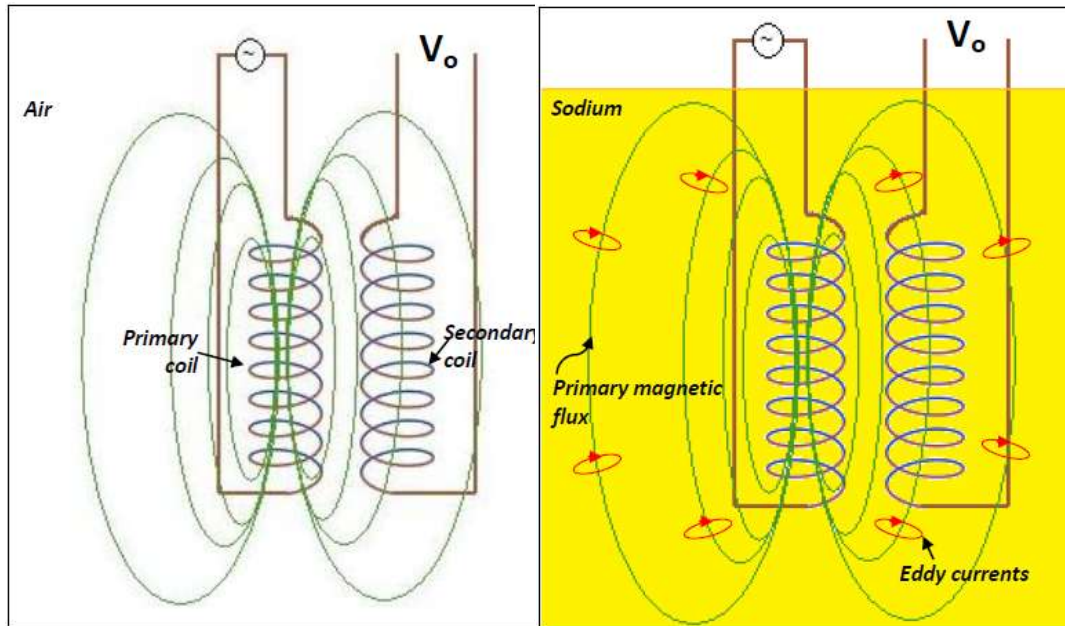
Fig. 2.2: Mutual inductance leak detector in air and in sodium

MI type leak detectors have several advantages such as:

- non contact operation with sodium as it is located inside a thimble

- facilitates easy maintenance, as the sensor can be removed from its pocket for inspection and/or replacement

- the sensor needs to be installed into the thimble only prior to sodium-filling of the vessel and not during the integrity (pressure/vacuum) tests, normally carried out on the vessel after fabrication

- immunity to sodium wetting

All the above factors are attractive to develop a miniature MILD. In order to optimize the design parameters of MILD, finite element modeling has been performed and details are discussed in next section.

2.4.   Finite element modeling of MI detector

2.4.1. Geometry construction

Schematic of the MILD is shown in Fig. 2.3. It consists of one primary winding and one secondary winding. The coils are made of MgO insulated SS sheathed copper core cable. This probe is placed inside a SS pocket.

Provisions are made in the pocket to collect sodium in case of leak. Presence of sodium in the pocket leads to decrease in mutual inductance between the coils, thereby detecting the sodium leak. Datasheet of the MILD is given in Table 2.1.
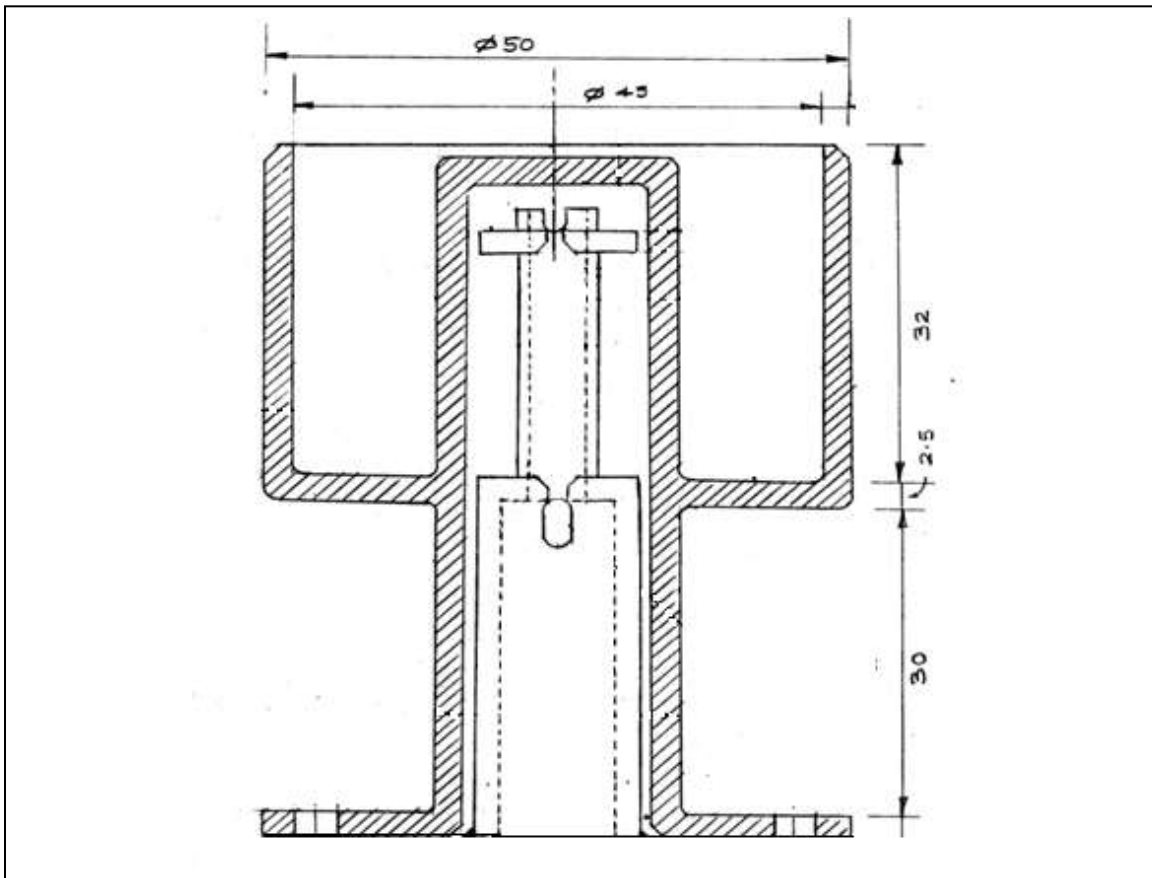
Fig. 2.3: Schematic of the mutual inductance leak detector

Table 2.1: Datasheet of MILD

Bobbin material	SS 316
Active length	20 mm
Total length	22 mm
Coil winding	Two layers
Cable	1 mm dia. SS sheathed copper conductor MI cable

2.4.2. Governing differential equation

The governing differential equation of the MILD is derived from the Maxwell's equations as given below [36]:

$$\nabla \times H = J + \frac{\partial D}{\partial t} \tag{2.1}$$

$$\nabla \times E = -\frac{\partial B}{\partial t} \tag{2.2}$$

$$\nabla \cdot D = \rho \tag{2.3}$$

$$\nabla \cdot B = 0 \tag{2.4}$$

where, H is magnetic field intensity, J is current density, D is electric flux density, E is electric field intensity, B is magnetic flux density, ρ is electric charge density and t represents time. MILD works on a quasi-static electromagnetic phenomena, the displacement current term $(\partial D/\partial t)$ in Equation 2.1 is insignificant and hence, neglected. Maxwell's equations are solved in conjunction with the following constitutive relations that describe the material properties:

$$B = \mu(H + M) \tag{2.5}$$

$$D = \epsilon E + P \tag{2.6}$$

$$J = \sigma E \tag{2.7}$$

where, μ is magnetic permeability of the medium, M is magnetic polarization, ϵ is permittivity of the medium, P is electric polarization and σ is electric conductivity of the medium. In the present case, the terms M and P are not relevant and hence, assumed zero.

The magnetic flux density is written in terms of magnetic vector potential (A) as follows:

$$B = \nabla \times A \tag{2.8}$$

Substituting Equations (2.5) and (2.8) in Equation (2.1) we obtain:

$$\nabla \times \left(\frac{1}{\mu(B)} (\nabla \times A) \right) = J \tag{2.9}$$

For the time varying magnetic fields, the current density is a combination of the induced eddy current density (J_e) in the material and the applied source current density (J_s).

$$J = J_e + J_s \tag{2.10}$$

Hence, Equation (2.10) can be re-written as follows.

$$\nabla \times \left(\frac{1}{\mu(B)} (\nabla \times A) \right) = J_e + J_s \tag{2.11}$$

The induced current density (J_e) obeys the constitutive relation mentioned in Equation (2.7) and hence, is expressed as:

$$J_e = \sigma E \tag{2.12}$$

The induced electric field (E) obeys Equation (2.2). Substituting the vector potential form of B in Equation (2.3) yields:

$$\nabla \times E = -\frac{\partial}{\partial t} (\nabla \times A)$$

This can be re-written as:

$$\nabla \times \left(E + \frac{\partial A}{\partial t} \right) = 0 \tag{2.13}$$

Equation (2.13) introduces the notion of a curl less quantity that can be written as the negative gradient of a scalar potential as follows:

$$E + \frac{\partial A}{\partial t} = -\nabla \psi$$

$$E = -\nabla \psi - \frac{\partial A}{\partial t} \qquad (2.14)$$

where ψ is electric scalar potential. Substituting Equations (2.12) and (2.14) in Equation (2.11) yields the governing PDE of the MILD.

$$\nabla \times \left(\frac{1}{\mu(B)} (\nabla \times A) \right) = \sigma \left(-\nabla \psi - \frac{\partial A}{\partial t} \right) + J_s \qquad (2.15)$$

$$\nabla \times \left(\frac{1}{\mu(B)} (\nabla \times A) \right) = -\sigma \frac{\partial A}{\partial t} + J_s - \sigma \nabla \psi \qquad (2.16)$$

Equation (2.16) is solved by FEM using the FEMM software.

2.4.3. Mesh generation

The MILD is modeled as an axis-symmetric problem, in which geometries are drawn in the r-z plane, on one side of the axis of the symmetry line. The primary and secondary coils were modeled as individual turns (including SS sheath). As it is not affordable to mesh and solve the problem in infinite space, it is necessary to specify a finite area to mesh. The model is truncated into a finite region by defining an external boundary model which limits the solutions to be calculated inside the assigned region. Properties of all the materials used in the model are given in Table 2.2. Simulation of temperature variation was taken care by varying the conductivity values for copper, sodium and stainless steel. Fig. 2.4 shows a typical model of MILD with the boundary region.
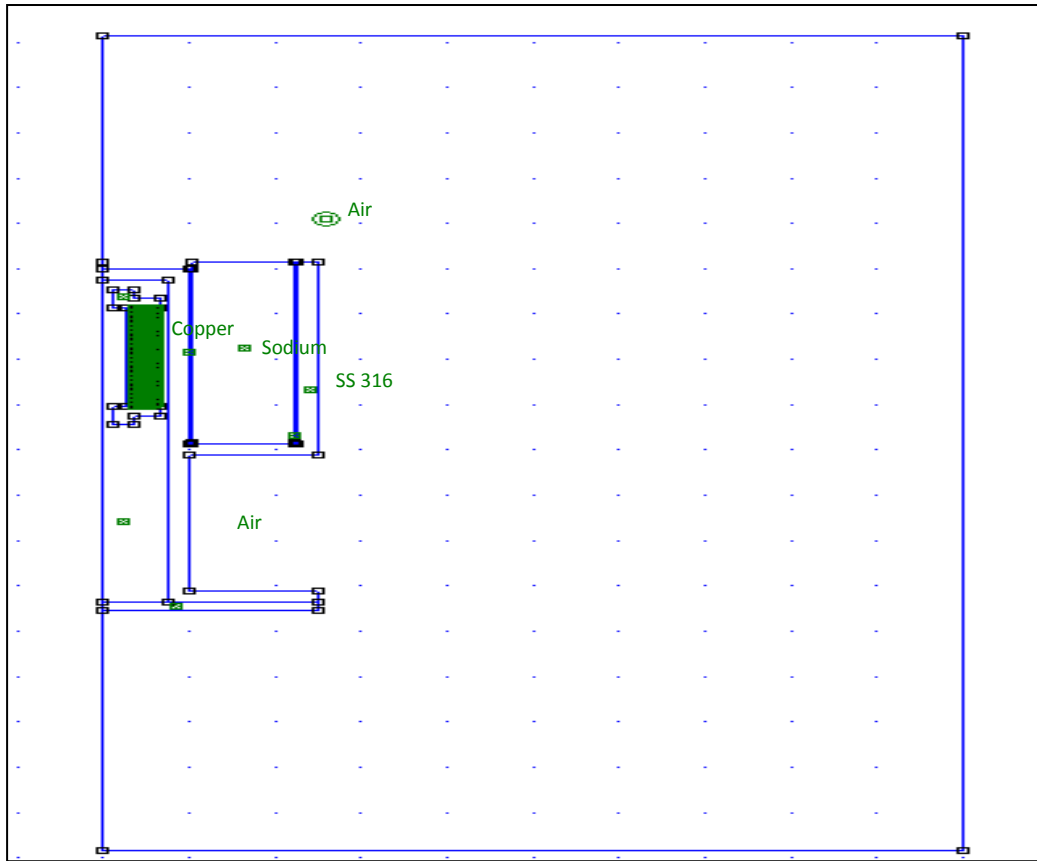
Fig. 2.4: Detector geometry drawn in FEMM

Table 2.2: Material properties

Sl. No	Material	Electric conductivity, σ (MS/m)		Relative magnetic permeability (μ_r)
		100°C	450°C	
1	Copper	47.51	23.5	1
2	Sodium	9.34	4.1	1
3	SS 316	1.28	0.97	1
4	Air	0	0	1

Table 2.3: Optimization of mesh size

Sl. No	Mesh size (mm)	Magnetic Vector potential (A) $\times 10^{-10}$ T-m		No. of mesh elements
1	2	8.27415		54971
2	1	8.2756		80813
3	0.5	8.27602	Saturated 'A'	186226
4	0.3	8.27602		436407

The model is divided into a mesh of small regions inside the problem domain. Hence, regions inside each individual turn were set at refined mesh size of 0.1 mm. The mesh size at larger regions were optimized after systematic trial and error that gives due emphasis to the solution accuracy and computational time. Table 2.3 gives the vector potential values at r = 15 mm and z =15 mm (inside the collection region of the pocket) for different mesh sizes. As seen from the table, the vector potential values tend to converge for mesh sizes less than 0.5mm. Hence, mesh size of 0.5mm was considered as optimum for larger regions in the problem domain. Fig. 2.5 shows the meshed MILD geometry in the region around the coil.

2.4.4. Boundary conditions

Boundary conditions are used to define the behavior of model at its boundaries [37]. The two popular boundary conditions used in FE methods are Dirichlet and Neumann conditions. Dirichlet boundary condition defines the vector potential values at the outer boundary. Neumann boundary condition defines the normal derivative of the vector potential at the outer boundary. In MILD model geometry, zero dirichlet boundary condition (A = 0) has been defined at the outer boundary of MILD as well as at the axis-symmetry line. This condition prevents the magnetic flux from crossing the boundary.

2.4.5. Solving the model

Solver is an algorithm to solve the system of linear equations obtained from the PDE of the MILD. The system of equations will be of the matrix form AX=B, where A and B are known matrices, and X is the unknown variable to be determined. In FEMM, the electromagnetic problems are solved by iterative Conjugate Gradient (CG) solver to find the unknown magnetic vector potential values at nodal points of the mesh. The global matrix of time-harmonic magnetic problem is complex symmetric in nature. Hence, FEMM uses the complex symmetric version of Bi-Conjugate Gradient (BCG) matrix solver in particular [38].

This solver allows one to operate directly on the complex symmetric matrix and take advantage of the symmetric structure to minimize the number of computations that must be performed per iteration. The long solution time of complex BCG algorithm was reduced by modifying it to include Symmetric Successive over Relaxation pre-conditioner [39]. The solver took around 30s of solution time to solve the MILD problem having 186226 degrees of freedom.
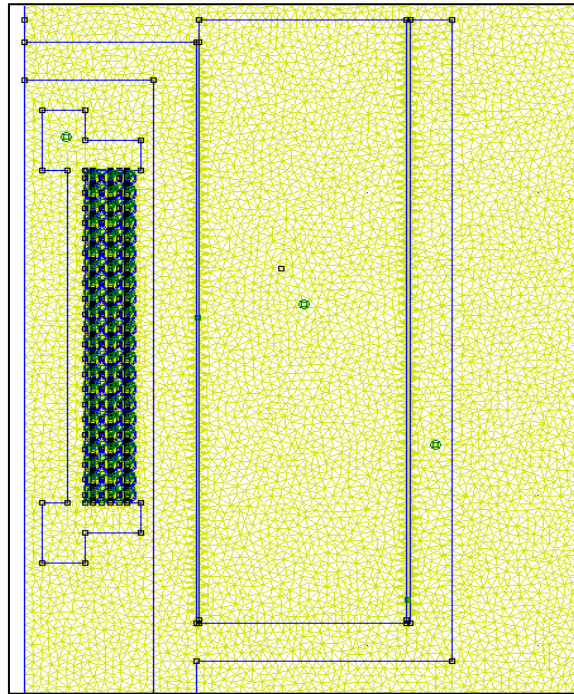
Fig. 2.5: Detector geometry near coil meshed with optimum size

2.4.6. Post processing

The functionality of post processing in FEMM is to view the solutions generated by the solver. On user requisition, the post processor computes the values of derived parameters, such as - magnetic flux density, induced voltage, inductance, etc. from the value of magnetic vector potential obtained from the solver. Based on these derived values, surface plots of them can also be plotted. The surface plots of MILD showing its magnetic flux density (B) without sodium and surrounded by sodium are respectively shown in Fig.2.6a and 2.6b.

It can be observed that, sodium surrounding the probe limits the magnetic flux lines to regions near the coil due to formation of eddy currents. To compute the leak detection sensitivity of MILD, induced voltage in the secondary winding of the probe was calculated for various excitation frequencies and ambient temperatures. Analyses were carried out for a frequency range of 1000 – 8000 Hz and a temperature range of 100 – 450°C.
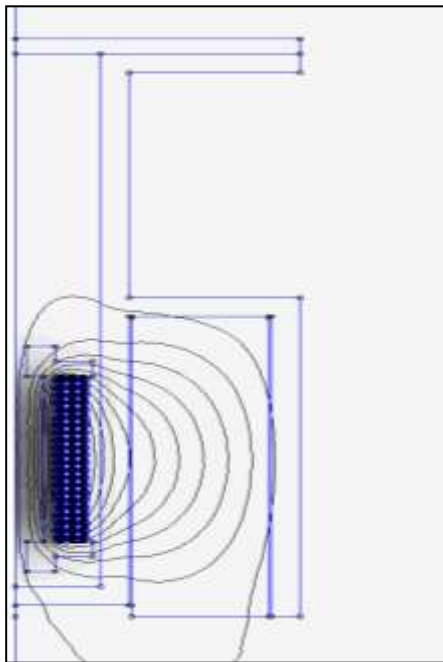
Fig. 2.6a: Magnetic flux density plot of MILD without sodium
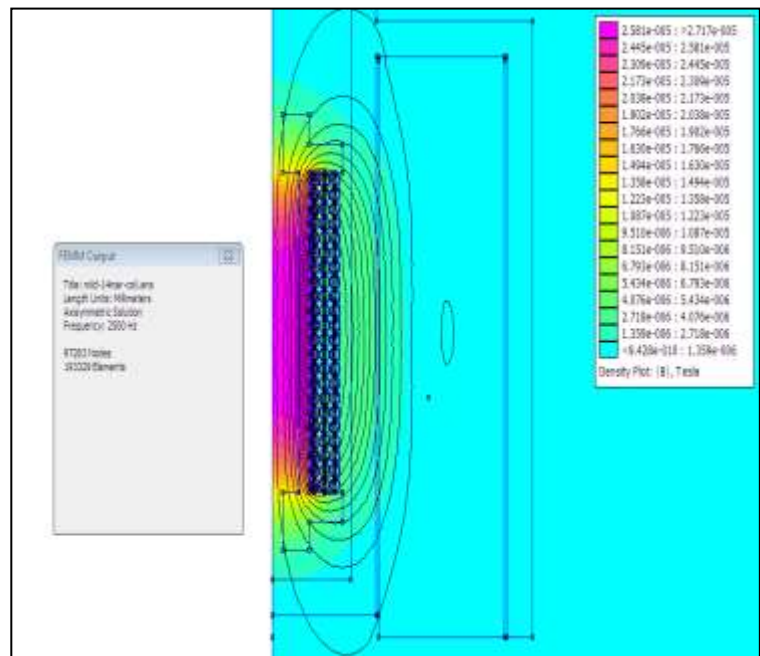
Fig. 2.6b: Magnetic flux density plot of MILD surrounded by sodium

Simulation of ambient temperature variation of MILD was done parametrically by varying the electrical conductivity/ resistivity values of all the materials used in MILD. This was done on the basis that electrical resistivity of most materials varies with temperature [40]. A linear approximation of temperature dependence of a material's electrical resistivity is given by:

$$\rho(T) = \rho_0 [1 + \alpha(T - T_0)] \tag{2.17}$$

Where, α is called the temperature coefficient of resistivity, T_0 is the reference temperature (usually room temperature), ρ and ρ_0 are the resistivity at temperatures T and T_0.

Higher accuracy of resistivity estimation can be obtained from non-linear approximations such as Bloch-Griineisen equation [41]. A typical electrical resistivity vs. temperature characteristics of sodium [42] is shown in Fig. 2.7.
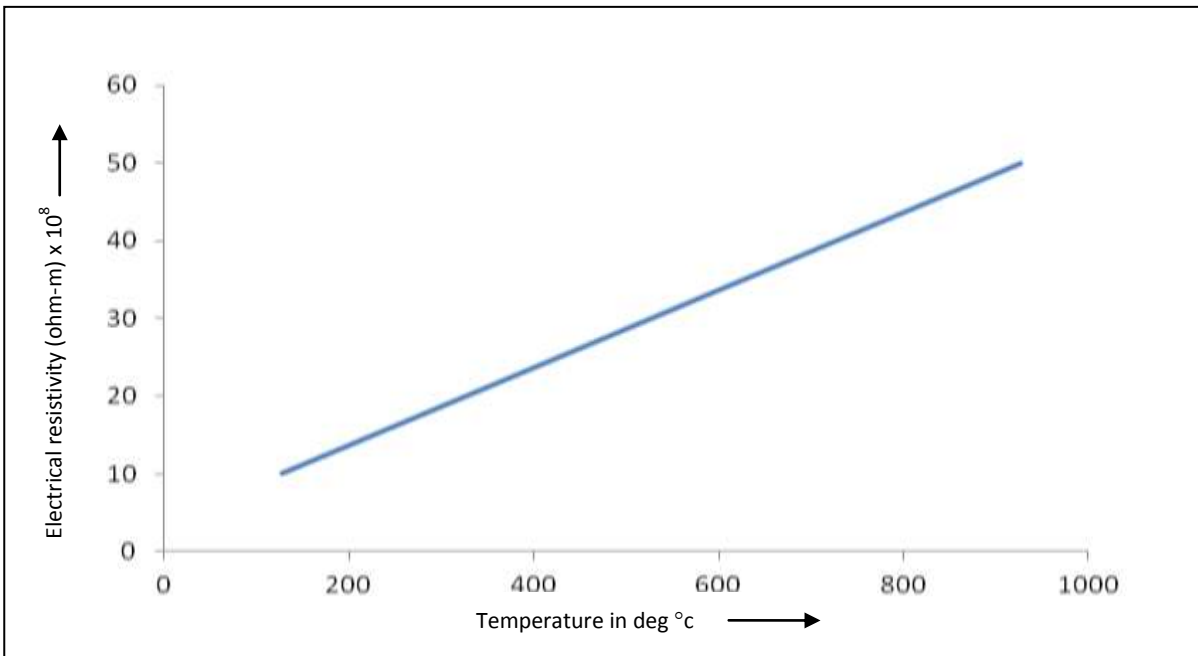
Fig. 2.7: Electrical resistivity variation with temperature for liquid sodium

Results derived from the FE modeling of the MILD were used to predict the performance of the MILD by simulating its operating conditions. The effect of primary excitation current, primary

excitation frequency, ambient temperature on the detection sensitivity of the MILD was studied.

Leak detection sensitivity, 'S' of the MILD is defined by the following equation:

$$S = \frac{V_{no} - V_{full}}{V_{no}} \times 100 \ (\%) \tag{2.18}$$

$$T_s = \frac{V_{450} - V_{100}}{V_{450}} \times 100 \ (\%) \tag{2.19}$$

where, V_{no} and V_{full} are the induced voltages in the secondary winding when the MILD is not surrounded by sodium and when the MILD is fully surrounded by sodium, respectively.

2.5   Finite element model predictions

2.5.1. Effect of primary excitation current
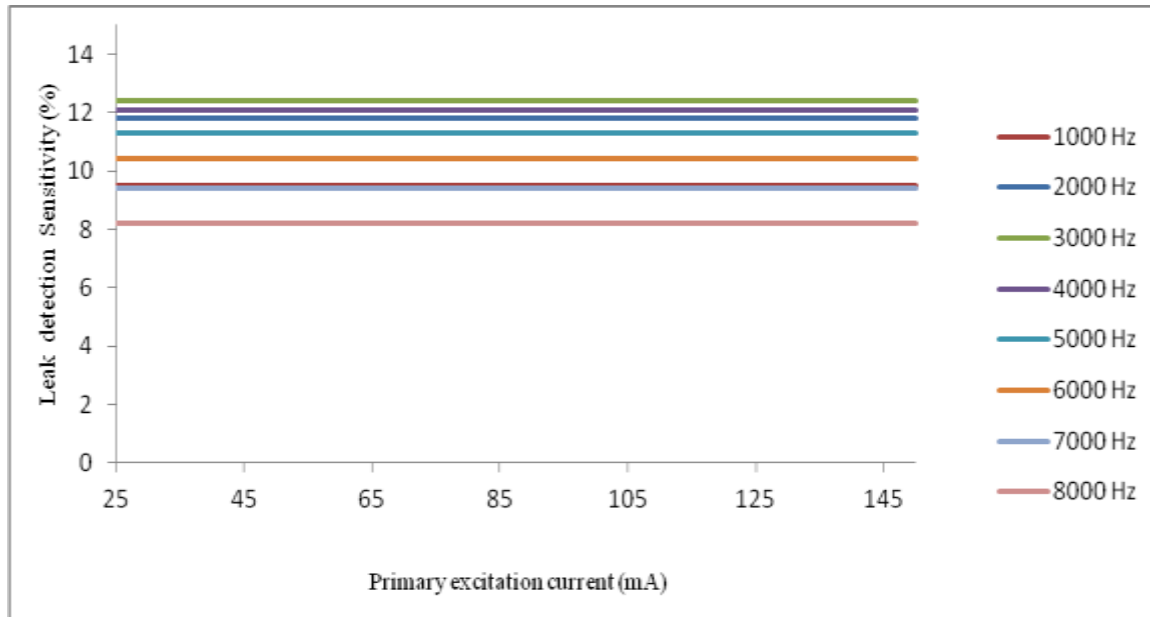
Fig. 2.8: Leak detection sensitivity vs. primary excitation current

Figure 2.8 shows the plot of leak detection sensitivity vs. primary excitation current for frequency range of $1 - 8$ kHz in steps of 1 kHz. The sensitivity of the MILD was predicted for various primary excitations currents in the range of $25 - 150$mA. It can be observed that the detection sensitivity of the MILD is unaffected by the magnitude of the excitation current.

Leak detection sensitivity of MILD is same for all excitation currents. However, a maximum of 100mA is selected based on the current rating of MI cable and power driving capability of the electronic circuits.

2.5.2. Effect of primary excitation frequency
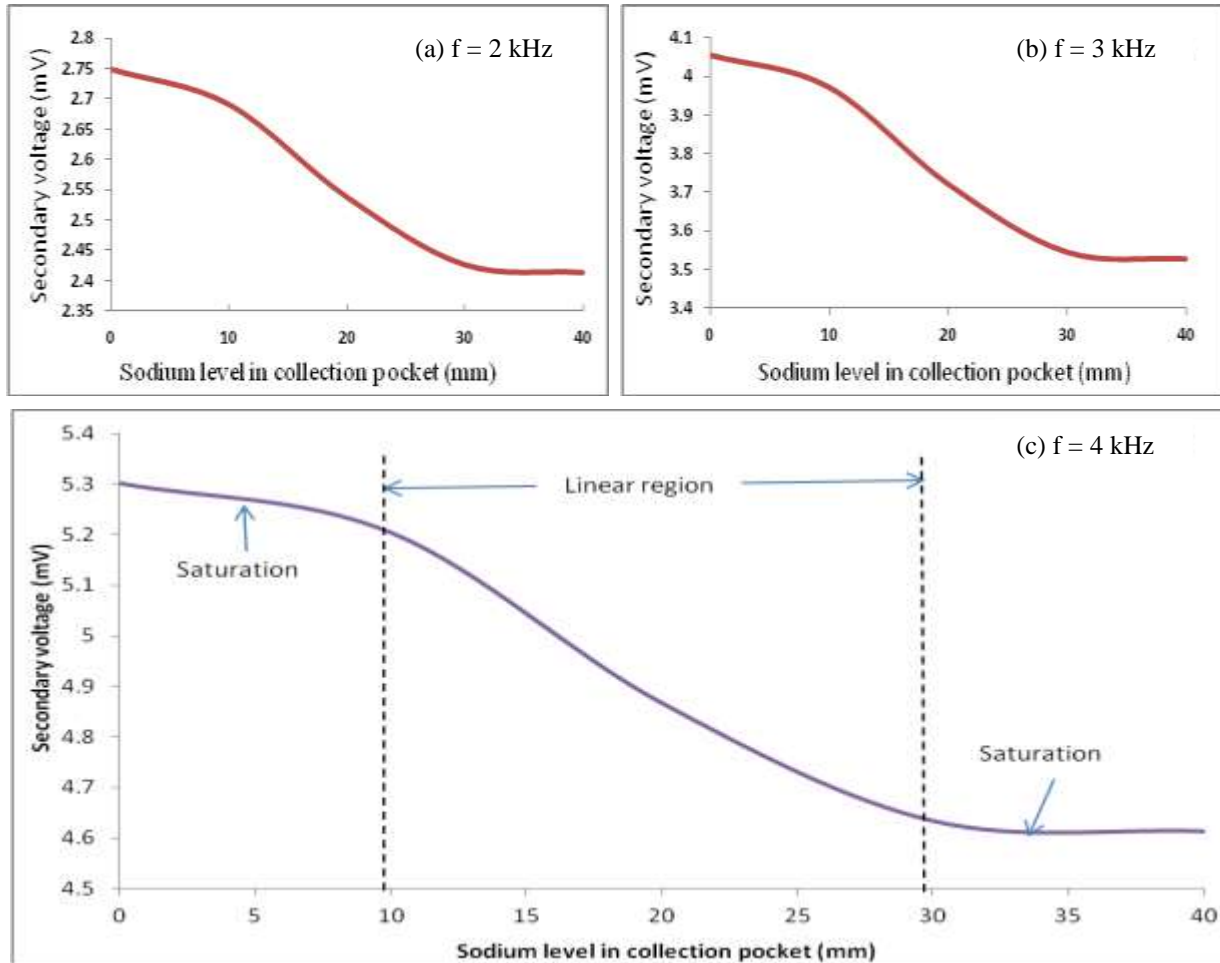
Fig. 2.9: (a) - (c) Secondary voltage vs. sodium level in the collection pocket

Figure 2.9 (a)-(c) show the magnitude of secondary voltage as a function of sodium level in the collection pocket of the MILD for the frequency range of 1k Hz – 4k Hz. At all frequencies, the curve is linear in the region of 10-30 mm, and gets saturated for sodium levels below 10 mm and above 30 mm. Though the total depth of the sodium collection pocket is 40 mm, active region of

the probe where the coil is present is from 10 mm – 30 mm only. Hence, the secondary output varies linearly in the active region and gets saturated in the end regions of the MILD. The linear increase of secondary voltage in the active region is caused by the increase in eddy currents generated in the sodium, that in turn is a result of increase in conducting volume (sodium) around the probe.
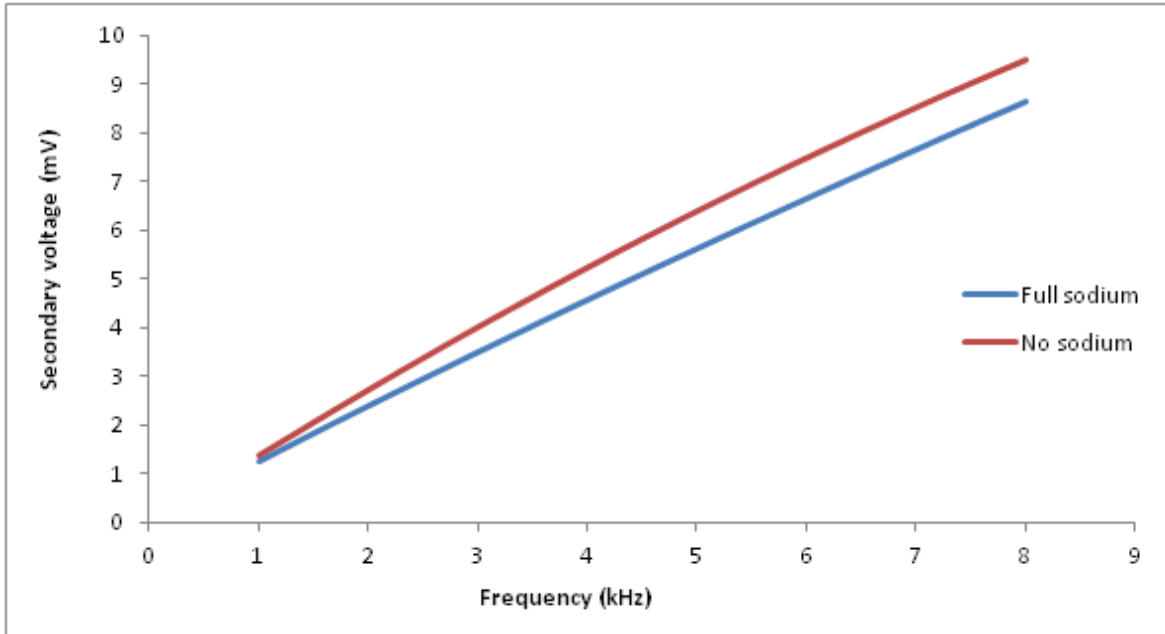
Fig. 2.10: Plot of voltage induced in secondary winding as a function of frequency

Figure 2.10 shows the secondary output vs. frequency plot of the MILD with and without sodium surrounding the probe. It can be observed that, independent of the sodium level in collection pocket, the voltage induced in the secondary winding increases with increase in frequency. Based on the Faraday's law, the induced e.m.f in secondary winding can be expressed as a function of frequency as

$$E = -2\pi \, n \, \varphi_m f \, \cos \, (2\pi f t) \tag{2.20}$$

where n is number of turns in the secondary winding, φ_m is the peak value of alternating magnetic flux generated by the primary winding and f is the primary excitation frequency.

Thus, induced voltage in secondary winding is a linear function of frequency as observed in Fig. 2.10. This induced voltage is not only dependent on the excitation frequency, but it also depends on the eddy currents generated in sodium surrounding the MILD. Power loss due to eddy currents is defined by,

$$P = \frac{\pi^2 B_m^2 d^2 f^2}{6k\rho D} \tag{2.21}$$

where, P is the power loss per unit mass, B_m is the peak magnetic field, d is the thickness of material, f is the frequency, k is an arbitrary constant, ρ is the resistivity of the material and D is the density of the material. Thus increase in frequency leads to non-linear increase in power loss that in turn, leads to decrease of the secondary voltage. Thus, for MILD fully immersed in sodium, its secondary output is a combined effect of two components, namely i) mutual induction and ii) eddy currents. Therefore, with increase in frequency, these two components counteract each other, leading to slow rate of increase of secondary voltage with frequency as shown in Fig. 2.10 whereas, in the case of MILD with empty pocket, its secondary output depends only on one component, i.e., mutual induction, leading to fast rate of increase of secondary voltage with frequency.

This difference in behavior of MILD with and without sodium has an effect on the MILD detection sensitivity as a function of frequency as shown in Fig. 2.11. It can be observed that the sensitivity of the probe is not same for all frequencies and is maximum at a frequency of 2.5 kHz.
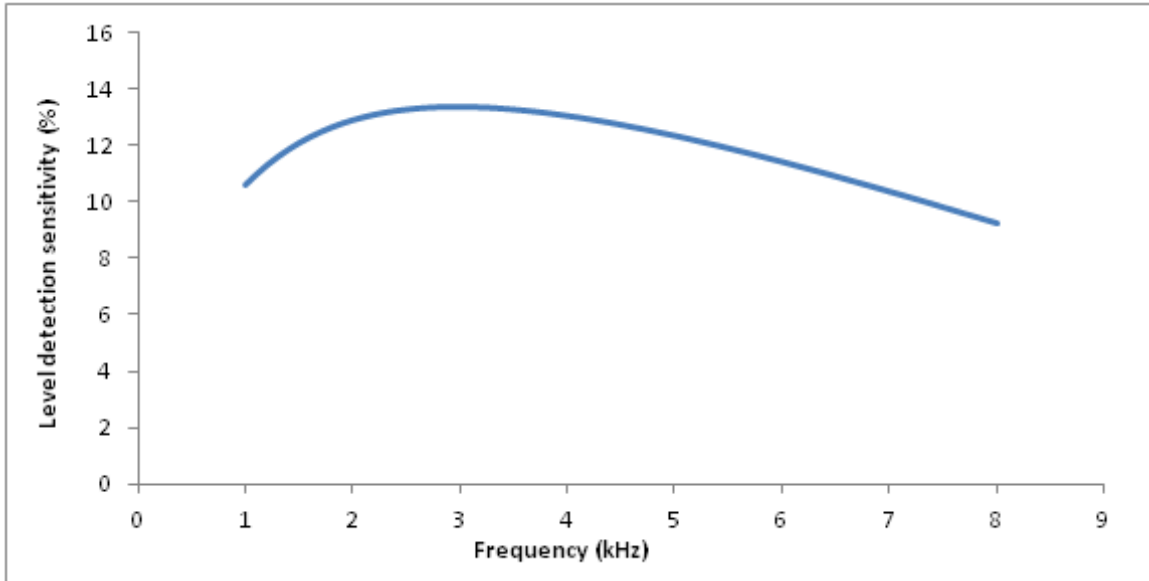
Fig. 2.11: Level detection sensitivity vs. frequency plot

2.5.3. Effect of ambient temperature

Figures 2.12 and 2.13 show the thermal characteristics i.e. plot of induced voltage in secondary winding for ambient temperatures varying from 100 to 450°C at 2 kHz and 8 kHz. This temperature range was chosen taking into consideration the operating temperature of sodium in the region where MILD is to be placed. It can be observed that there is not much change with temperature without sodium. However, the temperature effect is predominant with full sodium. As temperature increases, the electrical resistivity of sodium surrounding the probe increases, leading to reduction in eddy currents generated in sodium, that in turn leads to reduction in mutual inductance of the probe, which is seen as an increase in the secondary voltage. Thus, induced voltage in the secondary winding increases with increase in temperature.
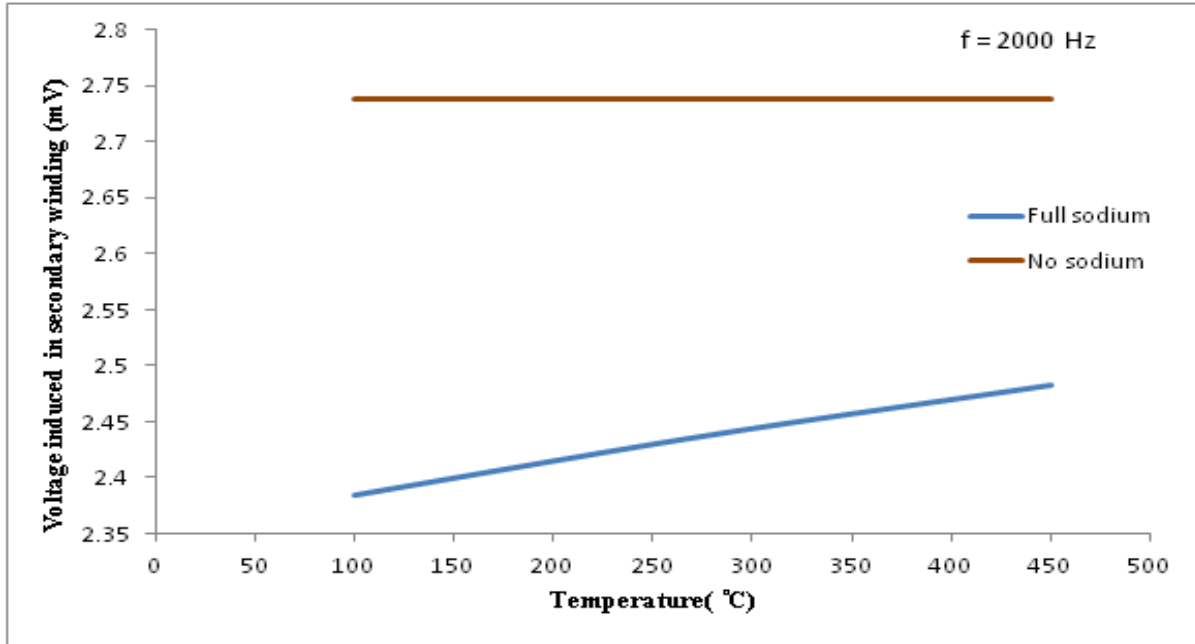
Fig. 2.12: Thermal characteristics at 2 kHz
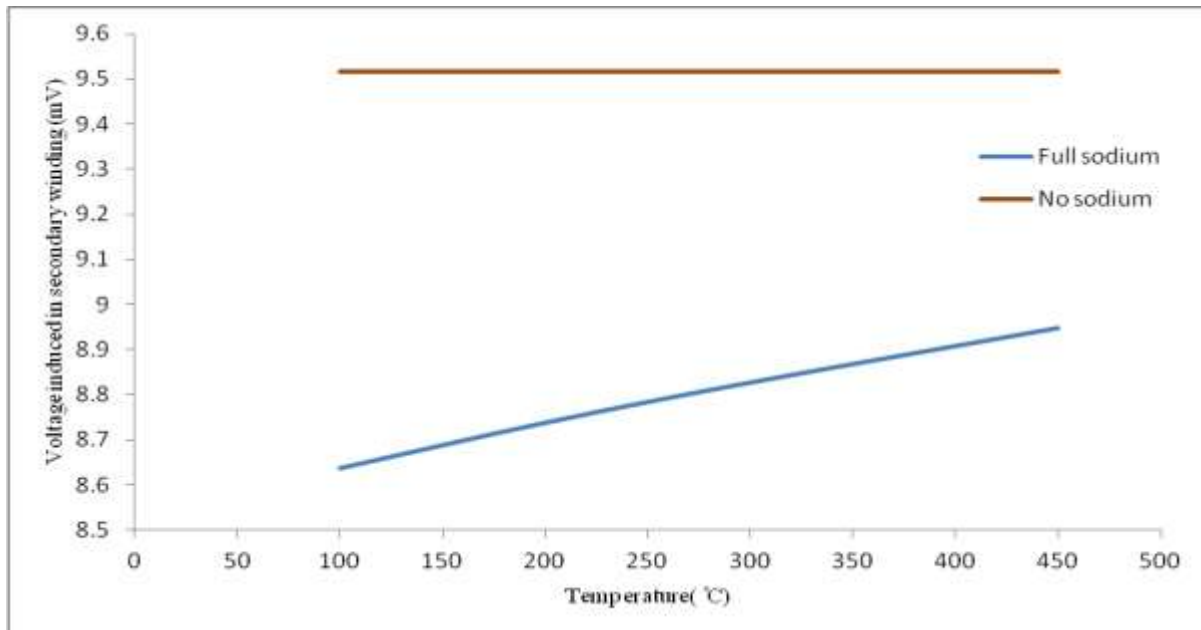
Fig. 2.13: Thermal characteristics at 8 kHz

Effect of temperature on performance of the probe is measured in terms of a parameter-temperature sensitivity defined as follows:

$$T_s = \frac{V_{450} - V_{100}}{V_{450}} \times 100 \ (\%) \tag{2.22}$$

50

T_s is temperature sensitivity of the MILD, V_{100} and V_{450} are voltage induced in the secondary winding of the MILD at 100 and 450°C respectively.

The plot of temperature sensitivity vs. frequency of the MILD fully surrounded by sodium is shown in Fig. 2.14. It can be observed that the curve peaks at around 2.1 kHz and dips at 6.7 kHz. Hence, the influence of temperature on performance of the MILD is dominant at 2.1 kHz and low at 6.7 kHz.
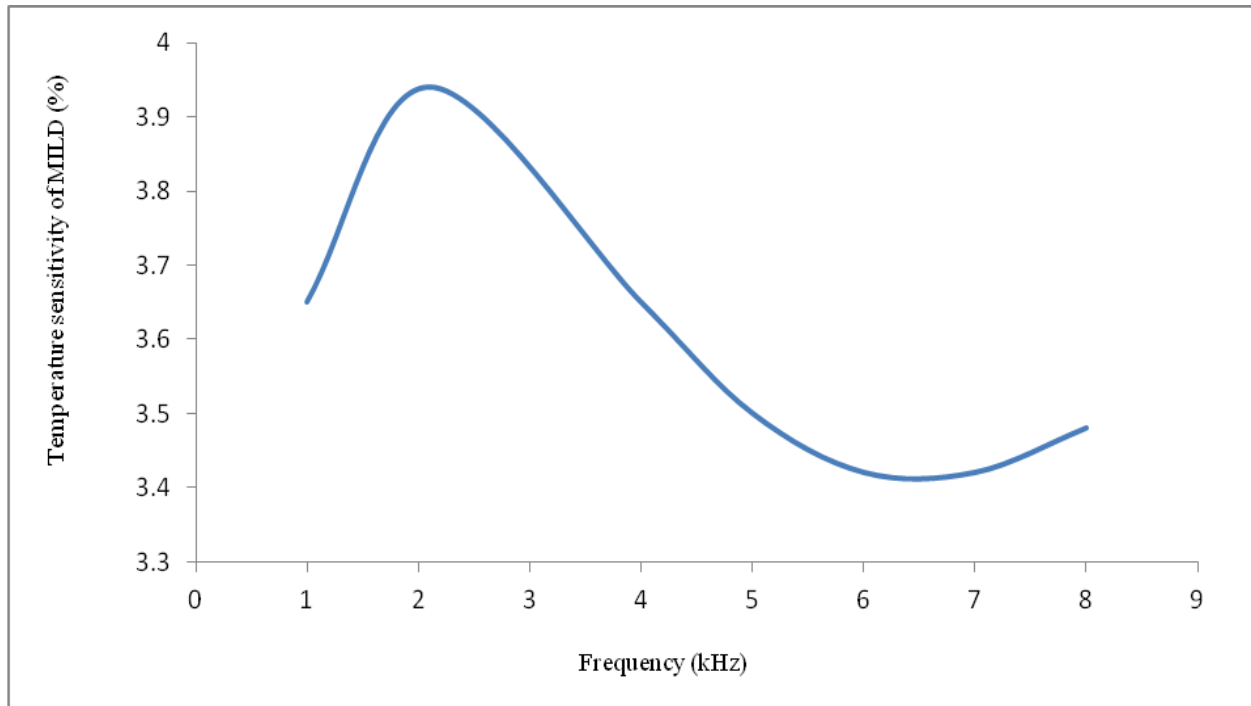
Fig. 2.14: Temperature sensitivity vs. frequency plot

2.5.4. Optimization of MILD

Optimization of the MILD is achieved by identifying and operating the probe at appropriate values for the coil parameters viz. excitation current, frequency and set point. This ensures high sensitive operation of MILD independent of the effect of temperature. Leak detection sensitivity of the MILD is unaffected by the magnitude of excitation current as shown in Fig. 2.8. By taking

into consideration, the current carrying capacity of the MI cable used for primary coil, the excitation current is chosen as 100 mA.

Performance of MILD is dependent on its primary excitation frequency. As observed in Fig. 2.11, the leak detection sensitivity is a non-linear function of frequency and peaks at 2.5 kHz. Hence, leak detection performance of the probe will be better, when operated at this peak frequency. However at this frequency, the MILD is more prone to temperature effects as shown in Fig. 2.14. Hence, it is essential to find the optimal frequency of MILD, where the leak detection sensitivity is unaffected by temperature effect. Towards this, leak detection sensitivity characteristics of the probe at 100°C and 450°C are studied as depicted in Fig. 2.16. It can be observed that at frequency other than 2.9 kHz, leak detection sensitivity of the probe is different for different temperatures. But at 2.9 kHz, the leak detection sensitivity of MILD is same for both temperatures. When operated at this frequency, though the secondary voltage is influenced by temperature, the leak detection sensitivity is unaffected by it. Thus, temperature dependence of MILD can be reduced by operating the probe at 2.9 kHz.
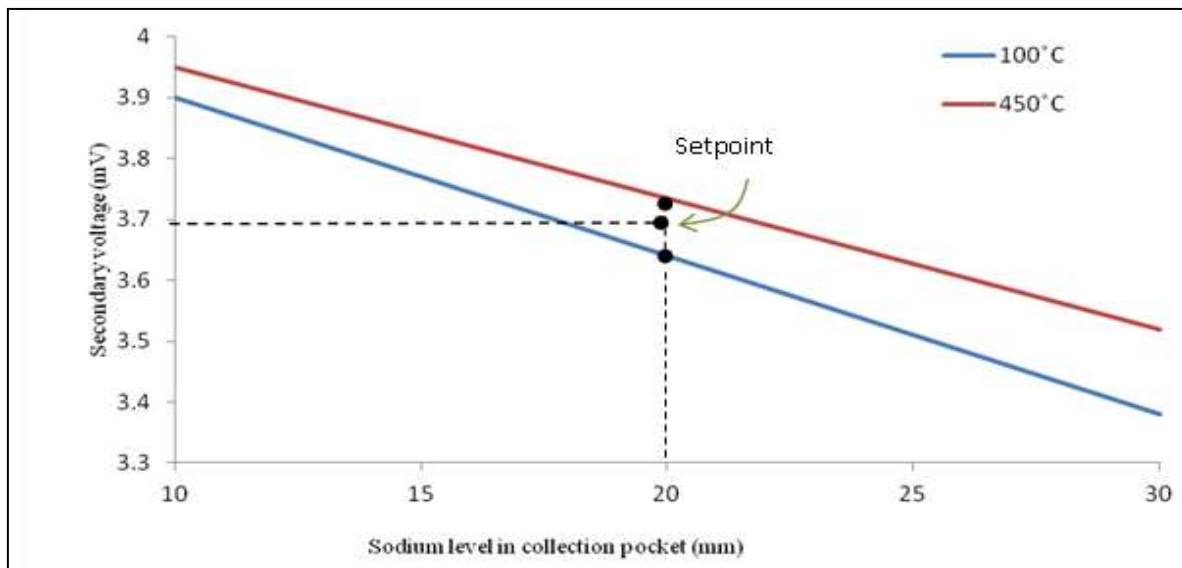
Fig. 2.15: Linear region of secondary voltage vs. sodium level plot at 2.9 kHz

Plot of voltage induced in secondary winding vs. sodium level in collection pocket of MILD excited with AC primary current of magnitude 100 mA and frequency 2.9 kHz is shown in Fig. 2.15. Variation in secondary voltage due to temperature is approx. 94.75 µV only. MILD along with its electronics should generate a leak signal / indication, when the sodium level in collection pocket goes above 20 mm. i.e., when the voltage induced in the secondary winding goes below 3.65 mV at 100°C or when it goes below 3.75 mV at 450°C as shown in Fig 2.15. Since the voltage set point for generating the leak signal is different for different temperatures, an average of the above mentioned values i.e., 3.7 mV is used as set point for generating leak signal. By this means, the set point and hence the leak detection is unaffected by temperature.

The sensitivity optimization of the detector at 100°C and 450°C is typically shown in Fig. 2.16. The physical dimensions of the optimized probe are given in Table 2.4 and photo is given in Fig.2.17.
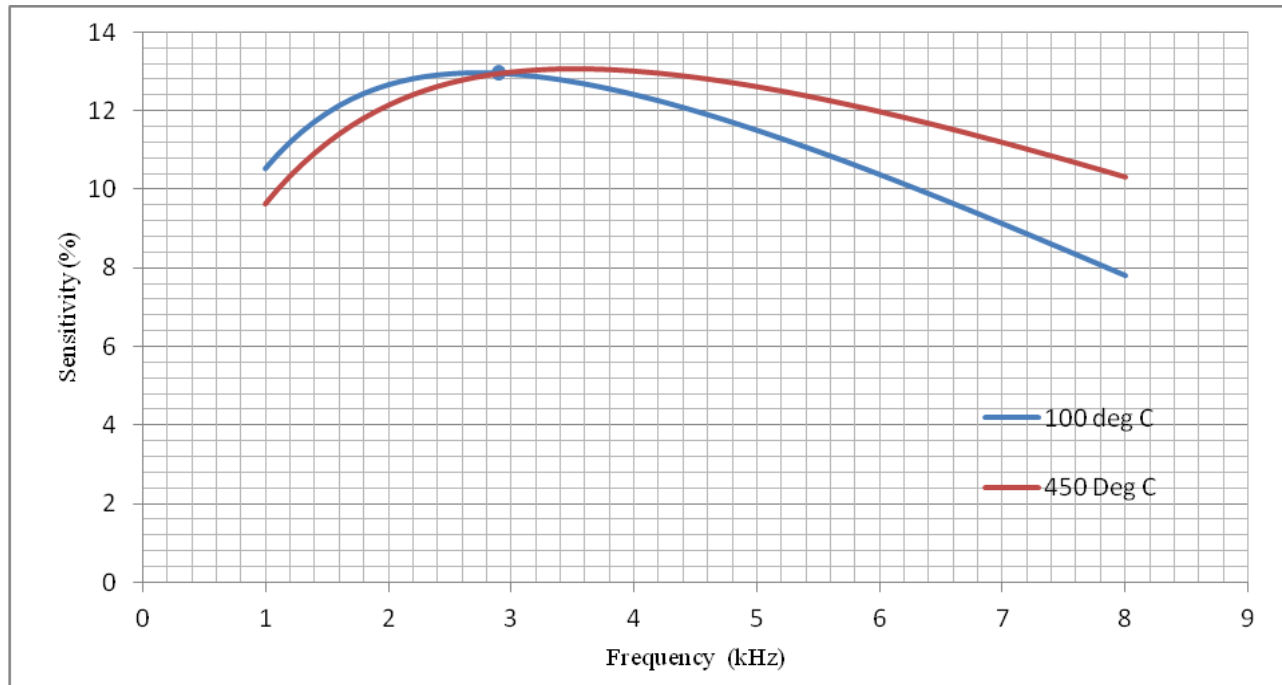
Fig. 2.16: Sensitivity vs. frequency characteristics of MILD

Table 2.4: Physical dimensions of the probe

No. of turns of primary/ secondary winding	22/ 44
Distance between winding	Tightly wound
Winding	1mm dia MI cable with 0.3mm Cu conductor
Sheath	SS 316L with MgO insulation
Height of bobbin	22 mm

2.5.5 Detector sensor cable properties

The insulating material of the cable is of electrical grade high purity magnesium oxide with 96% of MgO content. Impurity content in the insulation are kept within the limits as given in Table 2.5.

Table 2.5: Limits of impurity content

Boron plus cadmium	30 ppm
Sulphur	50 ppm
Carbon	300 ppm

The density of packing of the insulating material is high enough to give the required insulation resistance (IR) less than 10000 MΩ at room temperature. The metallic sheath over the magnesium oxide insulation is of seamless stainless steel tube. The sheath is of uniformly thick and hard and is to be free from any defects. The cable is annealed after manufacture to get required flexibility and chemically cleaned to get surface brightness.

2.6   Model validation

To validate the model predictions experiments were carried out. As in-sodium experiments are complicated and time consuming, room temperature experiments were carried out in lab with an aluminum block simulating the effect of sodium. Aluminum was chosen owing to its electrically conductive nature similar to that of sodium. In the FE model also, sodium was replaced by aluminum and the detector performance was predicted. For conducting experiments, a prototype

MILD based on datasheet given in Section 2.4.1 was developed. An electronics unit was also developed to energize the MILD, process the MILD signal and to display leak status in the form of alarms or indications. This section discusses the details of the electronics developed for MILD and the results of validation experiment.

Fig. 2.17: Photo of the developed MILD probe

2.6.1 Development of electronics unit

The schematic of MILD electronics unit is shown in Fig. 2.18. This comprises of two independent modules, namely – exciter module and receiver module.
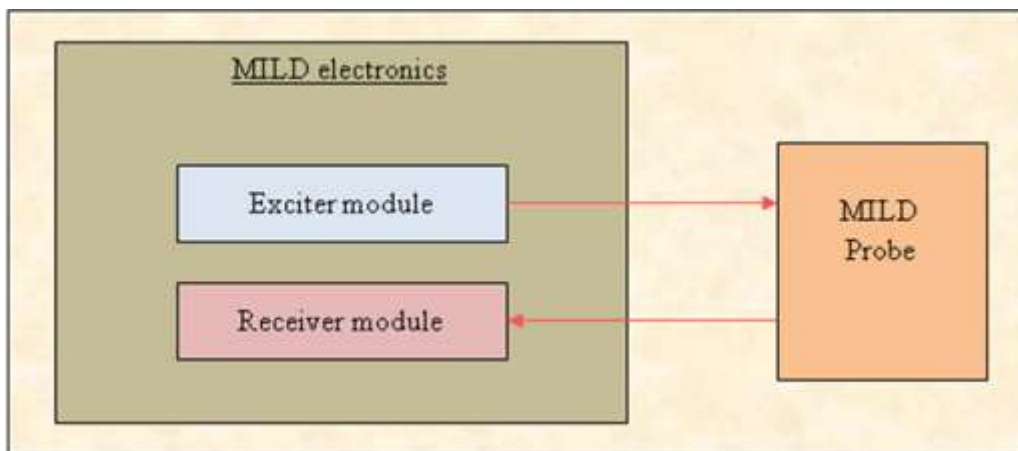
Fig. 2.18: Block diagram of the electronics unit for the developed MILD

The function of exciter module is to generate the excitation current required for primary winding of the MILD. It consists of (i) an oscillator to generate a sinusoidal signal, (ii) an amplifier to amplify the low level output of oscillator, and (iii) a constant current generator to feed AC signal of constant magnitude to the MILD primary winding. Provisions are given in the exciter module to adjust the frequency and magnitude of the excitation current signal.

The function of receiver module is to read the voltage induced in the secondary winding of the MILD, and indicate the leak status in the form of alarms or LED indications. It consists of (i) an amplifier to amplify the secondary voltage, (ii) a comparator to compare the secondary voltage with set point, and (iii) an alarm unit to generate leak alarms or indications whenever the secondary voltage goes below the set point. Detailed schematic of MILD electronics is given in Fig. 2.19. The instrumentation unit is based on an industry standard microcontroller. All passive and active components are made of industrial temperature grade with 85°C. The electronics modules use multi-layer PCBs. The PCBs are rigidly mounted on a chassis to reduce the effects of vibration induced flexing.
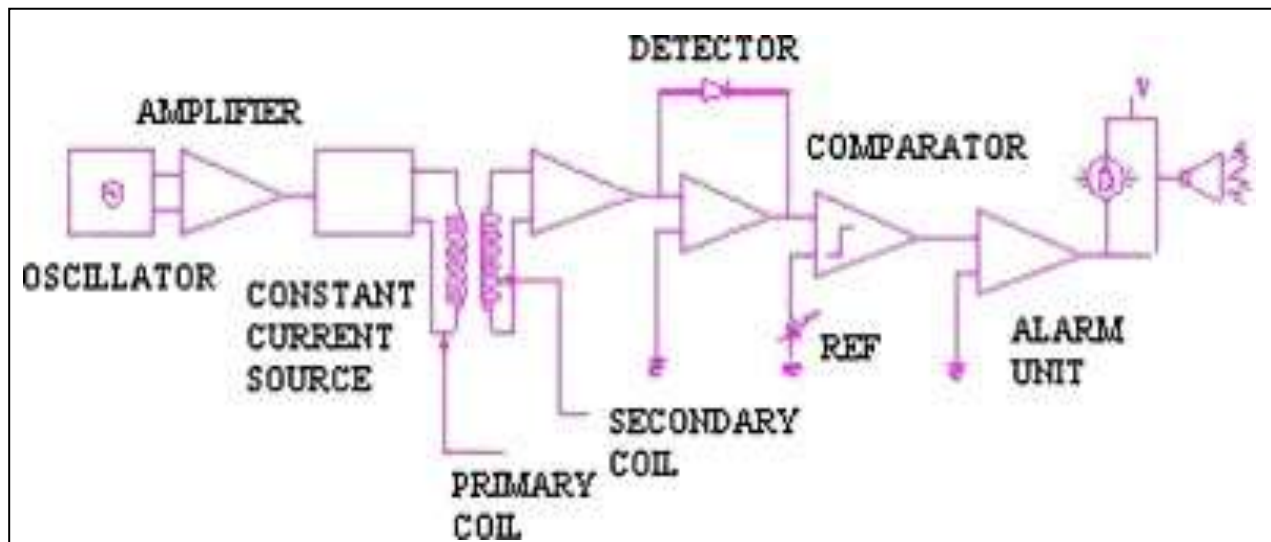
Fig. 2.19: Detailed schematic of electronics unit for the developed MILD probe

2.6.2 Test results

Room temperature experiments were carried out on MILD with an aluminium block simulating the sodium as shown in Fig. 2.20. For this purpose, an aluminium block with dimensions of the sodium collection pocket was fabricated as per Fig.2.3. Primary excitation frequency was varied from 1 kHz to 4 kHz. The secondary output of the probe with and without aluminium block were noted down. Same setup with aluminum block was modeled in FEMM. The secondary output of the probe for the above frequencies were predicted numerically. Figs.2.21 and 2.22 show the secondary output vs. frequency characteristics of the probe with and without aluminium block respectively.

Fig. 2.20: Simulated checking of the developed probe with aluminium block
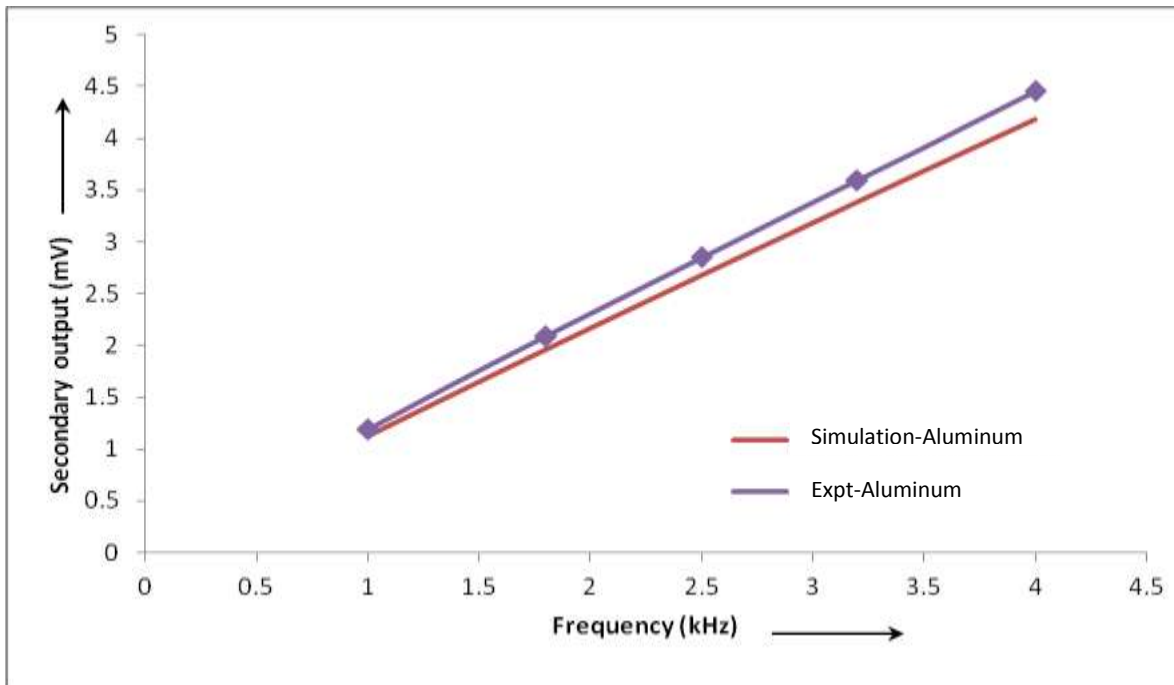
Fig. 2.21: Secondary output vs. frequency characteristics with aluminium block
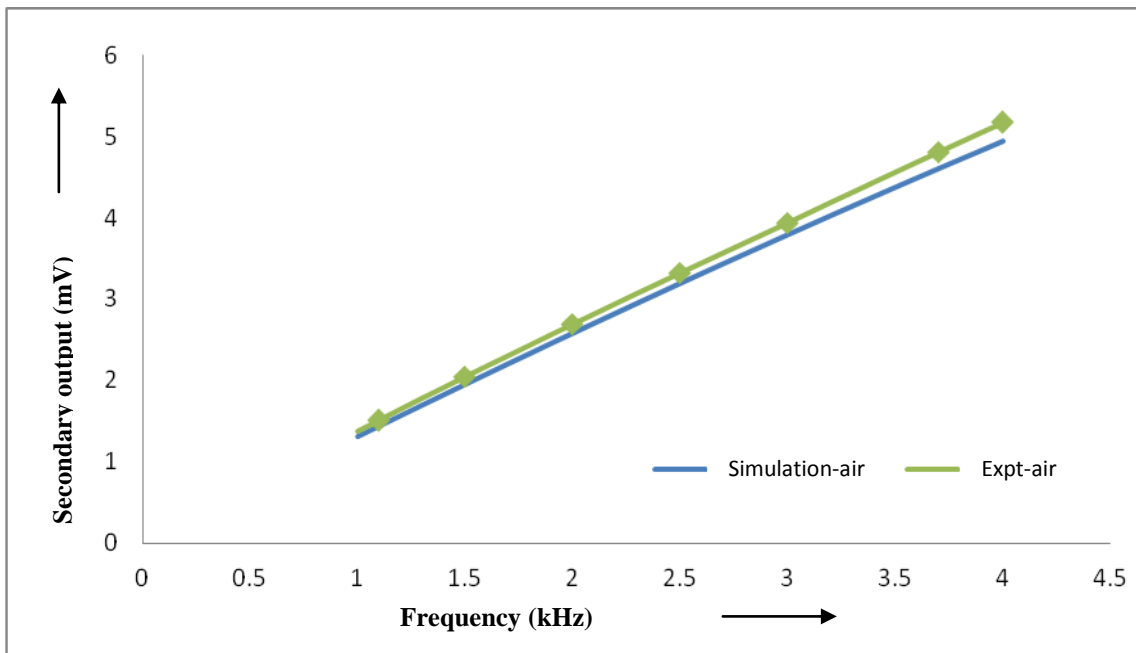
Fig. 2.22: Secondary output vs. frequency characteristics without aluminium block

The percentage relative error (e) between the FE model predictions and the experimental measurement was calculated as follows:

$$e = \frac{V_m - V_{exp}}{V_m} \times 100 \ (\%) \tag{2.23}$$

where Vm is secondary output during modeling and Vexp is secondary output during experiment. The plot of percentage relative error for various frequencies is shown in Fig. 2.23. A good agreement is seen between the model predictions and experimental measurement. The percentage relative error between the model and experimental results is found to be less than 7%. Thus, the closeness of both the experimental and analytical values has validated the model for further analysis. The small relative error between the model and experiments is attributed to be due to minor variations in coil dimensions, electrical conductivities of aluminum and stainless steel and spacing between the coil turns.
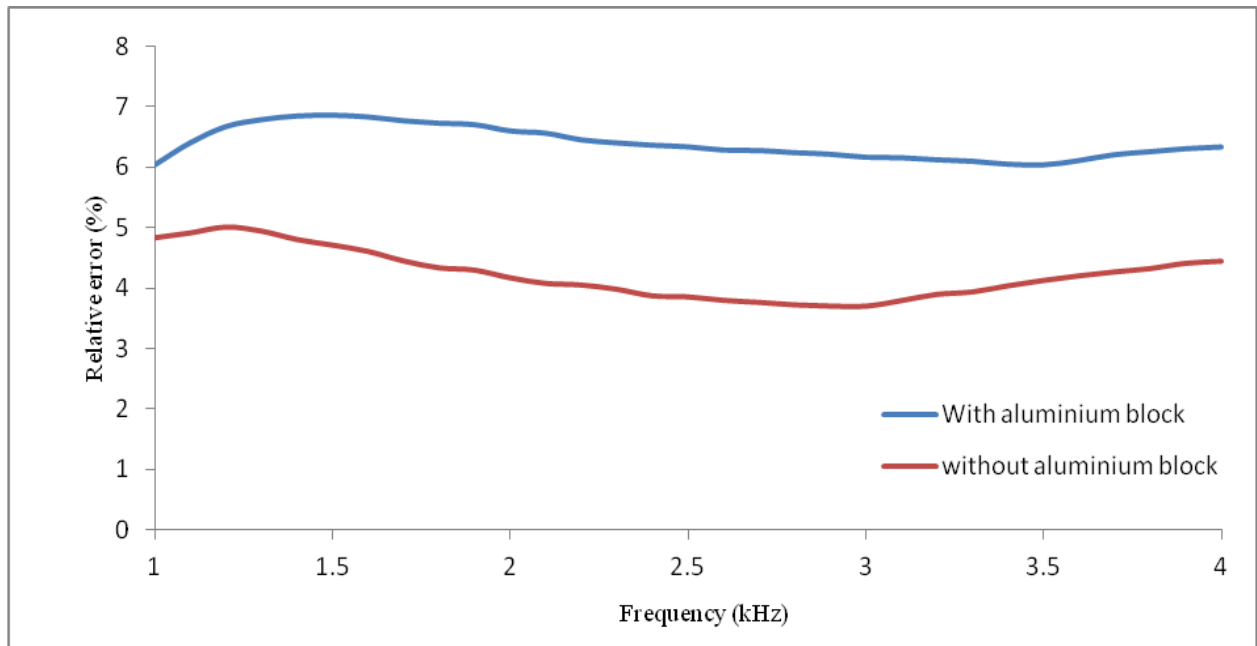
Fig. 2.23: Percentage relative error at various frequencies

The secondary output versus sodium level in the collection pot is given in Fig.2.24 and the sensitivity is found to be 1.183gm of sodium / mm as given in Appendix- 3.
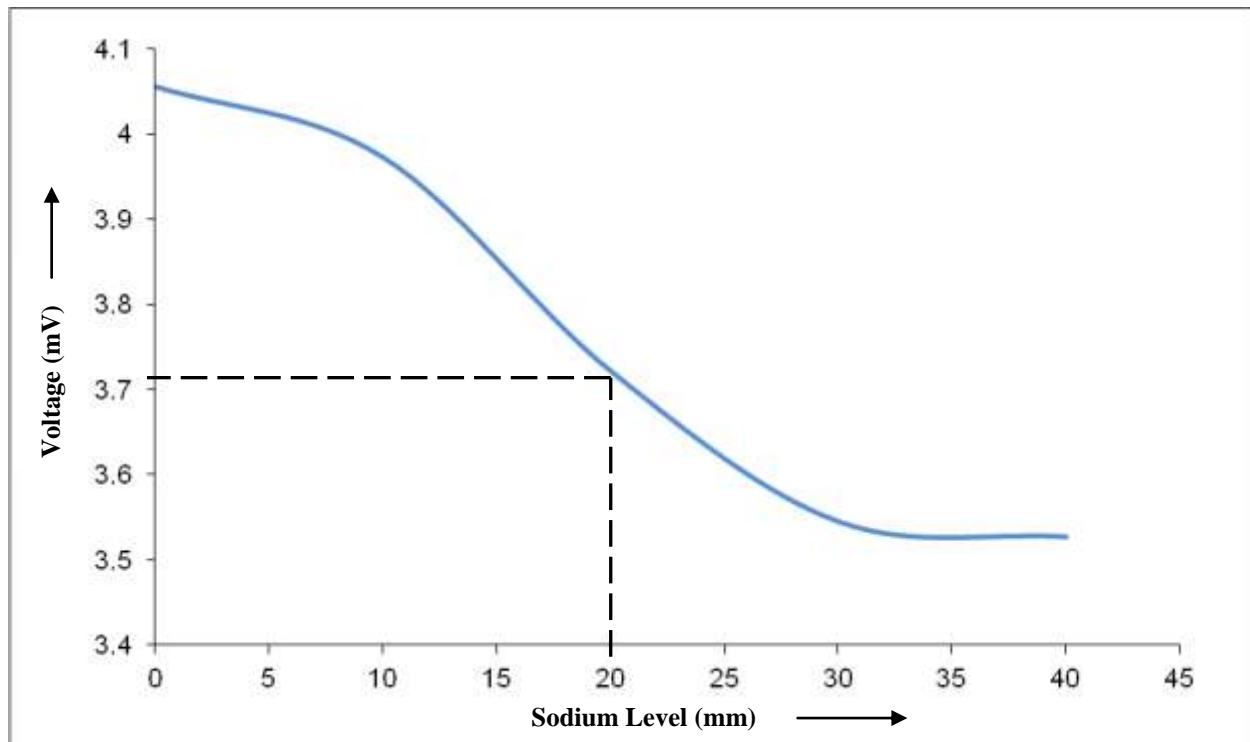
Fig. 2.24: Secondary output for different sodium levels

As given in Fig.2.24, the alarm is set conservatively at 3.7mV corresponding to 11.82gm of leaked sodium in the collection pot.

2.7 Deployment of the detector

The developed MILD was installed in the vacuum line very near to the nickel diffuser in secondary sodium west loop of FBTR and local leak indication and control room alarm annunciation was wired and commissioned. The detector with optimum frequency of 2.9 kHz and excitation current of 100 mA has been connected with the electronics unit and installed at site.

Fig.2.25, 2.26 & 2.27 show the photo and location of the MILD deployed at FBTR. The simulation tests were carried out periodically and the output from the detector was found to be steady. There were no spurious indications of the leak even when the vacuum lines were heated

for degassing purposes. After studying the performance for 6 months, two more detectors for the other two nickel diffusers in West loop were installed. Though the detector responds to 1.183g of liquid sodium as given in Annexure-1, the alarm annunciation is set conservatively for 11.83g which surely gives an early indication of the failure of nickel diffuser. In East loop also similar 3 more detectors were installed and commissioned. During simulated leak checking at site, the detector responds with a response time of less than 5 seconds.

Fig.2.25: Miniature detector for FBTR
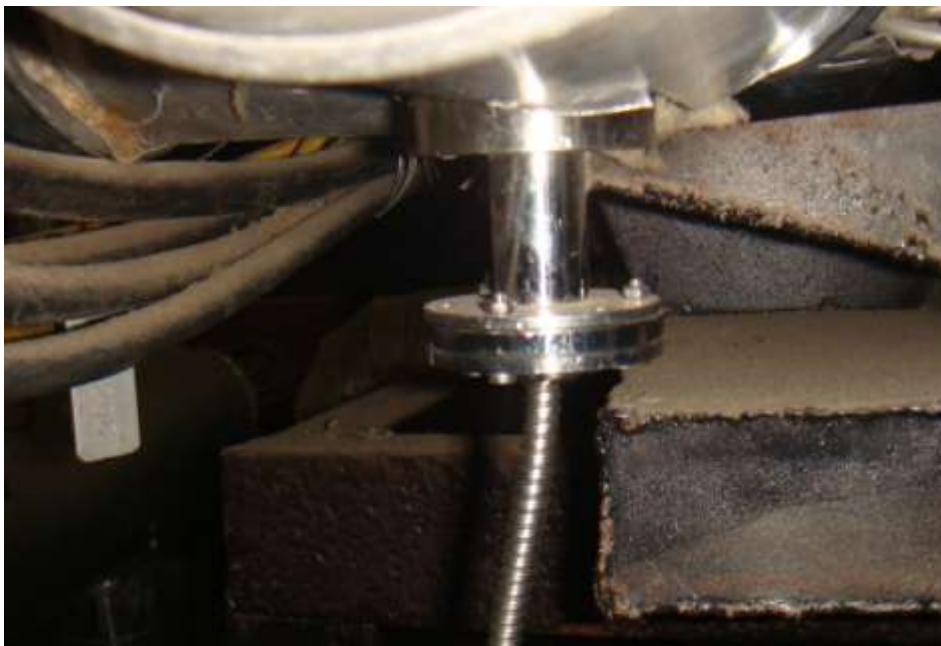
Fig.2.26: Miniature detector installed at FBTR
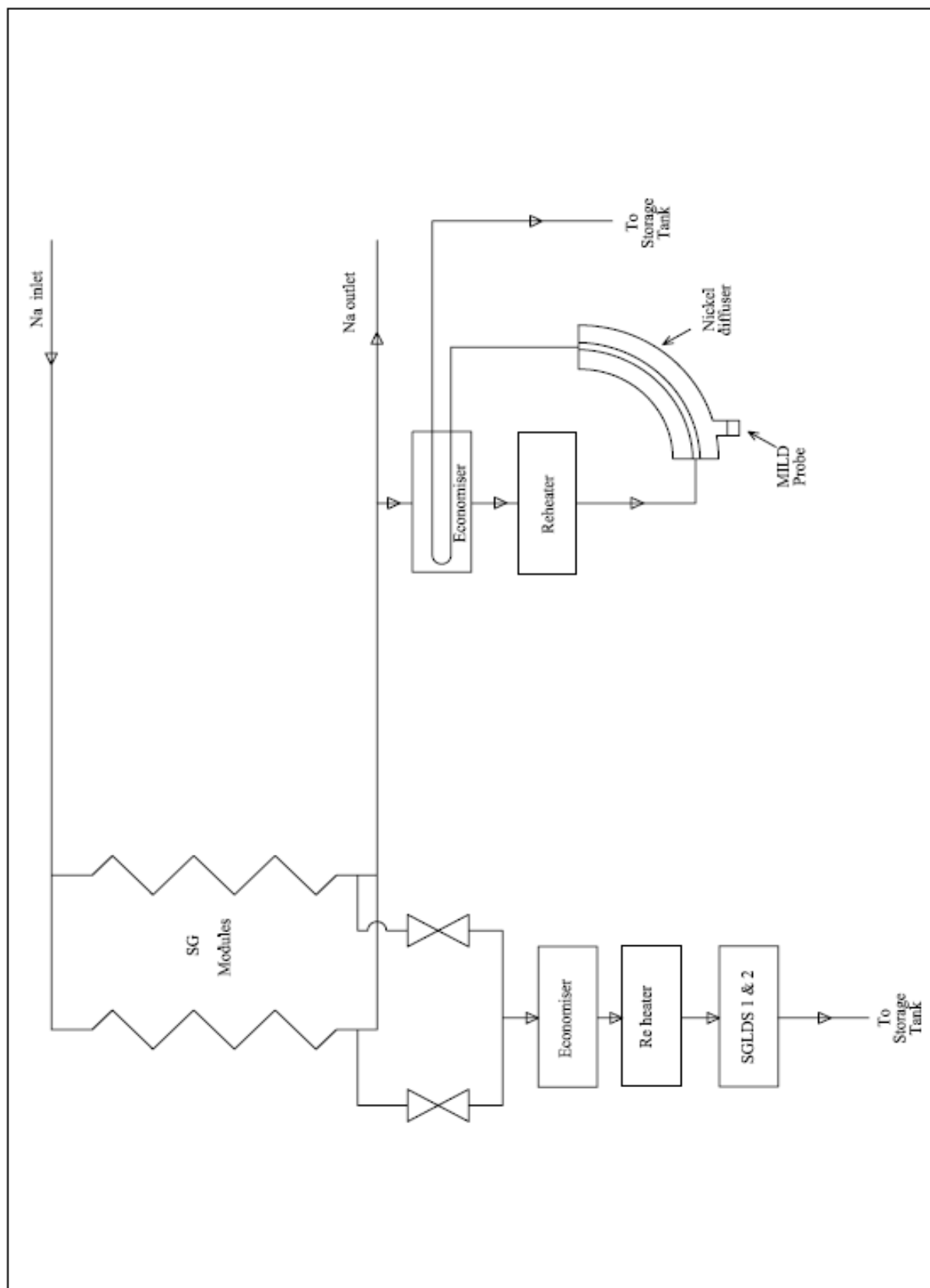
Fig.2.27: Location of developed MILD probe in SGLD system of FBTR

2.8 Summary

As conventional sodium leak detectors cannot be used for detection, a non-contact miniature mutual induction type leak detector has been developed for FBTR SG after finite element (FE) modeling and experiments. The major conclusions drawn are as follows:

- FE modeling was carried out to optimize the MILD for detecting sodium leaks independent of the effect of ambient temperature. MILD coil parameters, such as – excitation frequency, excitation current and voltage set point were optimized to be 2.9 kHz, 100 mA and 3.7 mV respectively.

- Prototype MILD and its associated electronics unit were developed and the FE model predictions were successfully validated through room temperature experiments carried out with an aluminum block simulating sodium.

- A good agreement was observed between model predictions and experimental results with a percentage relative error less than 7%.

- Detection of 1.183g of sodium leak due to the failure of nickel diffuser to the high vacuum in a diffusion based system in less than 5 seconds is possible with the developed detector. The MILD along with its electronics is deployed in SG leak detection system of FBTR to detect the failure of nickel diffuser membrane.

Chapter 3: Development of SIP Based SG leak detection system

3.1 Preamble

Determination of hydrogen concentration in sodium using sputter ion pump (SIP) or quadrupole mass spectrometer (QMS) is a widely accepted technique. However, in the QMS based system, availability is affected due to the random failure of QMS analyzer filament and its replacement necessitates calibration of the system. Hence, SIP system is preferred over a QMS based system. This chapter discusses the process of development of a SIP based system for the detection of small leaks in FBTR steam generators. The development stages involve modification of the SIP electronic circuit, evaluation and qualification of the output by conducting experiments and formulating safety actions.

3.2. Safety actions on SG leak

No sooner a leak is detected and confirmed in FBTR steam generator; safety action is initiated on the sodium and water/steam systems of the affected module. In order to maintain the consequence of a small leak in SG and the damage to the secondary sodium system, the reactor is shutdown and the affected loop is isolated on water/steam and sodium side by fast closing hydraulic isolation valves.

The nominal hydrogen concentration present in sodium as background is mainly attributed to the sources from Hydrogen injected during calibration tests, aqueous corrosion of the SG tubes and thermal decomposition of hydrazine added in steam water system.

The reactor is shutdown when any of the following occurs [43]:

1. Hydrogen concentration in SG outlet sodium high – 2 times the background signal

2. Rate of rise of hydrogen concentration in SG sodium > 25 ppb/ min.

3. Expansion tank cover gas pressure high > 0.5 kg/ cm^2 (due to the ingress of hydrogen in argon space above sodium)

4. Rupture of rupture disc (due to pressure build up in the system following large leak) which is detected by spark plug type leak detectors at the outlet

5. Actuation of SG safe configuration.

The first two inputs are generated by the SG leak detection (SGLD) system. These are automatically inhibited when SG is drained on water side to facilitate the following:

- SG leak detection system calibration by injection of hydrogen in sodium

- Calibration of quadrupole mass spectrometer by temperature cycling of nickel diffuser

- Replacement of QMS filament and SIP in vacuum system

Inhibition will be lifted automatically when any one of the SG on water or steam side is isolated. Due to small leaks developing into larger leaks, SGLD system orders reactor shutdown at 2 times the background or high rate of rise of hydrogen concentration in sodium. The other safety actions from expansion tank cover gas pressure and rupture of rupture discs detected by pressure switch and spark plug type leak detectors respectively are also available for safety action. The manual shutdown of the reactor can be adopted depending on the leak magnitude.

3.3. SGLD system

The SGLD system of FBTR consists of a sampling system which draws sample sodium from the outlet of SG which passes through a nickel diffuser as given in Fig.3.1. An ultra high vacuum (UHV) environment surrounding the nickel tube is provided by a vacuum system made of stainless steel type 304. The vacuum system has a volume of 1550 cm^3 and is fitted with a sorption pump for fore pumping and a sputter ion pump. This combination offers a dynamic pressure in the range of 10^{-12} to 10^{-8} kg/cm^2 of which 10^{-13} to 10^{-9} kg/cm^2 is contributed by the H$_2$

partial pressure. During steady state operation, the quantity of hydrogen diffusing from sodium through the nickel diffuser into the vacuum side is equal to that removed by the sputter ion pump, thus establishing equilibrium H_2 partial pressure which is proportional to the hydrogen concentration in sodium. A QMS installed in the UHV tuned for H_2^+, monitors the H_2 partial pressure in the dynamic vacuum system.
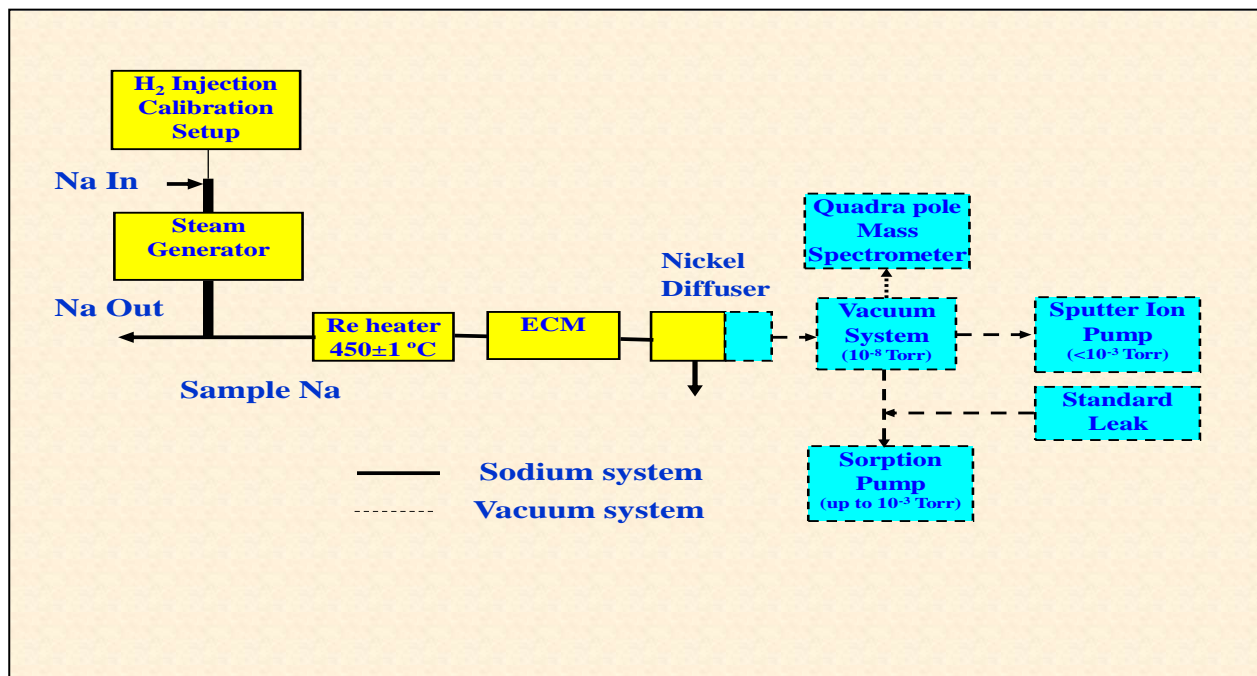
Fig. 3.1: Block diagram of SGLD system

The increase in the dynamic hydrogen partial pressure in UHV is interpreted as a leak. A computer system which monitors the QMS output and compares the processed signal against set thresholds and initiates safety action when they are crossed [44].

The detection of any water / steam leak into sodium is carried out by measuring the hydrogen concentration in sodium in ppb levels. Reaching the required vacuum and maintaining it is a challenge. Leaky spots were identified, leaks arrested and modifications were carried out to attain required vacuum in about 10 minutes, during commissioning of the SGLD system in FBTR.

3.3.1 Temperature control circuits

The reheaters provided to maintain the temperature of sodium at the inlet of the nickel diffuser at $450 \pm 1°C$ consisted of 50 mm pipe over which six MgO_2 insulated SS sheathed surface heaters had been mounted. Failure of heater elements (three on west & two on east loop) were noticed during the course of testing. To investigate the cause, thermocouples were installed on the sheath of the heaters and temperatures at different points were noted. In the proximity of pipe hangers, the heater could not be laid adequately close to the pipe line resulting in local hot spots. The sheath temperatures at these locations were found to be more than recommended value of $600°C$. Reheater was redesigned using immersion type of heater elements, fabricated and installed as shown in Fig.3.2.
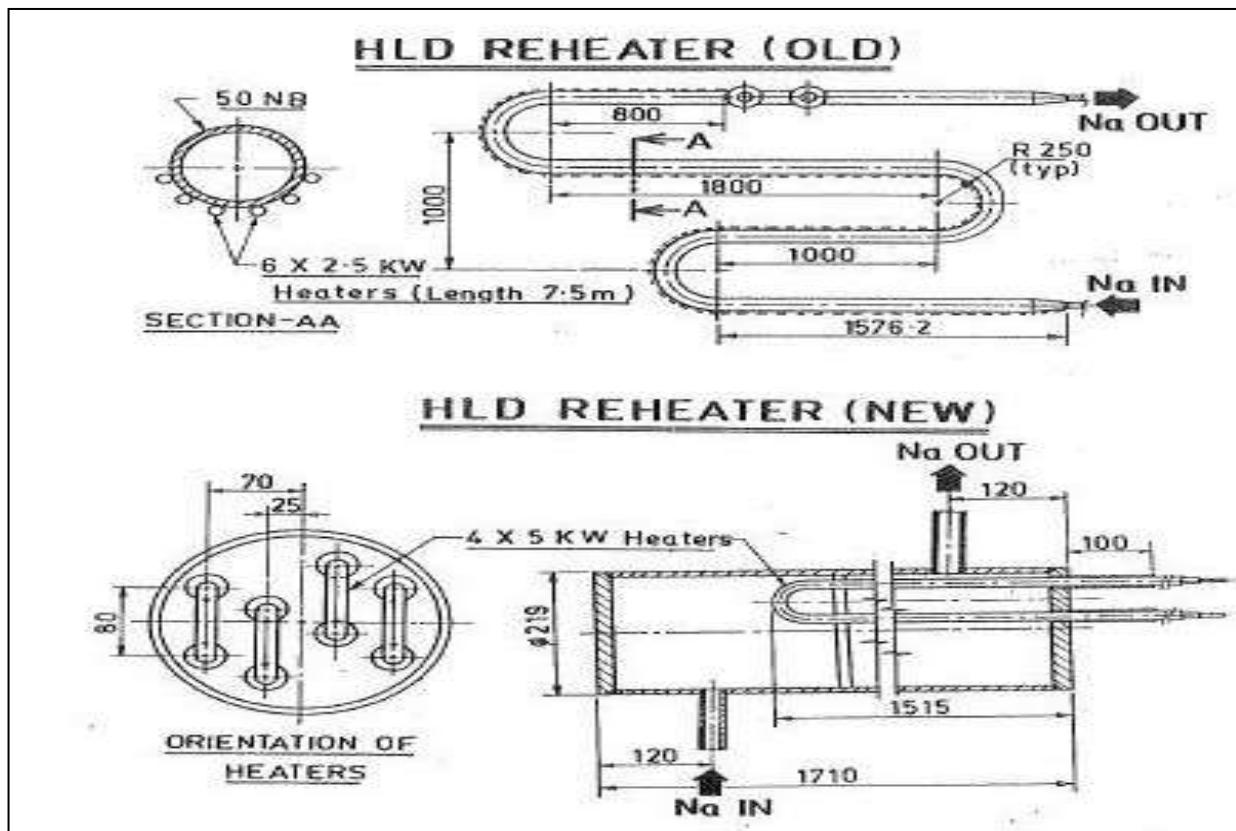
Fig .3.2: SGLDS reheater modification [2]

The reheater consists of a cylindrical vessel of 21.9 cm diameter and 171.0 cm long mounted horizontally. There are four immersion type heating elements of 5 kW capacities each. Three elements are connected in 3- phase delta and the fourth one is installed as in-situ spare. The sample sodium from SG outlet enters the heater vessel at the bottom and comes out at the top. In order to maintain the outlet sodium temperature of reheater within the design limits and to have a precise temperature control of $450 \pm 1^{o}C$ at the nickel diffuser membrane, a microprocessor based PID controller is utilized. This temperature controller receives feedback signal from chromel- alumel type thermocouple installed in the sodium outlet of the reheater. On comparing this signal with the set point of $450^{o}C$, depending on the error, the controller outputs the correction signal as per the PID algorithm to SCR which modifies the power through the heater elements. The control schematic is given in Fig.3.3.
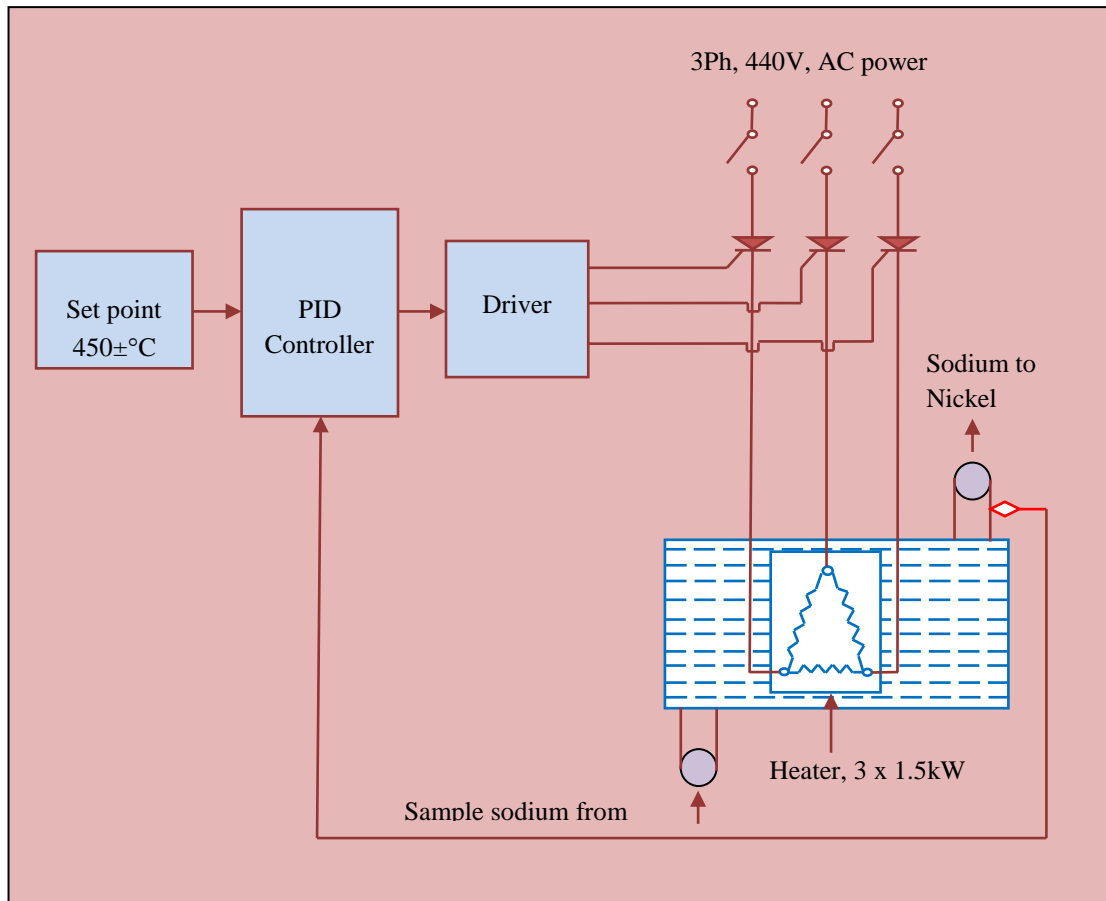
Fig.3.3: Nickel diffuser temperature control schematic

3.3.2   Valving in of water in SG

The SGLDS was put in service after establishing sodium flow through the SG modules and ensuring sufficient flow through the SGLDS sampling lines (> 1 m^3/h). To study the response of the system, hydrogen injection was carried out at various temperatures of 180, 250, 300 & 400°C in the sodium system and the Quadrupole mass spectrometer signals showing the partial pressure of hydrogen at these temperatures were recorded. The detector started responding after three minutes of injection which is the transit time from injection point to the detector. The sodium temperature upto 180°C was significantly affecting the detection capability. The response of the system was very poor at a sodium temperature of 180°C (20%) indicating that most of the injected gas remained undissolved in sodium and got released into the cover gas space. At 250°C, the response was very good (> 60%). This was useful to evolve a procedure to admit water into SG only at sodium temperature > 250°C. However, to admit water at 180°C, development of Hydrogen in Argon Detector (HAD) to detect hydrogen in cover gas is necessary.

3.4.   Nickel diffuser membrane

The assembly shown in Fig.3.4 is bent by 90° in order to accommodate the expansion between the nickel tubes and the SS shell. The nickel diffuser is made of nickel membrane in the form of tubes. Though the permeability of Hydrogen in palladium, platinum and copper is higher when compared to iron and nickel, in view of their poor compatibility with sodium, these materials are not considered. Amongst the other two, nickel is chosen due to its workability and oxidation resistance. The nickel membrane diffuser consists of 4 tubes of 0.3 mm wall thickness and OD of 7.2 mm made of 99.84% pure nickel with a surface area of 275 cm^2 placed in a stainless steel shell of 42.6 mm OD and 35.9 mm ID.

The temperature of the nickel tube is maintained 450 $\pm$1 $^{\circ}$C by a PID controller by controlling the temperature of sample sodium in the re-heater to avoid any variation in the diffusion rate of H_2 into the vacuum chamber on account of its temperature variations.

However, any variation in the membrane temperature would affect the hydrogen diffusion rate; but diffusion time constant being large the small temperature fluctuation ($\approx$1°C) gets averaged out and the effective temperature variation turns out to be much smaller [45].
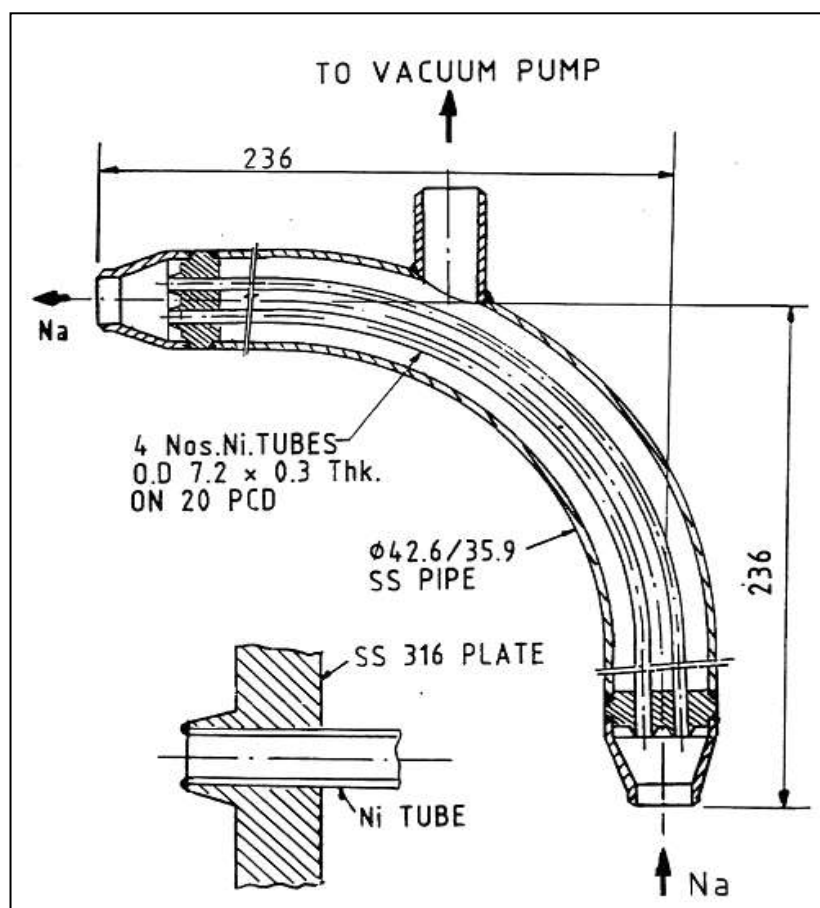
(All dimensions shown are in mm)

Fig.3.4: Nickel diffuser schematic

Table 3.1 gives the permeation coefficient of hydrogen in different materials. The permeation coefficient of hydrogen in nickel P = Db = 1.2994 x 10^{-6} mole.H_2.cm^{-1}.sec^{-1}.$atm^{-1/2}$. The selection

of Nickel as the membrane material is not only related to its magnetic permeability but also to its mechanical resistance to transients, embrittlement due to hydrogen, brazing reliability between membrane and steel.

Table 3.1: Permeability coefficient of H_2 in different material [46,47]

Membrane material	K^o_p (mol. $cm^{-1}.s^{-1}$,$atm^{-1/2}$)	Q (KJ/ mol)	Kp (mol.$cm^{-1}.s^{-1}.atm^{-1/2}$)		
			400°C	500°C	600°C
Palladium	5.0746 x10^{-6}	17.598	2.1852 x10^{-9}	3.2824 x10^{-9}	4.4917 x10^{-7}
Platinum	1.4513 x10^{-6}	75.420	2.0316 x10^{-12}	1.618 x10^{-11}	2.4559 x10^{-11}
Copper	2.8467 x10^{-6}	69.554	1.1370 x 10^{-12}	5.6773 x10^{-12}	9.9613 x10^{-11}
Iron	2.0172 x10^{-7}	4.224	1.5229 x10^{-10}	3.8598 x10^{-10}	7.9055 x 10^{-10}
Nickel	1.2994 x10^{-6}	56.146	5.69997 x 10^{-11}	2.0875 x10^{-10}	5.6785 x 10^{-10}

3.4.1 Permeation of hydrogen through nickel

Under the steady state conditions in the absence of any leak, the hydrogen permeation through nickel membrane into the vacuum circuit is proportional to the hydrogen concentration gradient across the membrane wall [45,48]. The permeation rate is estimated from

$$\dot{q}_{H_1} = \frac{DS}{d} (C_1 - C_2) = \frac{DbS}{d}\left[(P_{H_1})^{1/2} - (P_{H_2})^{1/2}\right] \tag{3.1}$$

where $\dot{q}_{H_1}$ is the hydrogen permeation rate across the nickel membrane, D = Diffusion coefficient of hydrogen in nickel, S = surface area of the membrane (cm^2), d = membrane thickness (cm), C_1 = Hydrogen concentration in liquid sodium, C_2 = hydrogen concentration in the vacuum chamber, b = Solubility of hydrogen in nickel, P_{H_1} & P_{H_2} are the hydrogen partial pressure (Pa)

at sodium and vacuum sides of the nickel membrane. Neglecting P_{H_2} for the flow calculation

purposes as $p_{H_2} \ll p_{H_1}$ the equation (3.1) can be rewritten as

$$\dot{q}_{H_1} = \frac{DbS}{d} \left(P_{H_1}\right)^{1/2} = \frac{PS}{d} \left(P_{H_1}\right)^{1/2} \tag{3.2}$$

This equation can also be written in terms of the hydrogen concentration C_H^{Na} in Na as

$$\dot{q}_{H_1} = \frac{PS}{db} \ C_H^{Na} \quad \because \left(P_{H_1}\right)^{1/2} \neq C_H^{Na} \tag{3.3}$$

The nickel membrane sensitivity $\rho_{Ni} = \dfrac{d\dot{q}_{H_1}}{dC_H^{Na}}$ is an important parameter and is found to be

0.865×10^{-12} g/ppb. Similarly, the time constant of nickel diffuser $\tau_{Ni} = \dfrac{d^2}{D\pi^2}$ is found to be

28s.

When a leak occurs in the SG at time t=0, the equilibrium is affected and the value of C_H^{Na} starts

increasing at a rate depending on the leak size. Correspondingly increased amount of hydrogen

permeates through the nickel membrane. The time dependant hydrogen flow rate across the

nickel membrane under this condition is given by [46, 48].

$$\dot{q}_{H_1\,(t)} = \frac{PS}{d} \ p_{H_1}^{1/2} \ \left[\ 1+2 \sum_{n=1}^{\infty} \ (-1)^n \ \exp\left(\frac{Dn^2\pi^2}{d^2} \ t\right) \ \right] + \ \dot{q}_{H_1\,(o)} \tag{3.4}$$

The higher order terms in the summation progressively diminish in magnitude and it is found

sufficient to retain only the leading term as

$$\dot{q}_{H_1\,(t)} = \frac{PS}{d} \ p_{H_1}^{1/2} \ [\ 1-2 \ e^{-t/\tau_{Ni}} \ ] + \ \dot{q}_{H_1\,(o)} \tag{3.5}$$

3.4.2 ANAVAC Quadrupole mass spectrometer

The ANAVAC make quadrupole mass spectrometers are provided to measure the partial pressure of H_2 in vacuum circuit. QMS consists of four electrodes in the form of cylinders in a square array. Mass separation is achieved on the basis of mass/charge ratio. A superimposed RF (AC) potential and DC potential is applied to the electrodes. Two alternate rods are supplied with $[U + V \cos\omega t]$ and other two rods are supplied with $- [U + V \cos\omega t]$ where $V \cos\omega t$ refers to AC voltage and U the DC potential. At a given frequency or amplitude of AC potential V, only those ions having a specific *m/e* (mass/charge) ratio can undergo stable oscillations and move axially to be collected at the other end of electrodes. Ions of other masses except the selected one undergo unstable oscillations and eventually lose their charges on hitting the electrodes.

Mass scanning is accomplished by varying the amplitude of AC voltage. A filament serves to ionize gas molecules before entering the electrode filter. The electrode rods must have uniform cross section and must be positioned parallel to each other. Quadrupole mass spectrometers are simpler than magnetic MSMs and have more sensitivity at low mass numbers [46].

There are two QMSs provided in both loops which measure total pressure over the range 10^{-7} to 5×10^{-15} kg/cm^2 and partial pressure over the range 10^{-7} to 2×10^{-14} kg/cm^2 in the mass range 2 to 60 amu. The units are provided with a range control knob for selecting appropriate pressure range (10^{-7} to 10^{-14} kg/cm^2). However only one filament is provided. Tuning for H_2 is done manually. During normal operation, QMS signal represents the background concentration of hydrogen present in sodium in terms of partial pressure of hydrogen. Hydrogen concentration in the loop can be read from the calibration charts.

3.4.3 Vacuum system

The vacuum system built around the nickel diffuser is made of stainless steel type 304 (SS304). All the joints are of FC 38 conflate flanges with OFHC copper gaskets. The vacuum system was initially cleaned with acetone and then baked up to 350°C for 48 hours in order to achieve effective degassing of chemisorbed gas molecules from the vacuum chamber walls. Subsequently during every startup the system is being baked up to 300°C. The vacuum system along with its components is shown in Fig 3.5.
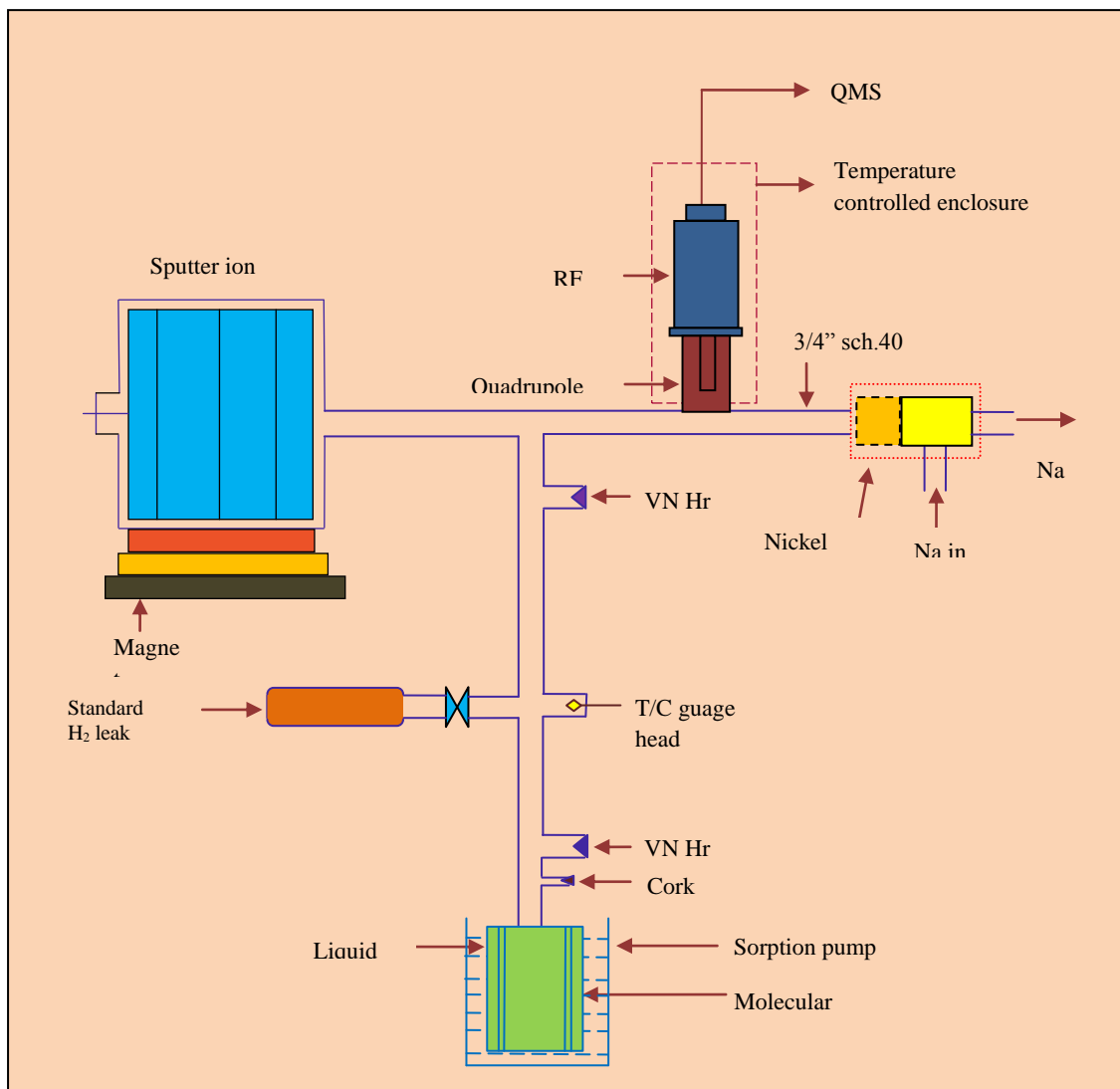
Fig. 3.5: Schematic of vacuum system

3.4.4 Sorption pump

During start up, the system is evacuated by the sorption pump till the vacuum of about 10^{-6} kg/cm^2 is reached. The pump used is of 50 lps capacity. In these pumps, the sorption property of gases by the porous material like the zeolite molecular sieve (alumina silicate) at liquid nitrogen temperature -196°C is utilized to pump down to 10^{-5} kg/cm^2 and below. Appreciable physical adsorption is achieved only when the surface is operated at a temperature close to that at which air would normally liquefy. This entails cooling of the molecular sieves by liquid nitrogen to achieve efficient adsorption. Sorption pump is cooled by pouring liquid nitrogen into the dewar surrounding it. These are ideal fore pumps for sputter ion pumps as they provide main advantages of freedom from oil vapour contamination and mechanical vibrations compared to rotary vacuum pumps. Since they saturate, they need to be reactivated by baking.

In our system this pump is connected to the vacuum system through a viton sealed bellows operated isolation valve. A thermocouple gauge is installed to read the rough vacuum upto 10^{-7} kg/cm^2. During start up, the vacuum system is evacuated by the sorption pump till the vaccum of about 10^{-6} kg/cm^2 is achieved. Then the SIP is switched on and is continued in service to maintain the dynamic vacuum in the range of around 10^{-11} kg/cm^2 and the sorption pump is isolated. The SIP and QMS analyzer head are connected to the vacuum system at right angles to avoid interference. The vacuum chamber enclosure materials are made of SS 304 and the volume of the chamber is 550 cm^3 [49].

3.5. Sputter ion pump

3.5.1 Pumping mechanism

The pumping effect of sputter ion pumps is produced by sorption processes, which are released by ionized gas particles. A sputter-ion pump consists basically of two electrodes, anode and

cathode, and a magnet. The anode is usually cylindrical and made of stainless steel. The cathode plates positioned on both sides of the anode tube are made of titanium, which serves as the gettering material. The magnetic field is orientated along the axis of the anode. Electrons are emitted from the cathode due to the action of an electric field and, due to the presence of the magnetic field, they move in long helical trajectories which improve the chances of collision with the gas molecules. The usual result of a collision with the electron is the creation of a positive ion that is accelerated to some kV by the anode voltage and moves almost directly to the cathode. The influence of the magnetic field is small because of the ion's relatively large atomic mass compared to the electron mass.

Ions impacting on the titanium cathode surface sputter titanium away from the cathode forming a getter film on the neighbouring surfaces and stable chemical compounds with the reactive of "getterable" gas particles (e.g. CO, CO_2, H_2, N_2, O_2). This pumping effect is very selective for the different types of gas and is the dominating effect with sputter ion pumps. The number of sputtered titanium molecules is proportional to the pressure inside the pump. The sputtering rate depends on the ration of the mass of the bombarding molecules and the mass of the cathode material. The higher this ratio, the higher is the sputtering rate.

In addition to the sputtering process a second important effect can be observed, the energy of the ionized gas particle allows some of the impacting ions to penetrate deeply (order of magnitude 10 atomic layers) into the cathode material. This sorption process pumps all kinds of ions, in particular ions of noble gases which do not react chemically with the titanium layer formed by sputtering. The cathode sorption process also works for hydrogen. Large amounts of hydrogen ions can diffuse deep into the bulk material beyond the range of the implanting ions and are permanently buried there.

The SIP is a vital component of this leak detection system. Apart from the usual pumping characteristics of the SIP for normal vacuum applications, a very high stability with ion current over a long period of time under continuous operation is required for this application as any momentary increase in its value is interpreted as leak signal and relevant safety action on reactor is initiated. While no genuine signal can be missed, any safety actions due to a spurious signal also is of serious concern as it affects the reactor operation and its availability besides resulting in large down time in confirming the leak tightness of the SG involving cumbersome experiments and test procedures.

Table 3.2: SIP Characteristics

Operating voltage (nominal)	3600 V DC
Magnetic field	1400 gauss
Pressure range	2.7×10^{-7} to 10^{-13} kg/cm^2
Nominal pumping speed for Nitrogen	14 l/s
Life (at 10^{-9} kg/cm^2)	30000 h
Maximum input power	40 W
Power consumption is proportional to the pressure below 10^{-7} kg/cm^2	
At 10^{-7} kg/cm^2 power consumption	10 W
Maximum bake-out temperature	400°C

The diode type SIP is of 14 lps capacity, consists of an anode made up of a series of small hollow cylinders of stainless steel and a cathode made up of a titanium plate separated by a gap between them. A high voltage around 3.6 kV DC is applied across the electrodes and the entire assembly is placed in the pole gap of a magnet, such that the magnetic field of strength of 1700

gauss is directed along the axis of the cylindrical anode and the cathode plates perpendicular to the cathode plates as in Fig.3.6. Table 3.2 gives the SIP characteristics.

The pumping capacity depends on the number of anode cylinders, the applied high voltage across the electrodes, the strength of the magnetic field and the operation history of the pump. Among these quantities, the stability of high voltage is achieved by careful design and regular maintenance of the electronics. Under the effect of an intense electric field between the cathode and the anode, a spontaneous discharge of electrons occurs.

Fig .3.6: Sputter ion pump with UHV system

These electrons hit the gas molecules and generate secondary electrons during ionization. The electrons are subjected to oscillation by the surrounding magnetic field, thus increasing the probability of collision with the gas molecules leading to further release of electrons and ionization before reaching the anode. The gas ions thus produced are directed towards the

titanium cathode of the pump where they get adsorbed and further get dissolved in titanium. The ion density in the vacuum circuit in the vicinity of SIP is proportional to the pressure in the vacuum system and hence the `ion current' realized by the movement of these ions is proportional to the gas pressure in the vacuum chamber. The rate of volumetric gas removal from the vacuum chamber or the pumping velocity of the SIP depends on the mechanisms which fix the gas ions on titanium. Normally the surface of the titanium cathode is covered by a layer of adsorbed gas, mostly N_2, preventing the free contact of hydrogen with the titanium surface. Only the hydrogen ions, which acquired sufficient energy under the effect of electric field, pass through this inhibiting layer and penetrate into titanium. Under the normal condition of operation, the rate of pumping of hydrogen Sp_n is $\sim$1.5 times that for N_2 as given in Table 3.3. When the hydrogen partial pressure is $>10^{-10}$ kg/cm^2, the number of ions formed become sufficiently high, so that the ionic bombardment scrapes the cathode surface which is cleaned off the passivating nitrogen molecules.

Table 3.3: Pumping speed of various gases with respect to that of air

Gas	Pumping speed
Hydrogen	252.5 %
Oxygen	56.25 %
Nitrogen	97.5 %
Argon	5.6%
Helium	10.6%

Thus at high hydrogen partial pressure, the impurity layer covering the titanium cathode disappears progressively by which the `activation' of the pump takes place. Under this condition the pumping rate of hydrogen Sp_a increases with the gradual increase of active capture surface of the titanium cathode and will be many times greater than the normal pumping speed Sp_n. The activated cathode surface area can neither be monitored nor maintained constant. Though the

cathode activation increases the pumping efficiency with no change in hydrogen measurement accuracy, it is ensured that the pump operates in non-activated mode by operating the vacuum system at low hydrogen partial pressure ($<10^{-10}$ kg/cm^2) [50]. In SIP, two flat plate titanium cathodes and a hollow cylindrical metal anode are mounted axially between the poles of a permanent magnet. When a high voltage is applied between cathode and anode electrons are emitted. These electrons ionize the gas molecules and the efficiency of ionization is good because of the helical motion of the electrons produced due to the magnetic field (The long helical path of the electrons produced by the magnetic field are much longer than the direct path, thus increasing the probability of ionization of gas molecules). Ions move towards the cathodes and get buried there as they strike it. At the same time bombarding ions knock out titanium atoms from the cathode in a process called "Sputtering". The sputtered titanium atoms are deposited on the pump walls and anodes and bury neutral gas molecules as well as act as getter for chemically active gases including hydrogen inside the pump, resulting in compound formation. Thus both ion and getter pumping are accomplished. Since titanium gets sputtered and there is a limited amount of titanium in this pump, it gets saturated after certain hours of operation (approximately 30,000 h).

 The life of the pump depends on the vacuum being maintained. At low vacuum the life is short. These pumps operate most effectively at below 10^{-9} kg/cm^2 and a vacuum of 10^{-12} to 10^{-11} kg/cm^2 can be achieved. Main advantage of ion pump is that oil-free vacuum can be achieved which is must in this system. When the vacuum circuit is put in service from rough pumping (sorption pump), if vacuum does not improve beyond 10^{-9} kg/cm^2, it could be due to degassing from the inside surfaces of vacuum line. Gases and moisture get adsorbed when the vacuum

system is exposed to atmosphere during maintenance. In such cases, baking is done by raising the temperature of the pump and the vacuum system using a tape heater for degassing [4].

If the vacuum circuit is exposed to atmosphere for a long time due to maintenance, hot baking at 300°C with sorption pump for 24h and with sputter ion pump for 40h is required. This is done during a fresh start-up and after prolonged exposure of the pump to atmosphere.
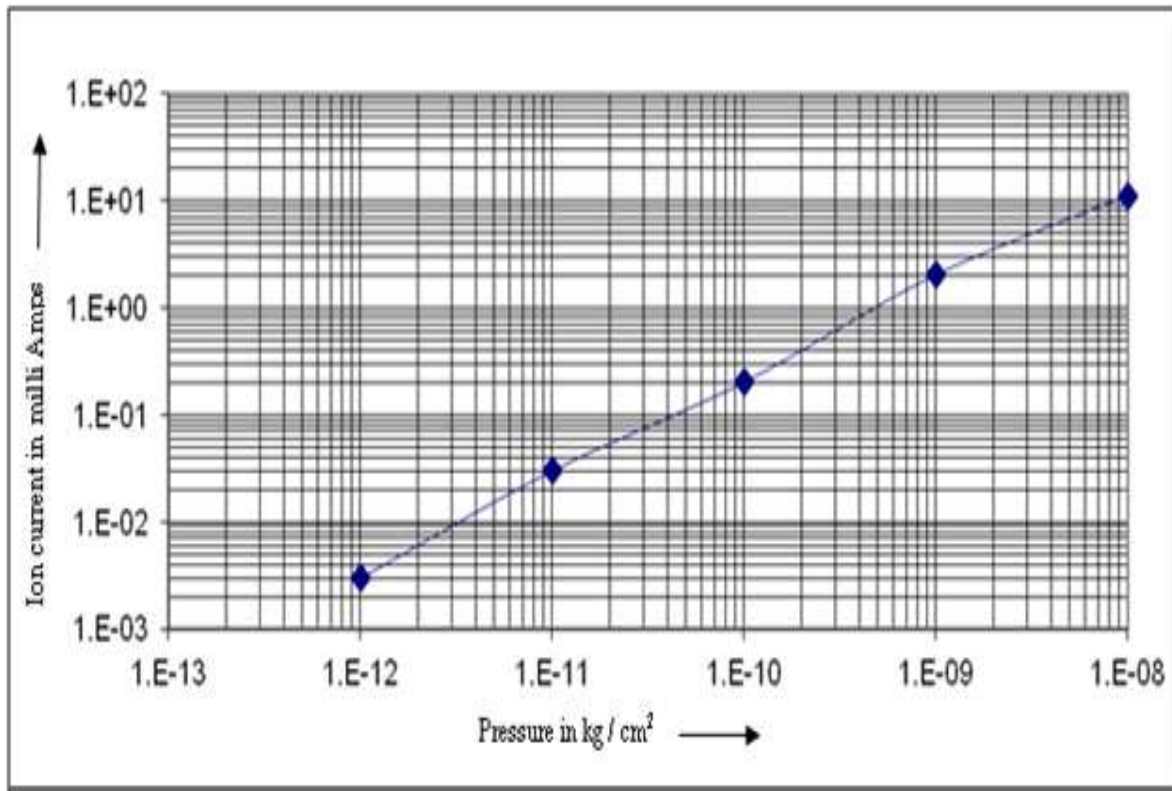
Fig.3.7: Calibration chart of sputter ion pump

The SIP current is a measure of the vacuum in the system. As the vacuum increases the current drawn by SIP decreases. Thus the ion current represents the vacuum created in the circuit. Interlock is provided to trip SIP and cut off the power supply to SIP if the pressure exceeds $10^{-7} kg/cm^2$ (20 mA). This is to protect SIP from operating at high pressure. Fig.3.7 shows the calibration chart of SIP [51].

3.6 Development of a robust technique for monitoring hydrogen partial pressure

After carrying out the necessary modifications, the SGLD system was put in to service and the reactor power was raised to 4 MWt. The performance of SGLDS was satisfactory. The SGLDS responded very well during the valving in of water and there was a significant increase in the background value. However, various problems forced unscheduled reactor shutdowns and increased down time of the plant. This was mainly due to the requirement of periodic ion source filament replacement in the QMS and subsequent calibration. There were a few occasions of premature filament failure of random nature which necessitated development of an alternate, robust technique for measuring the hydrogen partial pressure.

The concept of using the SIP ionization current, which is already in the circuit, in place of QMS was explored, as this current is a function of the total gas molecules in the UHV chamber as reported in the literature survey under section 1.7. This can be done because, although the sputter ion current is proportional to the total pressure in the vacuum circuit, after initial high temperature bake out is over, the availability of other gases are insignificant and only the dominating gas is hydrogen due to permeation through nickel membrane. Hence, the SIP current can be considered as proportional to the hydrogen partial pressure in the vacuum chamber. Implementation of this concept required the SIP riding over a very high DC voltage of 3.6 kV with adequate protection against high voltage and converting the SIP current into a 0-10V DC signal suitable for connecting to the real time computer system for monitoring and carrying out safety functions. After designing and testing the circuitry, a proto type was fabricated in collaboration with M/s. ECIL, Hyderabad and extensively tested in a separate experimental set up to study the performance pertaining to signal stability, noise immunity, repeatability etc.

The block schematic of modified SIP circuit is shown in Fig.3.8 and detailed electronic schematic diagram is given in Fig. 3.9. On obtaining satisfactory results, this unit was installed in the secondary sodium east loop.
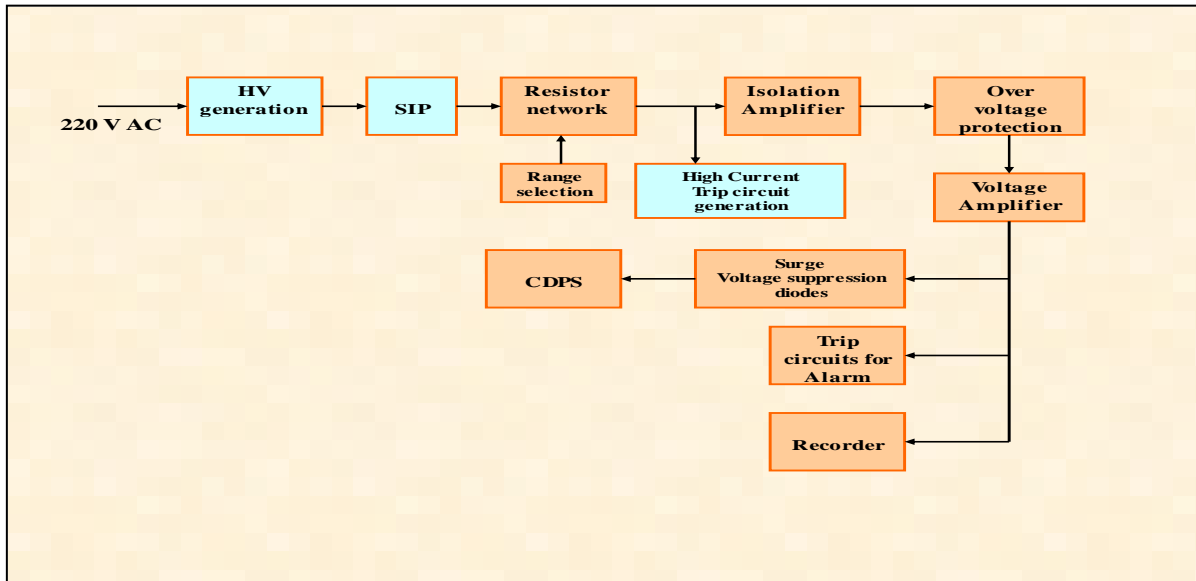
Fig.3.8: Modified SIP circuit
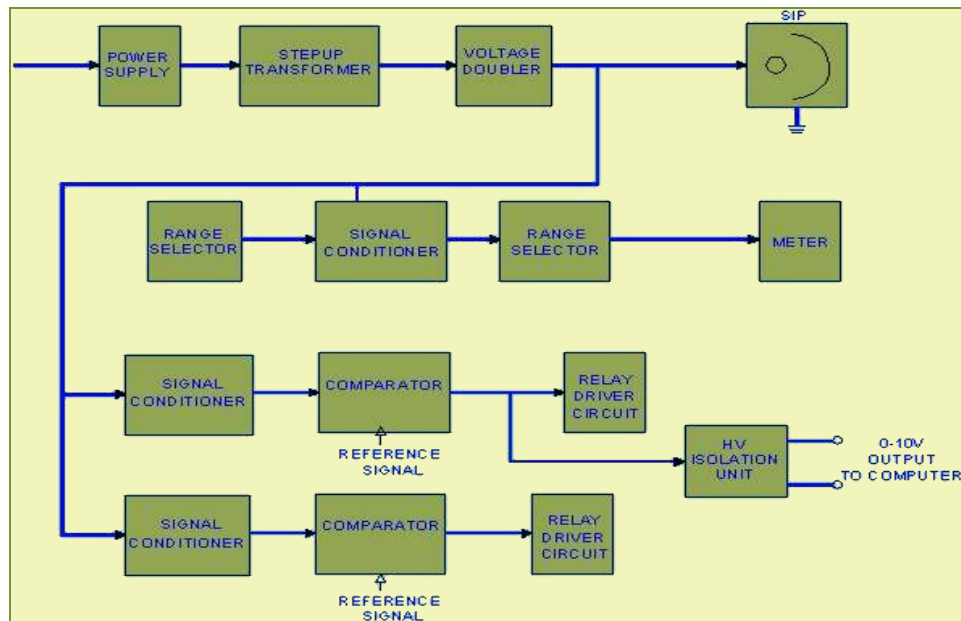
Fig. 3.9: SIP excitation, signal extraction and electronic schematic

3.7   Experimental results

Hydrogen injection tests simulating water leak were carried out by injecting known quantity of hydrogen in sodium at different loop sodium temperatures and the response was studied in the modified SIP unit and compared with that of QMS. A typical graph depicting three successive injection tests is given in Fig.3.10& 3.11. The response of SIP during each hydrogen injection is distinctly more than the corresponding increase in QMS.

The performance of the modified SIP unit was monitored for 40 days of reactor operation as given in Fig.3.12 and the hydrogen evolution in modified SIP unit was found to follow closely with QMS.
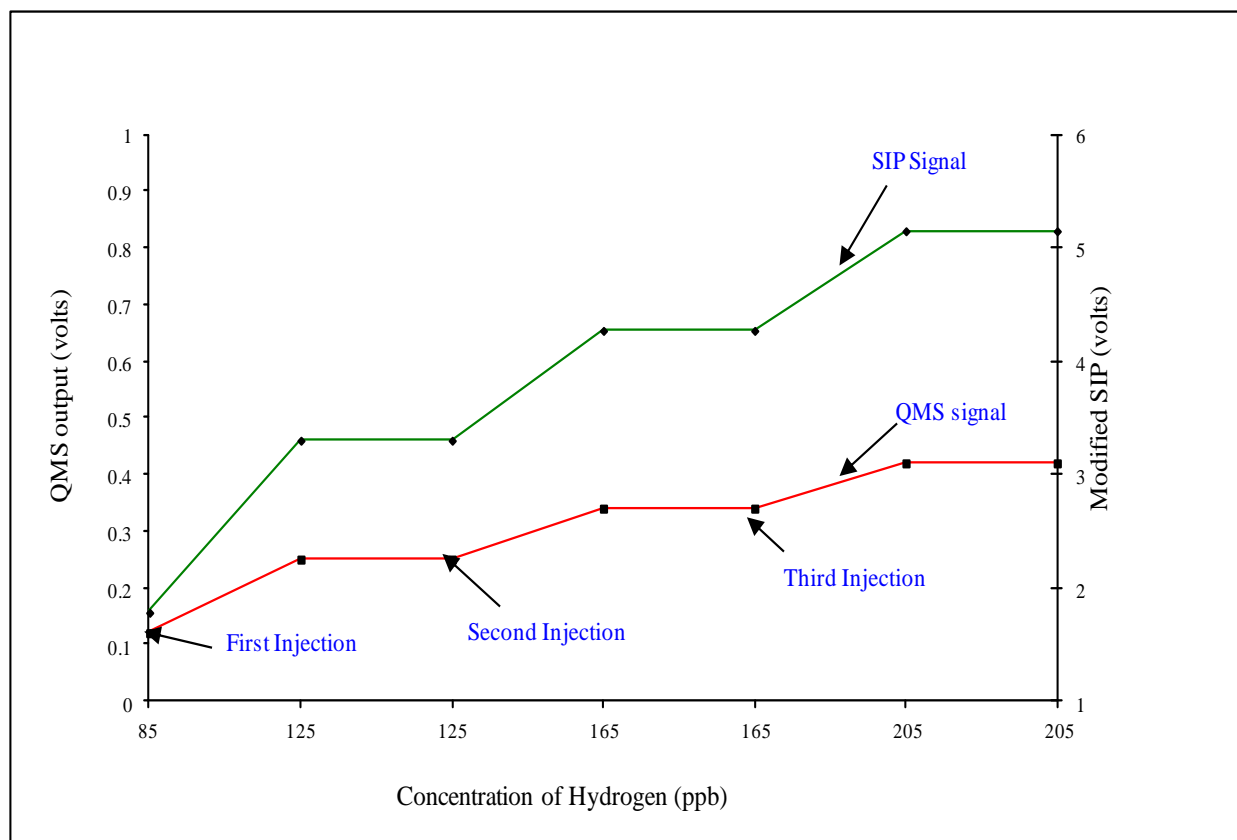
Fig 3.10: Response of SIP and QMS units to three successive injection tests
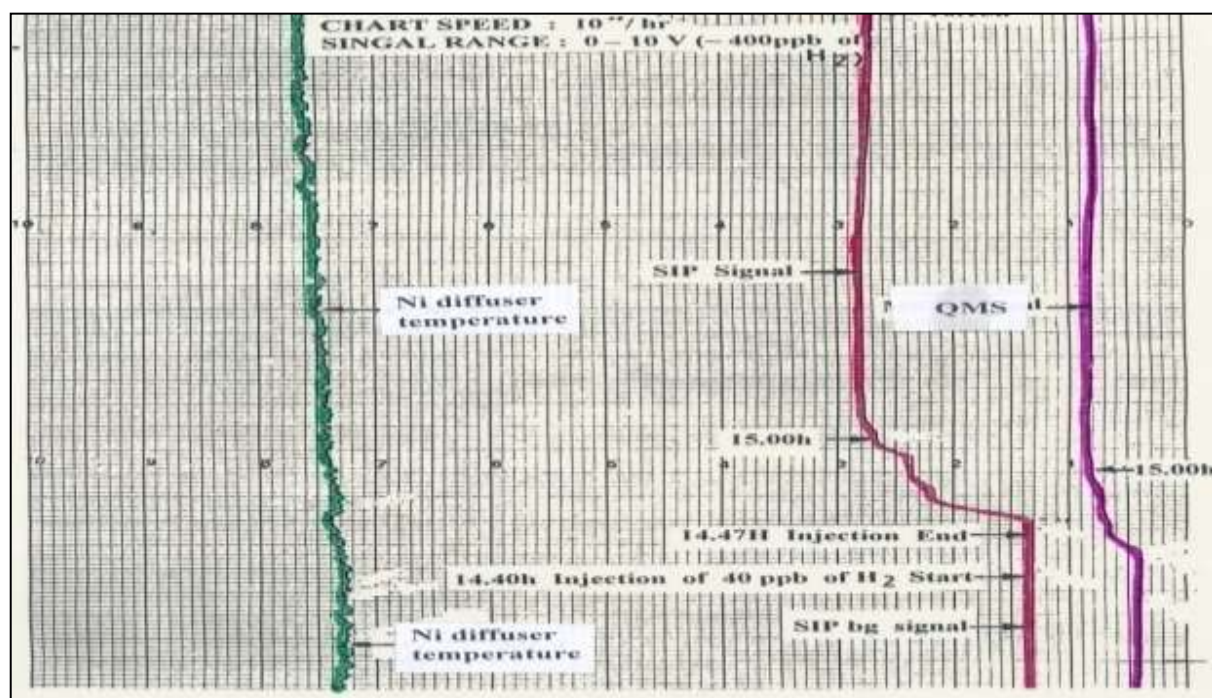
Fig. 3.11: Calibration chart of SIP & QMS signal real time
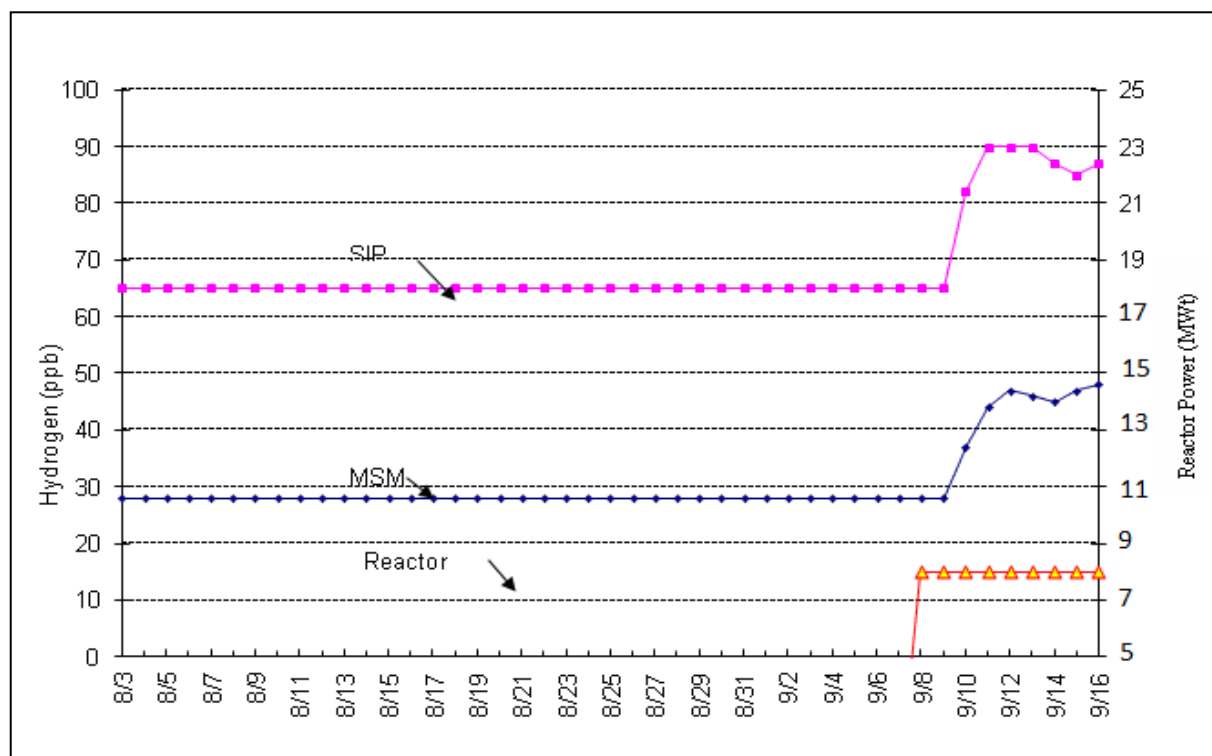
Fig. 3.12: SIP response during power operation

After ensuring the performance of the SIP unit along with QMS for two months, the second modified SIP was installed in the other sodium loop (west) and the hydrogen evolution in both east and west SIP units were monitored simultaneously for a period of 10 days with reactor power operation which involves SG valving- in, signal evolution during power operation and reactor shutdown the results are shown in Fig. 3.13.

These experimental results demonstrate the excellent performance such as accuracy, stability, reliability and detection speed of the modified SIP units for detecting SG small leaks.

This development obviates the need for QMS in the system with the associated problems of annual filament replacement and calibration leading to large down time. Besides, the modified SIP also eliminates the down time of three weeks due to premature QMS filament failure.
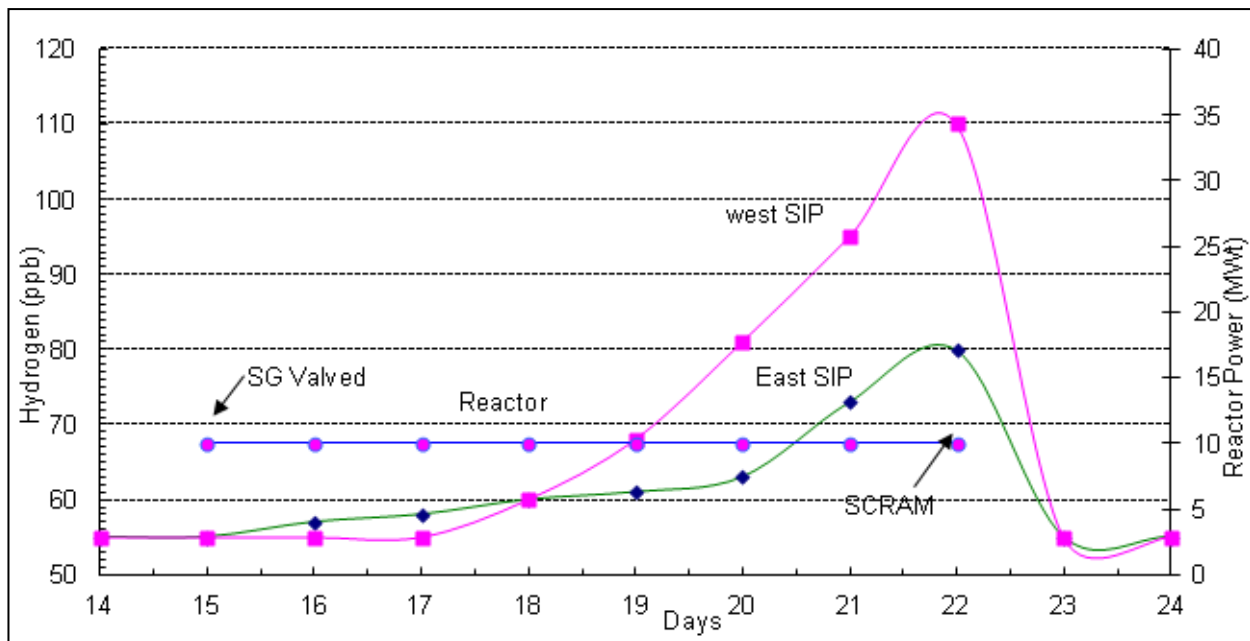
Fig. 3.13: Response of both east and west SIP during reactor operation

3.8 Variation of hydrogen pumping speed

The hydrogen pumping speed for the SIP is of the order of 250% of that for air. In order to arrive at the hydrogen pumping speed of the pump, the hydrogen partial pressure in the vacuum system

is noted down after the complete system has reached steady state condition. The pump is then switched off till the H_2 partial pressure increases by one order. Then by starting the pump, the time taken to reach the original hydrogen partial pressure back is recorded. With this the speed of the SIP for hydrogen can be calculated as below:

Hydrogen partial pressure in the vacuum circuit at time $t_0 = P_{H0.}$

Time at which the H_2 partial pressure reach $P_{H1 =} 10P_{H0} = t_1$

Time at which the pressure P_{H1} reduced to $P_{H2 =} P_{H0} = t_2$

$$\text{Speed of SIP} = \frac{(P_{H1} - P_{H2})V}{(t_2 - t_1)} \tag{3.6}$$

By repeating this experiment periodically (at $\approx$ 2000h intervals) the change, if any, in the pumping rate of SIP for hydrogen can be found. Taking the volume of the vacuum chamber as V liters, initial hydrogen partial pressure at time t_1 as P_{H1} and final hydrogen partial pressure at t_2 as P_{H2}, the average pumping speed of the SIP is determined using equation 3.6.

The hydrogen pumping speed of the SIP found in three consecutive measurements at an interval of 2000h are 3.06, 3.12 and 3.18 x 10^{-15} kg**.**l/cm ^{2} s. The slight apparent increase seen in the pumping rate with reference to time is due to the reduction in the desorption rate of hydrogen which are 1.27, 1.24 1.238 x 10^{-15} kg**.**l/cm ^{2} s. These studies confirm that there is no considerable increase in the pumping speed with time.

3.9 Appearance of argon spikes

The SIP ion current output signal was found to have a few spikes during the start up of the system following every opening of the vacuum system. The appearance of the spikes seems to affects the stability of the SIP output signal and can lead to spurious leak alarms. This is due to

the release of argon gas in spurts adsorbed in the system when exposed to the atmosphere and buried in the SIP cathode during the subsequent pumping.

This gas being inert, they are buried as they do not react with titanium to form stable chemical compound. Hence, when the sputtering of titanium surface takes place by the bombarding ions, during the pumping action, these argon atoms get released [49, 52, 53] as occasional spurts. Besides this, occasional argon instability causing series of spikes as in Fig.3.14 in the SIP current was observed. This was eliminated by permitting adequate N_2 blanketing on the internals of vacuum system whenever exposed to atmosphere.
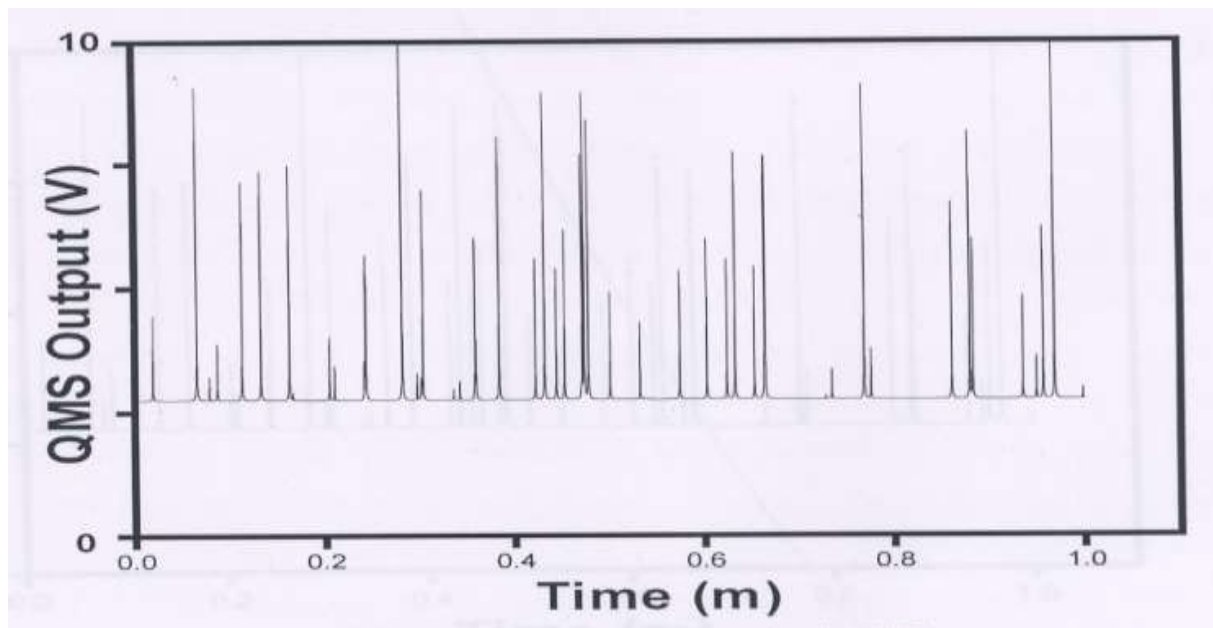
Fig. 3.14: Argon spikes in sputter ion pump due to instability

The nitrogen purging was provided to the entire vacuum system (blanketing) whenever the vacuum system was opened up and the argon spike problem could be eliminated.

3.9.1 Elimination of external noise interference

The external noise interference by electromagnetic coupling is due to production of time dependent magnetic field by any high current carrying cables running nearby. The 50 Hz noise

interference with the signal is frequently encountered with high power equipments drawing large current at 50 Hz. The high magnitude fluctuating magnetic field induces high amplitude noise voltages into the measurement circuit.

In our setup this interference was eliminated by (i) reducing the mutual inductance between the neighboring cables by physical separation of signal cables from the nearby power cables, (ii) by using twisted pair cables, (iii) by providing metal shielded cables, (iv) by arranging the power cables and signal cables to cross only at right angles and (v) by avoiding long parallel runs of cables [54, 55, 56]. Care was taken to ensure effective grounding. In addition, copper clad back plane also is provided for the ion current amplifier printed circuit board for effective shielding. These have virtually eliminated the 50 Hz electrostatic interference as noise current is diverted to the earth, and it does not corrupt the signal.

3.9.2 Reduction of intrinsic noise

Even if the entire external noise coupling could be eliminated in a circuit, a theoretical minimum noise level would still exist due to certain intrinsic or internal noise sources [54, 55]. Amongst these, the thermal noise, shot noise and burst noise are dominant. The thermal noise is generated in a conductor due to thermal agitation of electrons. It is non periodic and is related to temperature as $Vt = \sqrt{4Rk_bTB}$ where v_t is the noise voltage in volts, R the resistance in ohms, k_b the Boltzmann constant (1.38×10^{-23} joule/K), T the absolute temperature in K and B the band width of the noise in Hz. The noise voltage generated by the thermal noise sets the lower limit on the noise in the circuit.

The shot noise is generated due to current flow across a potential barrier, present in semiconductor devices. This noise is due to random diffusion of carriers through the base of a transistor and the random generation and recombination of hole electron pairs. The rms shot

noise current I_{sh} in a signal current I_{DC} is given by [57, 58] $I_{sh} = \sqrt{2eI_{dc}B}$ where e is the electron charge (1.6 X10^{-19} coulombs), B= noise in bandwidth in Hz.

The burst noise in the integrated circuits is caused by manufacturing defects in the junction, usually a metallic impurity at the semi conductor junctions. This noise occurs in burst and causes a discrete change in the signal level. Such a noise is characterized by its width varying from microseconds to seconds: frequency varies from several hundred pulses per sec to less than one pulse /min and their amplitude varying from 2 to 100 times that of thermal noise. Noise voltages produced by different sources independently with no correlation between each other are termed as uncorrelated and get added in root sum square sense as given by,

$$V_{total} = \sqrt{v_1^2 + v_2^2 + ... + v_m^2}$$ \hfill (3.7)

This gives an upper bound of noise in the measured signal. The thermal noise is minimized by using high quality metal film resistors with low temperature coefficients and high power rating. Additionally, a temperature controlled ambience is maintained around the electronics. The shot noise and burst noise are minimized by using type tested high quality low noise semiconductor components.

With the incorporation of these features in the measurement hardware, we obtained output signal with a maximum noise content of ±2mV. Though the signal with minimized noise content of this order is obtained with these hardware techniques incorporated, occasional possibility of some noise sneaking into the measurement process either by getting generated within the process such as argon re-emission in the SIP or getting induced in electronics or due to external interference cannot be ruled out under exceptional conditions. Hence to overcome such eventualities, software noise rejection technique is incorporated.

3.9.3 Evaluation and elimination of noise spikes by software

The noise induced in the signal due to any of the interference or by generation in the process itself could be of bipolar in the form of spikes. These are prevented from affecting the genuine measurement signal by the method of sampling, validating and averaging through software. First, the output signal from the SIP is sampled by the computer at one second interval. Each reading is compared with the previous sample. If the difference is more than a certain limit, the current scan value is rejected and the previous values replace the current value which is stored in separate location for comparison with four more subsequent reading. If the current value is more than the limit for five consecutive cycles, then rejection is not effected and the readings are validated. After taking five validated samples, the average value is recorded as the true signal.

This is used for comparison with the safety thresholds for effecting the safety actions. Any noise that may be present in the measurement signal gets eliminated and noise free measurement signal is obtained all the time. Choosing the comparison limit very low, the possibility of crossing the safety threshold increases and vice versa. In the set up described here, the limit is set at 0.5V.

SIP signal, after processing in isolation amplifier, is fed to computer system for initiating alarm and safety action based on rate of rise of the signal and CDPS software scans every second for rate of rise. For absolute value based safety action, this signal is fed to hard wired logic.

In order to avoid spurious alarm and trip due to noise pickup, the signal is processed and validated as explained above. All the supervisions are done based on these averaged values. Initiation of alarm and LOR is done if the averaged value or rate of rise crosses their respective threshold values in two consecutive cycles.

3.9.4 Long term stability of output signal

The long term stability in the output signal of the leak detection system is very important as the

signal is continuously monitored for detecting leak. Such variation in the signal without genuine variation of concentration of hydrogen in sodium can either rise to spurious alarm or contribute to increase in the response time for detecting a leak incident depending on the direction of the variation as discussed. The leak detection system is calibrated once a year by simulating a leak condition by injecting known quantity of hydrogen in sodium to restore the sensitivity of the total detection system in the realistic situation. This takes into account any variation in the operational parameters that contribute to the drift in this signal such as qualitative deterioration of the nickel diffuser and variation in the vacuum system parameters [56, 59].

The output signal of SIP is recorded by strip chart recorders in addition to processing by the online computer. After the calibration process by injection of hydrogen is completed and the hydrogen concentration is stabilized, the sodium temperature is maintained at 250 ^{o}C and the cold point temperature is reduced back to 120°C from 130°C. Only the secondary sodium is kept in circulation during the period under study. All the process parameters, which are known to contribute to the signal variation, such as cold trap temperature T_{CP}, nickel membrane diffuser temperature T_{Ni}, feed water/steam temperature and chemistry parameters and ambient temperature of SIP electronics unit were maintained constant.

3.10 Leak simulation tests

To study the evolution of the leak signal during an SG leak incident, the leaks are simulated by injecting desired quantity of hydrogen into sodium. Some of the signal evolution process steps are highly temperature dependent. Therefore, the simulation experiments were carried out at various temperatures of sodium such as 400, 300, 250 and 180°C to cover the entire operating range of sodium temperature. The hydrogen injection point is chosen at the sodium inlet header, which is located at the top of the SG. This will facilitate the study of the time taken for the

detection of the leak, when it occurs at the point at a maximum distance from the detector. It will be more appropriate if provisions are made to inject the hydrogen at different locations of the SG to simulate the leak in a real scenario. However, this loop being a part of the operating reactor, for safety considerations such a multi location injection facility for leak simulation is not available.

During the hydrogen injection, care is taken to maintain the sodium temperature at the desired value of 400, 300, 250 and 180± 10°C, reheater temperature at 450 ± 1°C, quantity of hydrogen as 0.557 g which corresponds to 40 ppb of hydrogen concentration C_H^{Na} in sodium if completely dissolved. This amount of hydrogen is equivalent to 5g of H_2O leak into sodium. The time taken to inject this is chosen as 420s, which is equal to the time for one sodium circulation in the loop. This corresponds to a leak rate of 0.0119g of H_2O/s. The main sodium flow q_{Na} is maintained at 135m^3/h and the cold trap is kept isolated during these simulation experiments to get the signal evolution data accurately by eliminating the uncertainty in the quantity of hydrogen removal by the cold trap simultaneously.

Injection of 0.557g of hydrogen was done at this temperature. The signal started increasing after about 140s and reached its peak value after about 780s and the increase in signal was 100% of the expected value corresponding to the increase of concentration by 40ppb. This is due to the fact that the dissolution of the hydrogen in sodium at this temperature is complete and the dissolved hydrogen concentration was detected by QMS and SIP.

3.10.1 Procedure for injection

Initially, before injection, the hydrogen tank RE_{Hr} 520 is thoroughly flushed with argon, evacuated and then Argon filled to 0.1kg/cm^2 pressure. Then the hydrogen is filled into this tank to the required pressure. This pressure is fixed such that, the final pressure after injection is more

than the sodium pressure which is ≈ 0.7 kg/cm^2 at injection location. This avoids sodium backing

up. The injection period is so chosen that the required rate of instantaneous hydrogen increase is

achieved. One complete circulation of sodium in the loop takes ~7 minutes and hence, an

injection time of 7 minutes is chosen. By this choice, the hydrogen concentration evolution can

be studied precisely. The following representative calculation shows an example of the injection

process.

In order to raise the $C_H{}^{Na}$ by 10ppb in the secondary sodium inventory of 13.92 tons the

hydrogen required to be injected is $\quad = \quad \dfrac{13.92 \times 10^6 \times 10}{10^9}$

$$= \quad 0.139 \text{ g} \quad\quad = 139 \text{ mg}/2.016 \text{ moles}$$

$$= \quad 6.895 \text{ x}10^{-2} \text{ moles.}$$

The pressure drop Δp required in the hydrogen tank RE $_{Hr}$ 520 to inject this amount of hydrogen

can be calculated from the ideal gas equation as:

$$\Delta p \quad\quad\quad = \quad \frac{mRT}{V} \quad\quad\quad\quad\quad (3.8)$$

$$= \quad \frac{6.895 \times 10^{-2} \times 8.3143 \times 303}{15.6 \times 10^{-3}}$$

$$= \quad 1.1134 \text{x } 104 \text{ N/m}^2$$

$$= \quad 0.11134 \text{ bar}$$

$$= \quad 11.134 \text{ kPa}$$

Initial pressure of RE $_{Hr}$ with the argon $= P_{Ar} = 0.1$ kg/cm^2

The required final pressure of tank P_f after injection should be $>$ Na pressure of 0.7 kg/cm^2 for

effective injection this is fixed at 2 kg/cm^2. Based on this requirement the hydrogen tank RE$_{Hr}$ -

520 can be pressurized to P_2 where

$$P_2 \quad\quad = P_{Ar} + \Delta p + P_f = 2.211 \text{ kg/cm}^2 \quad\quad\quad\quad (3.9)$$

The argon concentration in the H_2 tank = 0.1 kg/cm^2 /2 kg/cm^2 =0.0474

To inject the required quantity of hydrogen the actual pressure drop Δp required is 116 kPa. The injection of hydrogen into sodium has to be done till the pressure of the tank falls to

$$P_f \qquad = P_2 - \Delta p = 2.095 \text{ kg/cm}^2 \qquad\qquad (3.10)$$

Based on the specific requirement, in the above manner any quantity of H_2 can be injected into the experimental loop.

3.10.2 Leak simulation for 1g/s calculations

Leak simulation by injection of known quantity of hydrogen in sodium:

a) To simulate a leak of 1g/s of H_2O , the hydrogen to be injected in Na is

$$1/0.9 = 0.111 \text{g/s of } H_2$$

b) The rise of hydrogen concentration C_H^{Na} by the injection of 0.111g of H_2 in the inventory of 13.92mt of sodium =0.111 /13.92 x 106 =7.974 ppb

c) Since, the time taken for one circulation of the sodium is 7 min, hydrogen is injected for 7 minutes at a rate, which will increase the C_H^{Na} by 40 ppb, a round value, as given in calculation in Appendix-2.

Based on this, the total pressure after injection is 1.3 b (g) whereas the initial pressure is 2.0 b (g).

3.11   System calibration

The calibration is essential to establish the relationship between meter output and the concentration of hydrogen in sodium. The permeability of nickel membrane tubes decreases with time of operation i.e. for a given concentration of hydrogen in sodium at a given temperature, the quantity of hydrogen diffusing through the nickel tubes diminishes with time. This is called ageing. It is reported that, after 4000 h of operation, the permeability remains fairly

constant and the output of the SIP is approximately $1/5^{th}$ of the magnitude of the output signal prevailed initially. Such variations call for a periodic check up and calibration of the detector by injection of known quantities of hydrogen into sodium circuit.

The calibration is carried out when the reactor is in shutdown state or operating at power level below 500 kW so that the SG is not valved-in. The primary and secondary sodium temperatures are maintained at $375 \pm 10°C$ with the help of reheater or reactor power. The sodium flow through the SG is maintained at $135 m^3/h$. Tube side of the SG contains nitrogen at about $0.5 kg/cm^2$ pressure. The cold point temperature of sodium is maintained at $130°C$ till the QMS and SIP signals stabilize.

The flow through the SGLD system is maintained at $> 1 \ m^3/h$ from each module. The vacuum circuit of SGLD system is maintained at a vacuum of 10^{-11} to $10^{-10} kg/cm^2$.

The calibration is achieved by injecting known quantities of hydrogen gas into sodium. For this purpose, an injection line of φ 20 mm is connected to the sodium header at the upstream of the SG. Hydrogen is stored in an upstream tank of 15 liters volume and the rate of injection can be controlled by a needle valve provided in the line. The quantity of hydrogen injected is calculated from the drop in pressure in the hydrogen tank. The evolution of signals of QMS and SIP are monitored during hydrogen injection. The safety thresholds are fixed based on the calibration results of three successive (triple) injections of hydrogen in sodium. All the data are tabulated typically as in Table 3.4. From the Table, concentration of H_2 (ppb) in sodium versus SIP output is plotted.

Table 3.4:Calibration data format

Injection. No.	H_2 conc. (ppb)	SIP output(V)
1	Background (85)	
2	Background (125)	
3	Background (165)	
4	Background (205)	
5	Twice Background (170)	

(When the purification system is in continuous service, the background is 85 ppb with the cold point temperature at 130°C.)

3.11.1 Initial conditions for calibration

a) Primary and secondary sodium temperatures are maintained at 375 ±10°C with the help of reheater.

b) Sodium flow through the steam generator is maintained at 135m³/h with the pump operating at 350 rpm. Tube side of the steam generator contains nitrogen at > 2.5 kg/cm² pressure.

c) After stabilization of signal, cold trap is isolated and cold point temperature is maintained at 130 ± 5°C with the help of electrical heater.

The vacuum circuit of SGLD system is maintained at a vacuum of 10^{-11} to 10^{-10} kg/cm². Flow through the each SG module at 1 m³/h.

d) The nickel diffuser temperature is maintained at 450 ± 1°C.

e) EM pump flow is maintained at 3m³/h.

f) Temperature of H_2 injection line is maintained at 150°C using line heaters.

g) The calibration is done by injecting 0.557g of H_2 into sodium through the hydrogen injection circuit. This raises H_2 concentration in 16 m^3 hold up of sodium by 40 ppb.

3.12   Online calibration method

The calibration is generally carried out when the reactor is in shutdown state or operating at power level below 500 kW so that the SG is not valved-in. As the calibration is carried out with the SG in drained condition on water side, the reactor is not available for high power operation till the calibration is completed which may take about 10 d. As an alternative, on an experimental basis, a controlled online injection of 20 ppb of Hydrogen in sodium has been carried out in west loop with the reactor operating at 13 MWt and the measured results are matching with the estimated values. Hydrogen injection of 20ppb was selected so that the increased values after injection do not exceed the reactor safety thresholds. Hence it is demonstrated that the calibration can be done with the SG valved-in condition and at sodium inlet (SG) temperature of about 400 ^{o}C. The reactor need not be shut down for calibration and continued operation of reactor at high power can be maximized.

As there is diverse method available for SG leak detection from expansion tank cover gas pressure rise and rupture disc rupture along with the protection from SGLDS on absolute value threshold, the calibration of the system will not prejudice the safety of SG while done on-line with reactor operating at high power. Besides saving time and efforts towards raising and maintaining sodium temperature at 375°C, when the reactor is in shutdown state, this method will yield more realistic data for fixing thresholds as the calibration is done on line.

The calibration is achieved by injecting known quantities of hydrogen gas into sodium. For this purpose, an injection line of φ 20 mm joins the sodium header at the upstream of the SG. Hydrogen is stored in an upstream tank of 15 litres volume and the rate of injection can be

controlled by a needle valve provided in the line. The quantity of hydrogen injected is calculated from the drop in pressure in the hydrogen tank. The evolution of signals of QMS and SIP are monitored during hydrogen injection. The safety thresholds are fixed based on the calibration results of Triple injection of hydrogen in sodium.

3.13 Precautions during measurement

a) During the calibration of the leak detection system by injecting hydrogen into sodium through the injection set up, safety precautions regarding fire protection are taken. All the gas connections of the injection set up are checked for leak tightness with argon pressure at 4 kg/cm^2 before pressurizing the tank RE_{Hr} -520 with hydrogen. The injection line from RE_{Hr}-520 to sodium header is purged with Argon thoroughly before admitting hydrogen into sodium.

b) A pressure trip in the UHV system is provided at $>10^{-5}$ kg/cm^2 which turns off the SIP to prevent damage due to high ion current in case of a vacuum leak. Before the trip an alarm is set at $>10^{-6}$ kg/cm^2.

c) It is also important that during start up of the system, the electrical heating tapes for baking the system and the equipments are laid for uniform heating of the components, in particular those around ceramic feed through of the SIP. Non-uniform heating may develop cracks in the metal-to-ceramic seals due to differential expansion across them, which may end up in damaging the SIP.

d) The sequence of opening of hydrogen injecting valves should start from the hydrogen tank RE_{Hr} to avoid backing up of sodium.

3.13.1 Background hydrogen in sodium

There is always a certain amount of hydrogen present in sodium as background due to the following important sources:

1. Hydrogen injected during calibration tests.

2. Hydrogen generated due to aqueous corrosion of the tubes of the SG and its diffusion through the SG tubes.

$$3Fe \quad + \quad 4H_2O \quad \longrightarrow \quad Fe_3O_4 \quad + \quad 4H_2 \qquad (3.11)$$

3. Decomposition of hydrazine added in steam water system to control oxygen concentration and its diffusion through tubes.

Hydrogen injected during the calibration tests is known. Diffusion of hydrogen from water side of SG to sodium side is high as soon as valving- in of SG, till the formation of Fe_3O_4 layer is complete on tube side. The initial rate is around 8.0×10^{-11} gH/cm^2/s. After thousands of hours of operation, this reduces to half (4.2×10^{-11} g H/cm^2/s).

In order to confirm the ingress of H_2 to the sodium system during the addition of hydrazine in feed water system, an experiment was conducted to study the evolution of H_2 during the addition of hydrazine with the cold trap in isolated condition.

3.13.2 Variation in hydrogen concentration in sodium due to ingress from feed water

The entire secondary sodium system was kept in operation at an isothermal temperature of 375 ^{o}C and the cold point temperature maintained at 120°C for 72 h. In order to quantify the H_2 flux diffusing through the steam generator walls, an experiment was carried out by isolating the online purifying cold trap when the SG is in operation. The isolation of the cold trap was carried out after SIP signals were found steady for about a week. The electromagnetic pump discharge to

the cold trap was stopped and the inlet and outlet valves of the cold trap were closed. The SIP outputs were recorded. The increase in C_H^{Na} with reference to time is given in Fig 3.15.
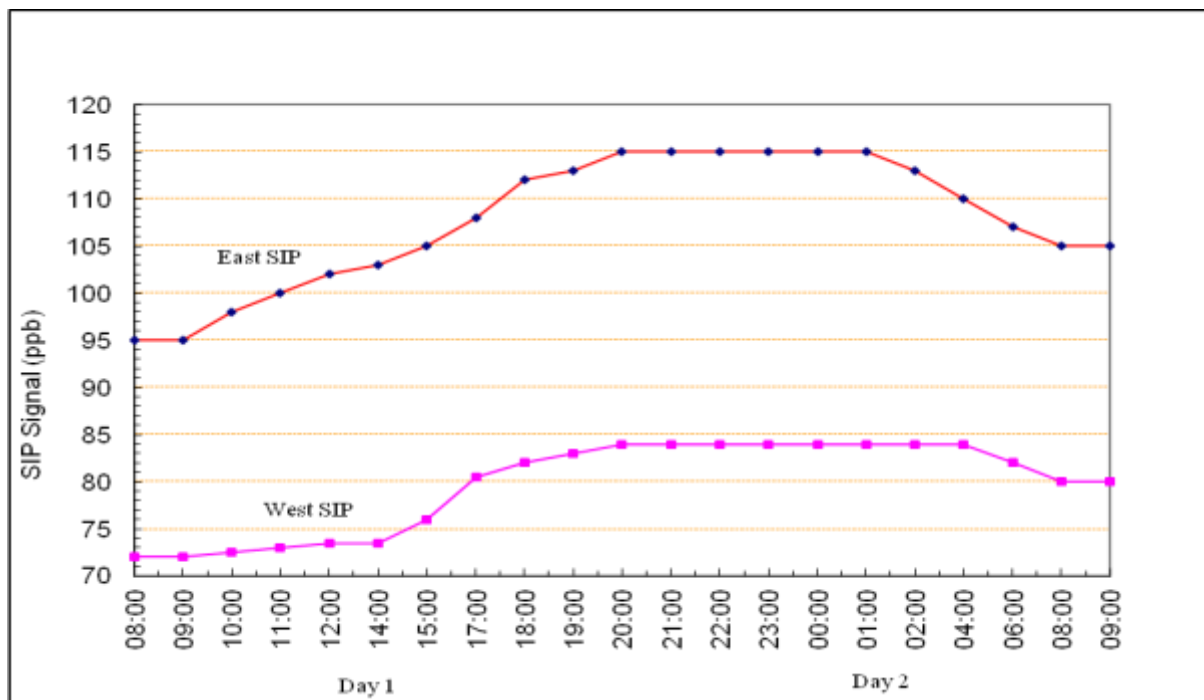
Fig. 3.15: Evolution of H_2 from feed water during experiment of isolation of cold trap

The initial C_H^{Na} before isolating the cold trap was 95 ppb as read by east loop SIP and 72ppb by west loop SIP. However, the stabilized values of C_H^{Na} after isolation of cold trap was 115 ppb and 84ppb. Later on valving in of cold trap, C_H^{Na} has started decreasing to the background value.

3.13.3 Variation in hydrogen background due to SG tube internal surface parameter

On first time valving- in of water in SG, the evolution of hydrogen was found to be very high. The hydrogen signal gradually increased and reached a maximum value of 220 and 70 ppb after 12 hours of valving-in water in SG from the background values of 105 and 45 ppb for west and east loops respectively [2]. The higher value logged for west loop is attributed to the lower trapping efficiency of the cold trap in west loop. The high value of hydrogen signal increase

during valving-in was analyzed and found to be due to the variation in the amount of hydrogen diffusing from water side of the SG walls into the sodium [60, 61]. This is strongly influenced by the chemical reaction process of forming magnetite which release hydrogen on the inner surface of the SG tubes. While this reaction produces hydrogen, it also coats the inner surface with magnetite, which reduces the H_2 diffusion.

Thus the hydrogen load in the flowing sodium depends on the Fe-H_2O reaction and on the extent of the free (from magnetite covering) fresh surface of the SG wall. The magnetite layer loses integrity and develops cracks due to the thermal and vibration induced shock. This also contributes to the hydrogen load. However, large H_2 load does not develop during continuous operation of the reactor with SG. There could be a minor increase in H_2 concentration in sodium due to occasional cracking of the magnetite layer, but it gets repaired soon. These increases are very small as compared with the very large signal increase on the occasion of a leak. Thus, a leak condition either simulated or actual gets positively detected.

3.14   Triplication of the System

Each secondary loop was initially provided with one SGLDS. There was no provision to confirm the genuineness of a leak signal and the availability of the system was very much dependent on the accuracy and performance of the single channel. To improve the availability of the plant by avoiding spurious actuation of leak signal, the system was duplicated in the first phase by adding one more nickel diffuser-vacuum system in each loop in series with the existing SGLDS.

 A third system with its own re-heater & economizer, nickel diffuser and SIP was then added, taking sodium sample from the common sodium outlet header as given in Fig.3.16 & 3.17. The output from the modified SIP units of the additional systems were connected to the computer system and the reactor trip from SGLDS is modified to incorporate 2/3 coincidence logic.

The calibration of the six SIP units installed in the triplicated systems in both loops of FBTR show good response to the leak simulation tests by injection of hydrogen as given in Fig.3.18 and 3.19. These tests provide useful data for evaluation of the performance of the SIP units.

The excellent experimental results on accuracy, reliability and detection speed obtained in these tests demonstrate the success of the selection of modified SIP units in place of QMS for leak detection.
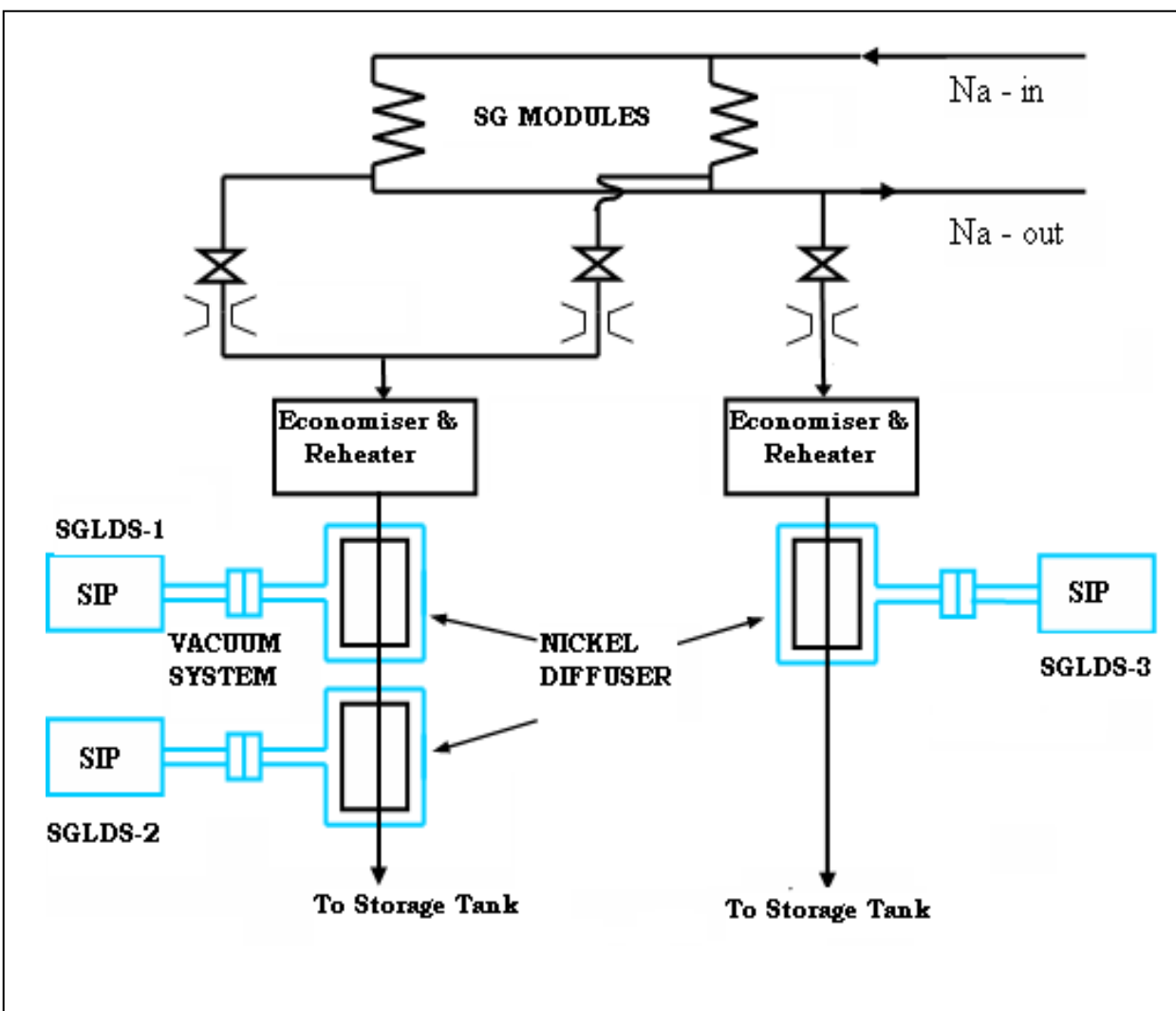
Fig. 3.16: Triplicated systems of SG leak detection loop

Fig. 3.17: Triplicated systems of SG leak detection photo
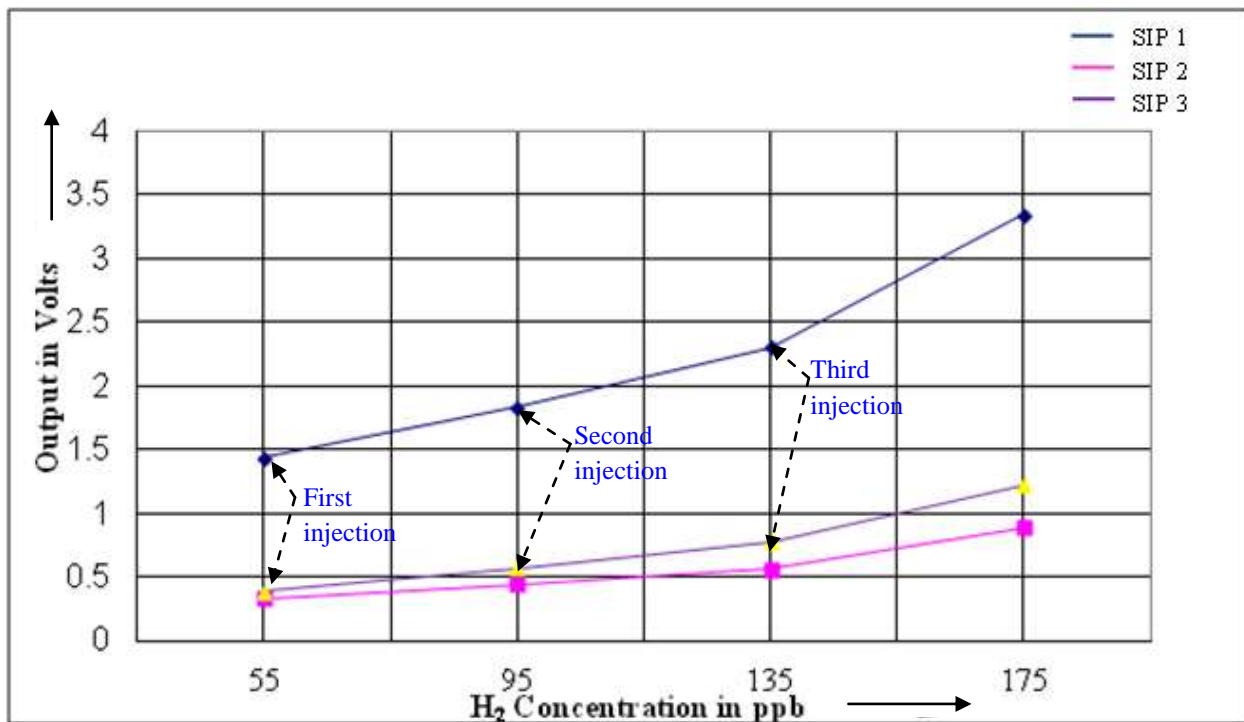
Fig. 3.18*:* Response of 3 nos of SIP in triplicated channels of east loop
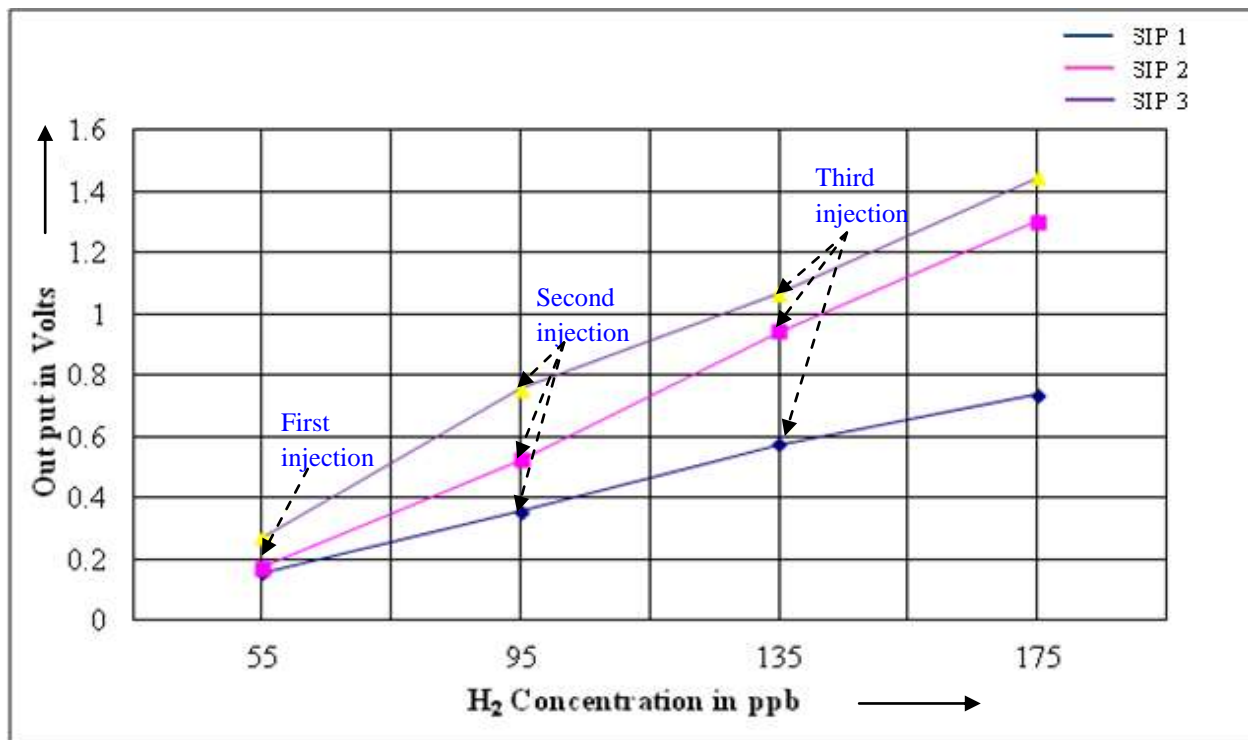
Fig. 3.19*:* Response of 3 nos SIP detector in triplicated channels of west

3.15. Summary

Sputter ion pump based SG leak detection system is reported to be used in some of the fast reactors, but information is not available in open literature regarding the processing of the sputter ion pump current signal for safety actions. The SIP circuit has been modified and the response has been evaluated and qualified by conducting various experiments. Calibration and testing procedures have been developed and safety actions have been formulated and implemented as given below:

- The reheater and temperature control circuit are modified to achieve the temperature at the nickel diffuser inlet within $450 \pm 1°C$ continuously.

- The evolution of hydrogen signal during the first time valving- in of water in SG was very high. The signal reached 220 ppb from the background value of 105 ppb of hydrogen in sodium. This increase was analysed and found to be due to the fresh internal surface of SG tubes generating H_2 by chemical reaction with H_2O.

- The SIP electronic circuit has been modified and after testing, the output signal has been wired for safety circuits. The QMS which takes approximately 2-3 weeks for replacement of analyzer filament and subsequent calibration, is removed from the safety circuits.

- Software algorithms have been incorporated which eliminates noise and spikes in the signal.

- A new approach by triplication has been proposed and implemented by retrofitting two more identical systems in each secondary loops and enhancing the safety logic to 2/3 redundancy.

- The developed SIP based system was found to respond well to leak simulation by hydrogen injection tests and during reactor power operation. Response time of the system was approximately 3 min.

- On-power calibration procedure (online calibration by the injection of reduced hydrogen concentration of 20 ppb during reactor operation) is formulated which can reduce the period of calibration by three weeks.

- The developed SIP based SG leak detection system has detected hydrogen concentration as low as 7ppb in sodium or a water leak of 1g/sec in three minutes.

Chapter 4: Acoustic leak detection system

4.1   Preamble

 The diffusion based hydrogen detectors used for detecting small leaks in SG have large response time of the order of 3 minutes and hence the leak cannot be detected at the incipient stage. Faster response of acoustic detector and its ability to detect leaks even in stagnant regions within the SG are the advantages of acoustic system in comparison with the diffusion system. This chapter compares the performance of detectors based on hydrogen in sodium with the acoustic detection technique under development.

4.2   Basic Principle

There are two methods in the acoustic technique. One is the passive method [62, 63], which detects leak by receiving sounds generated due to sodium-water reaction. Another is the active method [64] using ultrasonic waves. As is well known, hydrogen bubbles are generated at the time of a sodium-water reaction. An emitter is attached to the outside of a fluid component to generate a sound field, and the attenuation of sounds due to the passing of bubbles through the sound field is detected using a receiver. However, it is difficult to install this sensor close to the expected leakage place because of the relatively large thickness of the steam generator wall compared to the wavelength of the ultrasound. Thus, the ultrasonic sensors are located at the steam generator outlet nozzle using a waveguide through the penetration of the pipe. Thus, the sensing performance such as the leak detection sensitivity and response time depend on the transportation of the sodium bubble from the starting point of a sodium-water reaction to the steam generator outlet nozzle [65]. The ALD system consists of transducer, charge amplifier and signal processing circuits. The schematic of acoustic leak detection (ALD) system [66] is shown in Fig.4.1.
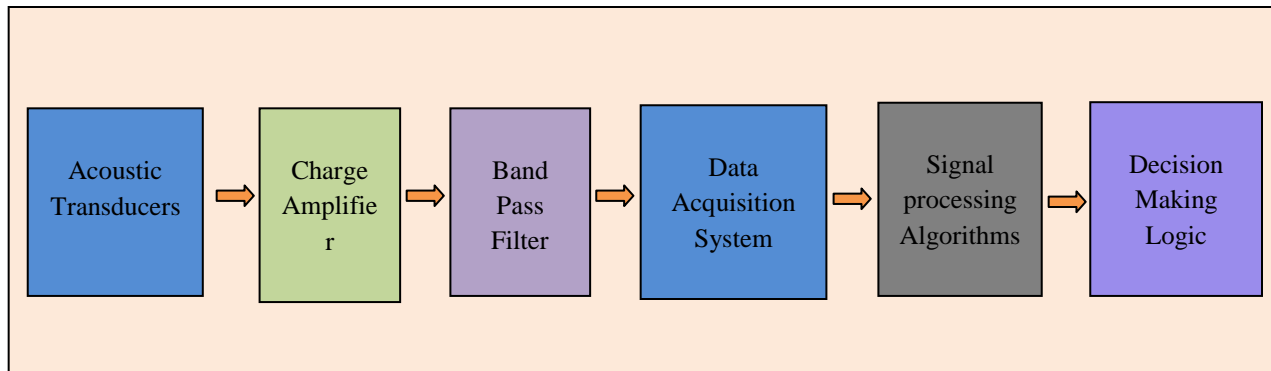
Fig. 4.1: Schematic of Acoustic Leak detection system

When water/steam at high pressure leaks into sodium, the main mechanisms of acoustic noise generation are:

a) Jet Noise: When water/steam at high pressure flows through the crack, acoustic energy is released due to turbulent flow conditions existing in the crack. The mechanism of conversion of kinetic energy to acoustic energy is based on the fluctuations in the flow momentum across the fixed crack surface. Acoustic signal from this source lies in the frequencies greater than 100 kHz [67].

b) Bubble Noise: Generation of pressure waves in sodium due to primary bubbling (water) and secondary bubbling (gaseous products of the reaction, like hydrogen) gives acoustic noise up to 10 kHz frequency range. This type of noise is characterized by strong low frequency peaks due to bubble resonance. Bubbles generate noise during inception, volume or shape oscillations and collapse.

At the first stage of leakage, steam jet noise and hydrogen bubble noise occur. Acoustic noise generated by the above mentioned mechanisms during leak in steam generator units can propagate either through the metal structure, or through the sodium or more likely through an

exchange of the mechanical energy between the two media. These signals finally appear on the external shell of the steam generator unit, where acoustic sensors convert them into electrical signals. When water/steam at high pressure leaks into sodium, acoustic noise will be generated whose signal to noise ratio is of the order of -10 to -16 dB [68, 69]. From the normal RMS of time signals, it is very difficult to judge the initiation of leak. Special signal processing techniques are required which can detect the leak whose signal/noise ratio is about -16dB.

4.2.1 *Waveguide as transducer*

Piezoelectric accelerometers mounted on wave guides are generally used as transducers in ALD. Piezoelectric sensor develops charge corresponding to the mechanical vibrations (acoustic signal). Charge amplifiers convert the charge into electrical voltage. Band pass filters are used to separate the leak noise signals from the prevailing background noise signals. Signal processing techniques are then used to discriminate the leak signals from the background noise. Decision logic gives alarm signal and initiates the safety actions in case of a leak.

4.3 Initial measurements at FBTR

As explained in Section 1.3, the FBTR SG is housed inside an insulated casing and temperature inside the casing is expected to be around 400°C. Initial experiments were carried out to study the detection capability of acoustic detector on the steam generator modules [70]. Measurements were carried out on two modules, one in each secondary loop. 20 mm diameter and 1 m long 2 ¼ Cr- 1 Mo ferritic steel wave guides were welded to the SG shell on the `U` bend portions and the wave guides were extended to casing outside through suitable penetration as in Fig 4.2.
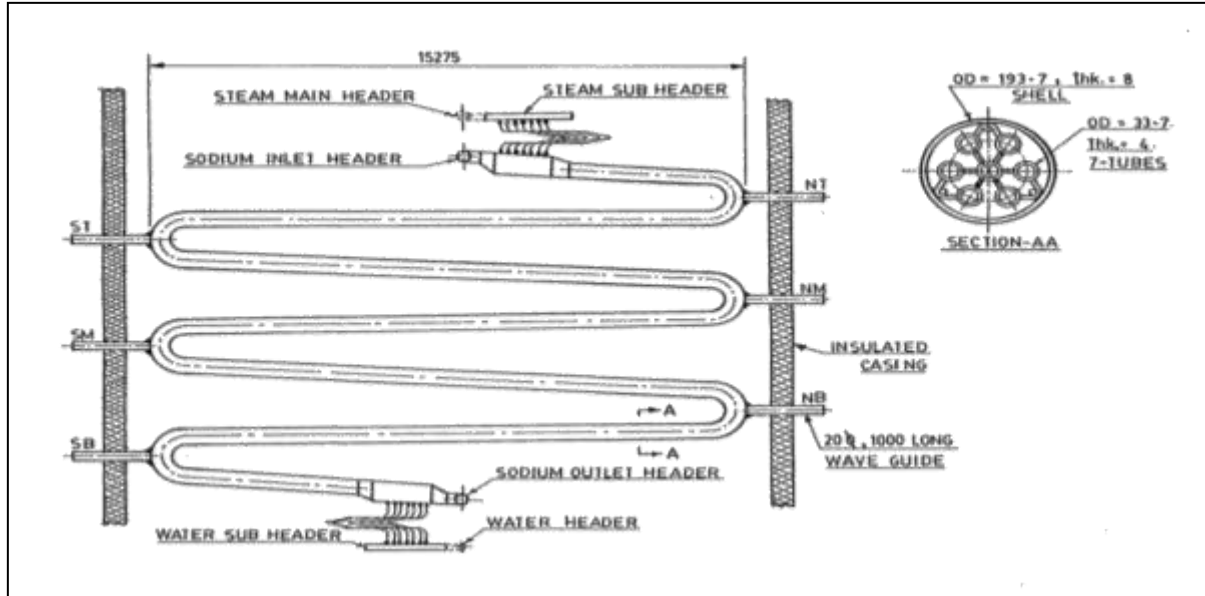
Fig. 4.2: FBTR SG Waveguides

These arrangements enabled installation of low temperature transducers at the cold end of the wave guide. Wave guides were installed on the `U` bend because this region contains tube to tube weld zones, a likely zone of failure. Piezoelectric accelerometers and acoustic emission sensors, which cover a wide frequency range, were selected for background noise and its characterization. The specifications of the transducers are given in Table 4.1.

Table 4.1: Specifications of the transducers

	Accelerometers		A.E.Sensor
	Type-1	Type-2	-80dB ref . 1 volt per Microbar
Sensitivity	45 pc/g	12 pc/g	
Mounted resonance frequency	27kHz	110kHz	
Frequency range(3dB)	to 9kHz	to 30kHz	100-100kHz;flat response type
Dynamic Range	2000g	2000g	

Sodium was filled into the SG modules and background noise measurements were carried out with only sodium flow. Preliminary measurements indicated that at sodium temperatures below

250 °C, diffusion type in -sodium hydrogen detectors are not very effective in detecting a leak. Only 40% of the injected hydrogen was found to be in dissolved form when the injections were carried out at different temperatures upto the sodium temperature of 250°C. At low temperatures hydrogen generated tends to remain in the form of gas bubbles. Hence measurements were carried out to check whether the acoustic transducers installed on the modules can detect gas bubbles in sodium flow. Known volumes of argon and hydrogen were injected into sodium through 20 mm inner diameter pipe at a point upstream of SG sodium inlet for these measurements. These were carried out at a sodium flow corresponding to a reactor power level of 10.5 MWt.
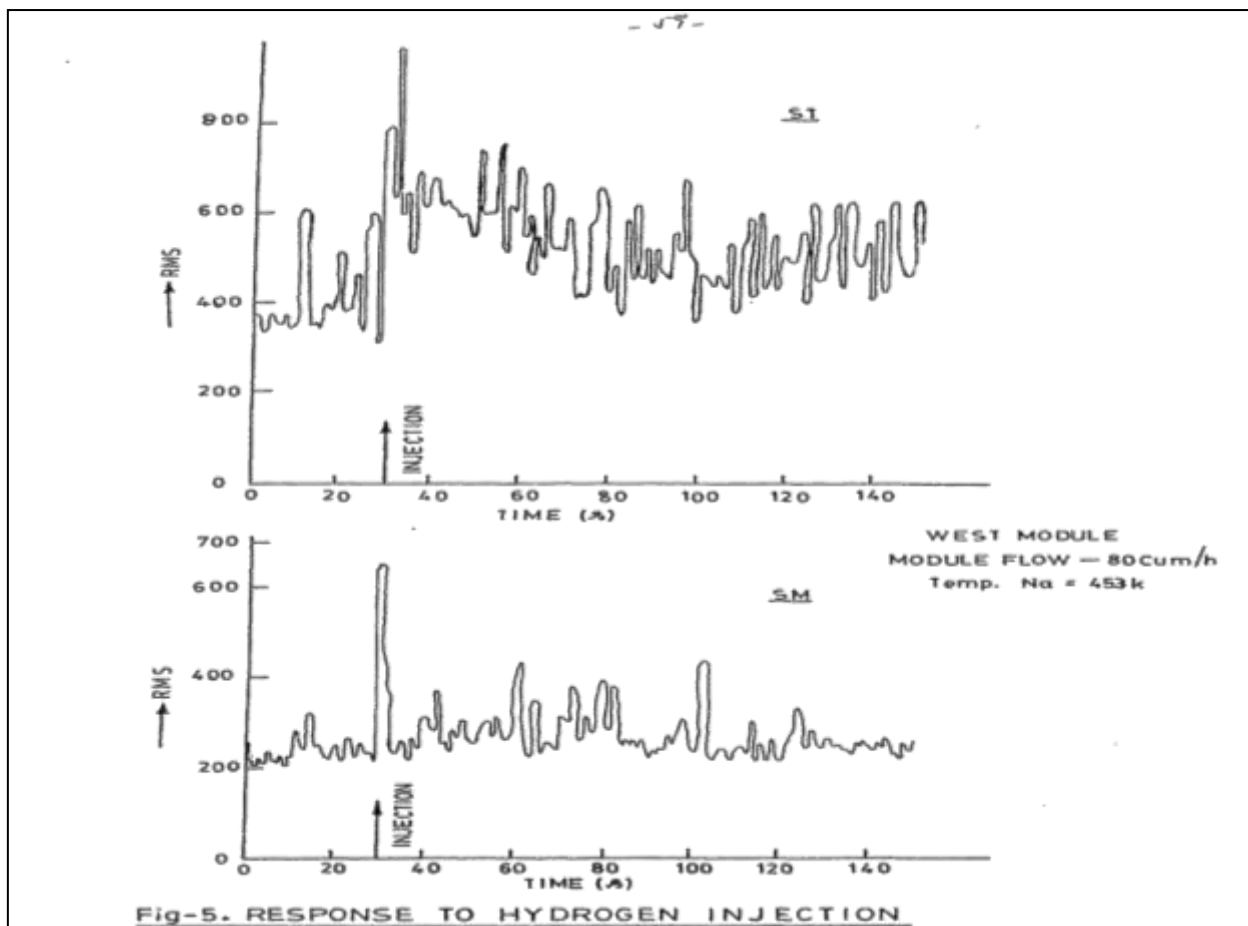
Fig. 4.3: Response to Hydrogen injection

From argon injections, it was established that the transducers responded when the volume of argon injected was about 1.4 liters at STP (circulating sodium volume was 16 m^3) and the response was not positive at much lower volumes like 0.2 liters. Signal level increased due to sodium flow containing gas bubbles. 1.4litres of hydrogen gas was injected into sodium in the west module at sodium temperatures of 180°C and 400°C. This corresponds to 40 ppb increase in hydrogen concentration in sodium, if all the hydrogen goes into solution. Fig.4.3 shows the response of transducers ST and SM to hydrogen injection at 180°C in the west loop [70].

All the above measurements were carried out over a bandwidth of 100Hz to 20 kHz at wave guide locations ST and SM. The two instrumented modules are identified as east module and west module, based upon their physical location in the plant. The sodium flow noise was measured and found to be random in nature. The RMS value of the signal was found to increase with flow with an exponent of 2 to 3 when measured at different flows between 0 and 143 m^3/h. Experiments showed that the acoustic transducers respond to the presence of hydrogen bubbles in sodium flow and hence has the potential for detecting leaks into low temperature sodium, when hydrogen tends to remain in gas form. The experiments indicate the detection capability of the acoustic detector and the requirement of developing signal processing techniques to have rapid response without any transport delay of the leak signal.

4.4   Experimental simulation of   sodium-water reaction

In a steam generator, the sodium and water/steam are separated by the wall of the steam generator tubes. If there is a hole or break in a tube, leakage of the water into the sodium may occur, resulting in a sodium-water reaction. There are several reaction equations during the sodium-water reaction [67].

The sodium-water reactions under actual steam generator conditions can be expressed by the combined reactions as follows:

$$aNa + bH_2O \rightarrow cNaOH + dNa_2O + eNaH + fH_2 \quad \text{(-31.8 Kcal/g.mol)} \tag{4.1}$$
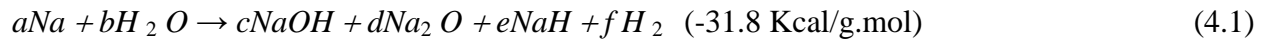
Where, a, b, c, d, e, and f are the mole fractions of the reaction. The hydroxides as shown in Eq.4.1 can activate the wastage effect of the steam generator tubes by erosion and corrosion, and result in multiple tube damages. The pressure of the steam generator during the sodium-water reaction eventually increases due to an increase of the heat and hydrogen gas pressure by the exothermic reaction. The leakages could be classified into four categories; micro leaks, small leaks, intermediate leaks, and large leaks. Table 4.2 shows the leak rates and its effect [71].

Table 4.2: Leak size and their effects

Category	Water leak rate[1]	Major effect
Micro leak	under 5×10^{-2} g/s	Self-wastage
Small leak	5×10^{-2} g/s ~ 10 g/s	Single target wastage
Intermediate leak	10 g/s ~2 kg/s	Multiple target-wastage & pressure increase start
Large leak	over 2 kg/s	Pressure increase

The micro leaks are in a leak range where practically no target wastage occurs, but the phenomenon of an enlargement of the diameter of the leak hole itself, called the self-wastage, can be seen. In the range of small leaks, the wastage of the impinged target is observed as a principal effect of the leakage.

These values are typical. Values of leak rate differ with the type, capacity and other conditions of steam generators. According to the IAEA co-ordinated research results, when a small leak (1g/sec.) occurs, the dominant noises are jet noise, bubble noise and droplet noise. The frequency bands of each noise were 600 kHz, for a low band, and 100 to 1000 kHz, respectively. It is noted

that the frequency band of each noise is not fixed. They depend on the leak size, leak propagation, and steam generator structure.

Originally, sodium-water interaction takes place with the formation of gaseous hydrogen, which is one of the reaction products. In the final stage of this process, a hydrogen bubble grows and separates from the section. At the moment of separation, the hydrogen bubble oscillates and generates sound with the resonance frequency. In the bubbling mode, hydrogen bubbles in liquid sodium oscillations are the main source of acoustic noise generation. The main source of SG background noise from the points of view of acoustic power level and wide frequency band is the water boiling noise generated inside the heat transferring tube and penetrating through the tube wall to the sodium. Measurements of background noise signals during the initial commissioning phase of the SG are very important from the point of view of choosing frequency range for acoustic leak detection.
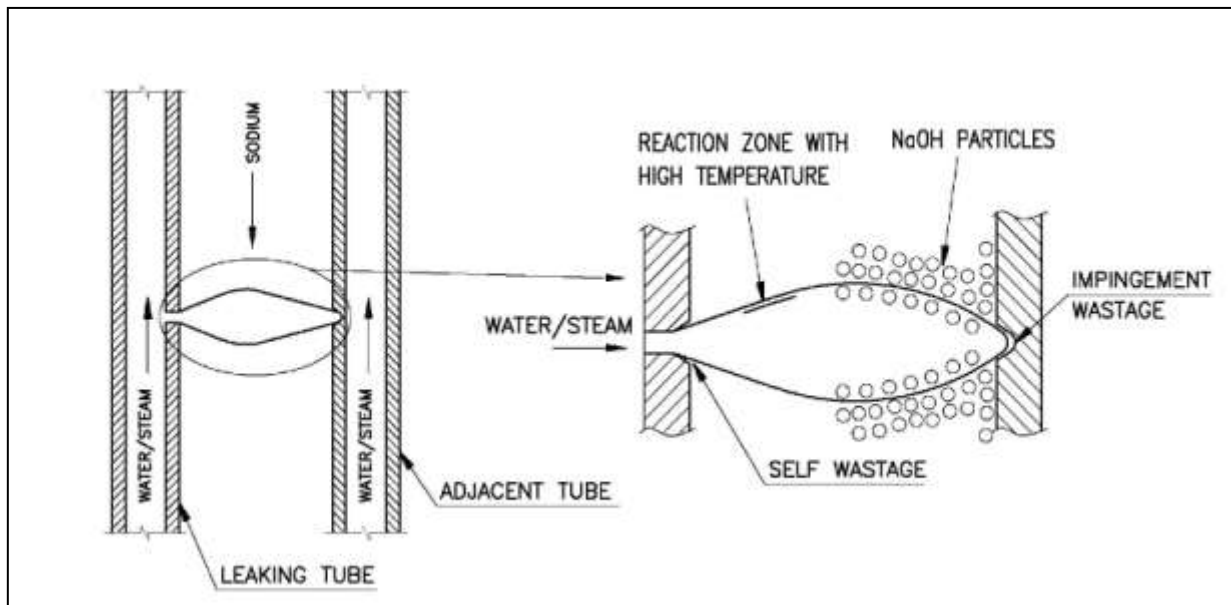
Fig.4.4 Impingement Wastage

The reaction products impingement on an adjacent tube of the leaking tube cause damage called impingement wastage which can puncture the adjacent tube in a short time as shown in Fig 4.4.

Impingement wastage is often expressed in terms of wastage rate, mm/s. It is the ratio of maximum depth of wall thickness penetrated to the time taken for penetration. The main parameters affecting impingement wastage are steam/water leak rate, sodium and steam temperatures, tube material, distance between leak tube to adjacent tube and sodium velocity. Wastage characteristics are important design data required for leak detector developments and for fixing the thresholds for SG safety logics.

A series of tests, simulating small leak in SGs of Monju reactor had been carried out in sodium water reaction test loop [72]. Injection nozzle used had a 0.3–0.7 mm diameter opening that was sealed with a rupture disc. It was kept at a distance of 26.5 mm away from the target tube. The quantity of steam injected was calculated from the pressure in the steam reservoir before and after the injection. The duration of injection was calculated from the opening and closing signals of injection valve. The target tube assembly, pressurized with 100 kg/cm^2 argon, could be pulled up after each steam injection to conduct the wastage tests successively. Tests were conducted with target tubes of 2¼Cr 1Mo steel and 9Cr Mo steels. Based on experiments, wastage correlations were obtained and are available in literature. They are used to quantify the development of SG leak which is needed to assess the requirements of SG leak detection and protection systems. Two of such correlations are shown in below.

$$WR = 15120 \times e^{\{[-0.255 \times \ln(3.42\, m/x) \times 2] + [5460/T]\}} \tag{4.2}$$

For 2.25Cr–1Mo steel, based on steam injection experiments with TN at 330–480°C and x at 6.35–25.4 mm [73]

$$WR = 6.0 \times e^{-[0.214 \times \ln(4m/x) \times 3]} \tag{4.3}$$

For 9Cr–1Mo steel, based on steam injection experiments with TN at 470°C and x at 12.5 mm. Experiments are conducted to develop suitable signal processing techniques for acoustic

detectors in a Sodium Water Reaction Test facility (SOWART), which is constructed to study various aspects of sodium-water reaction phenomenon. It consists of sodium circuit, water circuit and other auxiliary systems as shown in Fig. 4.5.
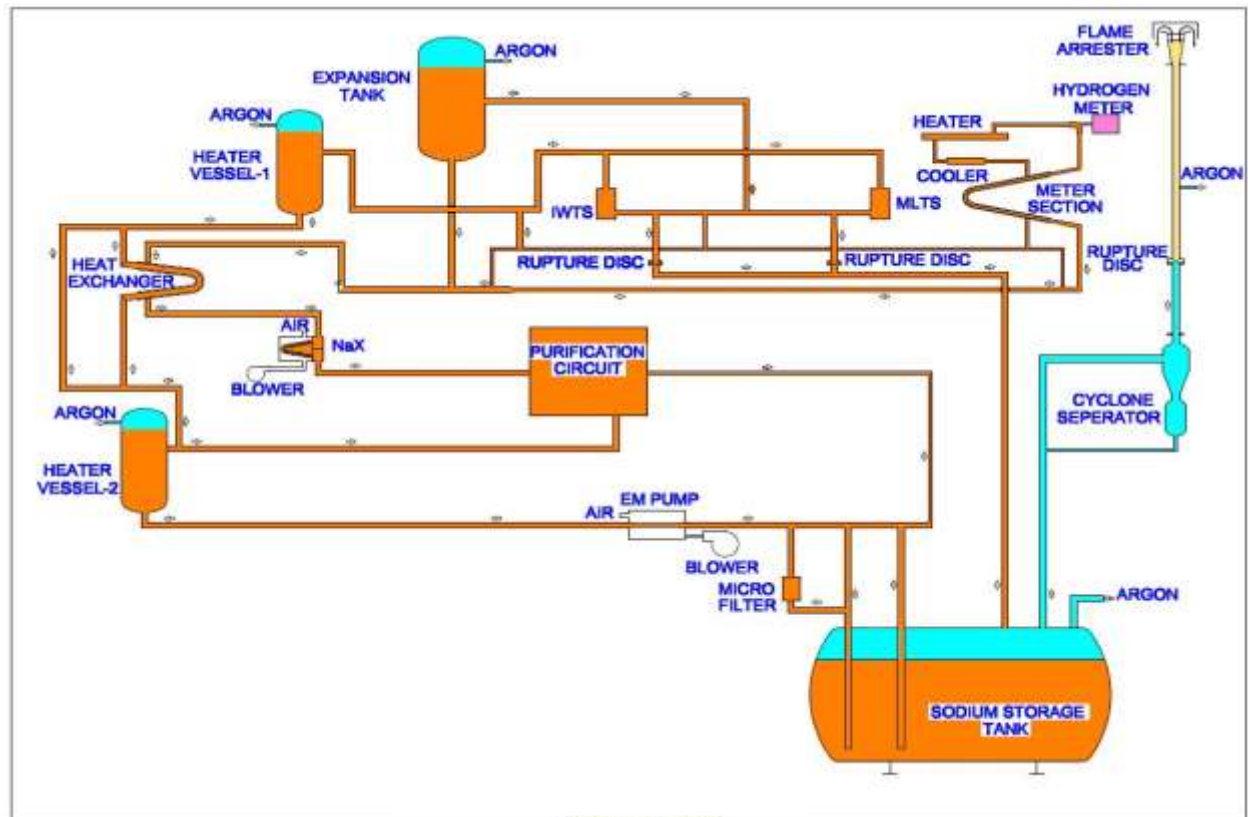
Fig.4.5: Sodium water reaction test facility (SOWART)

The total sodium inventory is 10 t. An electromagnetic pump is used to circulate sodium. The hot leg is designed to handle sodium at a maximum temperature of 530°C. A large cold trap is made available so that contaminated sodium can be purified in a short time. Two heater vessels and an expansion tank are provided with argon space over sodium free surface.

The facility is equipped with other diverse detectors such as SIP based hydrogen in sodium detector, hydrogen in argon detector (HAD), electro chemical hydrogen meter (ECHM) in addition to acoustic detectors. The steam system comprises of a 12 litre vessel and associated

piping. Water in steam vessel can be heated up to 353°C to produce saturated steam at 172 kg/cm^2. Further, steam will be passing through heater lined pipe lines to get superheated to 480°C. Both sodium and steam systems are provided with rupture discs as safety against over pressurization.

4.5 Leak simulator test setup and methodology

Test section with leak simulator is shown in Fig.4.6. Tubes made of 9Cr-1Mo, 15mm outer dia and 2.2 mm thickness were used for fabricating injectors and target tubes. A piece of the tube, sized to 160 mm length, was used for manufacturing injector. The tube was locally thinned down to about 0.5 mm/1mm to make 0.1 mm or 0.2mm pinhole by mechanical drilling (depth of the pin hole is limited to about 5 times the dia of hole, due to machining constraints). Through-hole was ensured by passing argon at around 100 bars at room temperature.
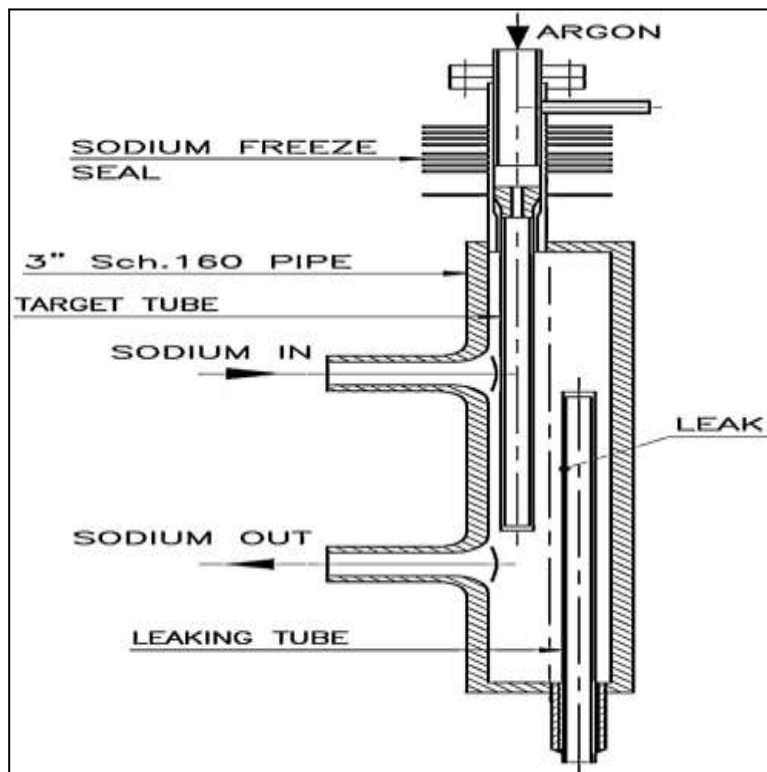
Fig.4.6: Leak simulator schematic

The hole diameter was measured using an optical measuring device. One end of the injector was dummied and the other end was welded with a SS 316 extension tube. Target tube was kept pressurized with argon at 4 bars during the test. It was fixed with flanged joint below which a sodium freeze seal would be established due to the cooling fins provided. The locked up pressure in target tube would be monitored during the experiment. The pressure falls as soon as the tube gets punctured. An orifice is provided inside the assembly which will regulate the sodium entry into the top part of target tube after the tube gets punctured.

Injector was placed in such a way that leak was oriented towards the centre line of the target tube. Once steam is admitted into the injector, it leaks out, forming a sodium water reaction jet that impinges on the target tube.

SOWART was filled with sodium with test section isolated. Sodium circulation, heating and purification were carried out to bring the loop to the experimental conditions. Cold trap and storage tank would be isolated. Prior to sodium admission to test section, argon was purged through the injector, so that sodium entry into the injector, which was connected to the steam line, was prevented. When steam of required quality was produced, argon would be isolated and steam would be charged. Sodium water reaction was monitored and instantaneously detected by acoustic detectors and subsequently by hydrogen meters. The maximum length of steam injection time was limited by a timer controlled by a PLC. At the end of reaction, steam supply to test section would be cut off automatically by using pneumatically operated steam inlet valve and vent valve. During experiment, target tube was pressurized to 4 bars with argon, a pressure higher than that of sodium. Puncturing of target tube could be noticed from the argon pressure fall in the tube [74].

4.6 Results

Tests were carried out with sodium at 500°C for a leak rate of approximately 500mg/sec as per the conditions given in Table 4.4 [75]. As steam was admitted, there was immediate response of acoustic signal. But after 150 seconds, ECHM and SIP signals also increased indicating sodium water reaction. Steam injection was continued for 720 seconds. Towards end there was sudden drop in target tube pressure from 4 kg/cm^2, indicating puncture of target tube. Immediately, steam was vented and sodium was dumped. Once removed the target tube was found punctured.

The response of acoustic sensors during the steam injection experiment in SOWART facility is given in Fig. 4.7, 4.8, 4.9, 4.10 [76]. During this test, large variation in acoustic signal level was observed. The acoustic detector continued to work even after the sodium water reaction whereas the ECHM and flow meter reached the saturation limits. SIP indicated leak and immediately tripped due to over hydrogen concentration. ECHM showed its peak but gradually decreased. Sodium flow meter signal was fluctuating, indicating presence of hydrogen bubbles.

Table 4.3: Experimental Conditions

Sodium velocity through test section(m/s)	Sodium/Steam temperature (^{o}C)	Steam pressure (kg/cm^2)	Sodium pressure (kg/cm^2)	Duration of injection (sec)	Increase in Hydrogen concentration ECHM (ppb)
1.65	500	172	1.6	720	>1450
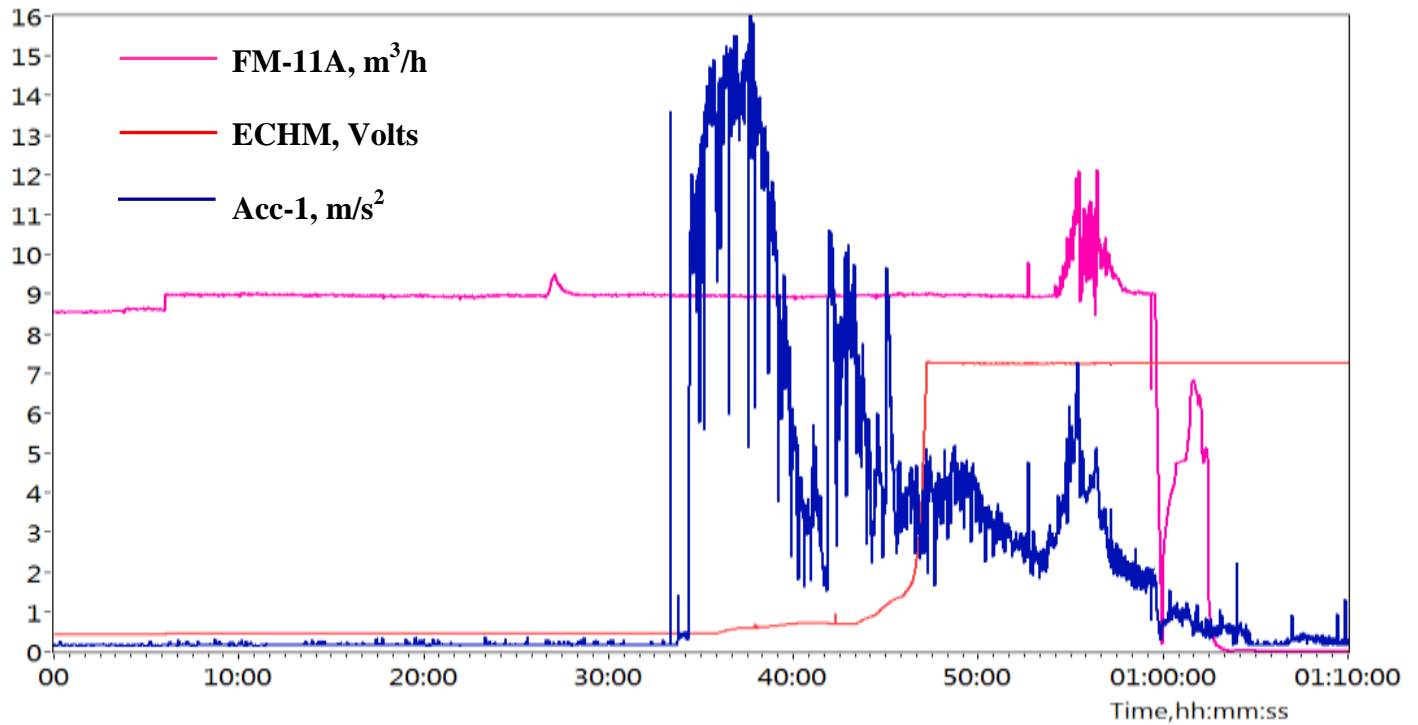
Fig. 4.7: Response of Acoustic sensor-1, PMFM and ECHM during Experiment

Fig.4.8: Zoomed Portion

RMS Plot
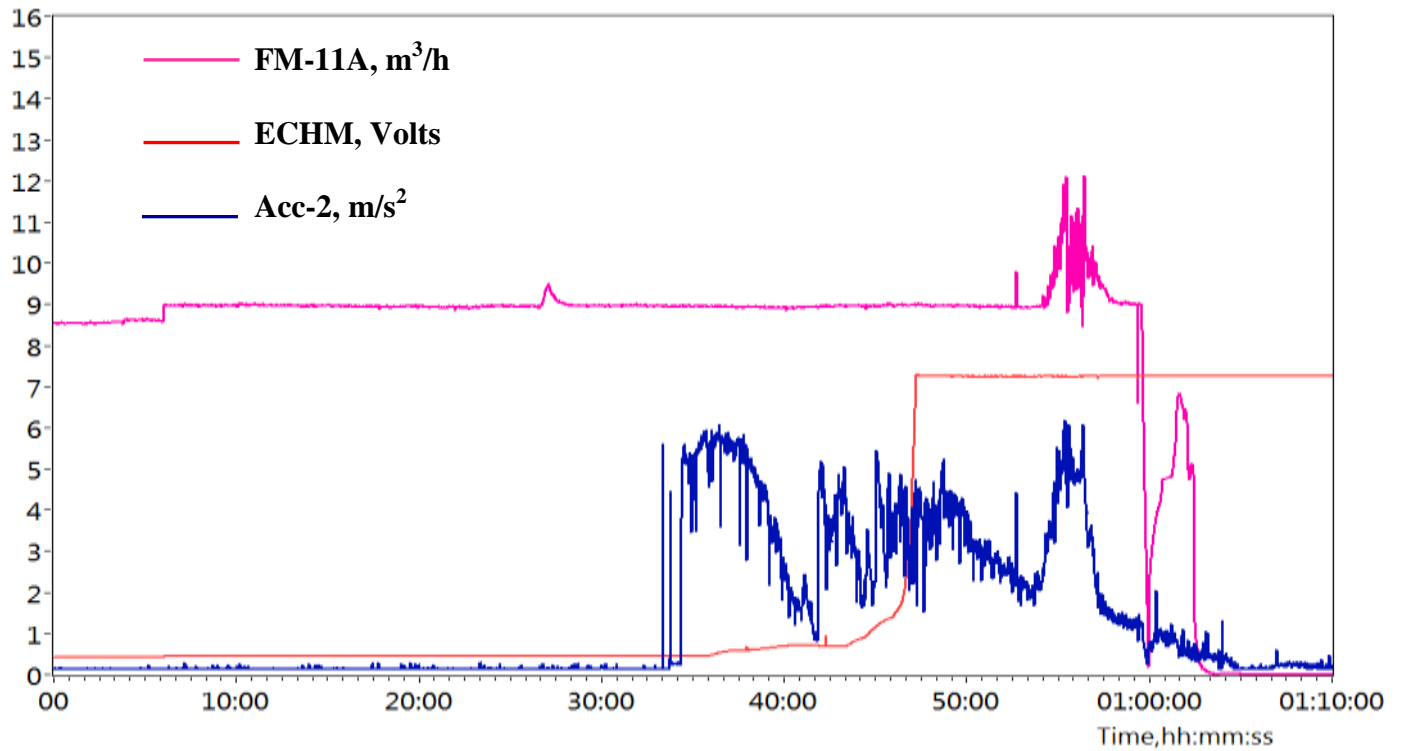
Fig. 4.9: Response of Acoustic sensor-2, PMFM and ECHM during experiment

RMS Plot
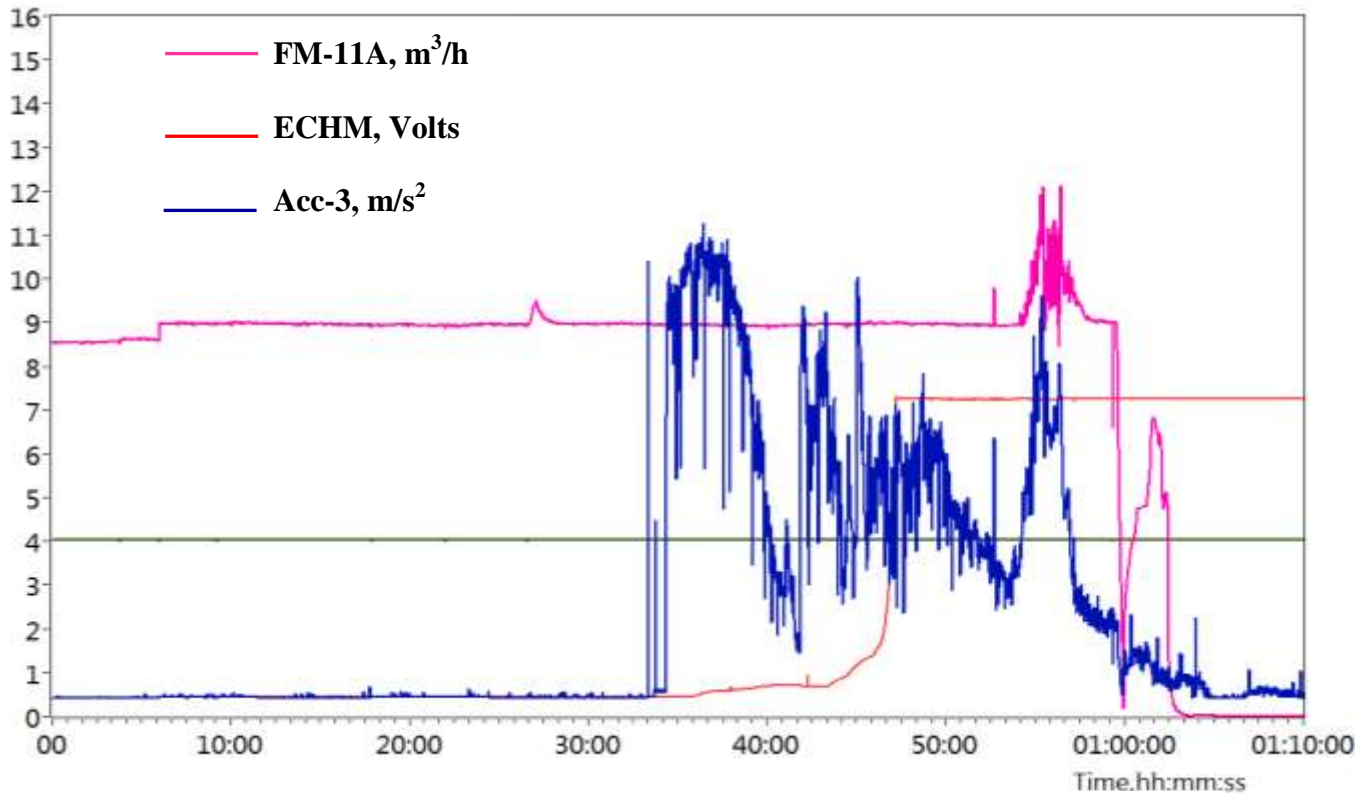
Fig. 4.10: Response of Acoustic sensor-3, PMFM and ECHM during experiments

Though the start of sodium water reaction can be fairly identified, all the acoustic detectors signals are dominated by noise. Second experiment was carried out at higher leak rate of 3.2g/sec. During the experiment the flow through test section was kept around $10m^3$/h. Steam pressure was 172 kg/cm^2. Tube to tube distance was approximately 18-19 mm. SIP, ECHM and TCD were in service. As the flow through IWTS is very low (compared to SG) the hydrogen concentration rise due to a leak would be very high. Even though it is a small leak, the local concentration would rise by many ppm, which is beyond the operating range of SIP. Hence, it trips as soon as hydrogen is detected. Similarly ECHM also rises to its upper limit value, 1440 ppb. Throughout the experiment, the intensity of steam injection was sensed by acoustic sensor.

4.7 Summary

The response of diffusion based hydrogen detectors are compared with the response of acoustic detectors by analyzing the signals from FBTR and SOWART leak simulation experiments and found that the acoustic technique is faster than hydrogen detection based techniques. The acoustic detector also responded for extended period of time despite tripping of SIP and ECHM during the SOWART experiments.

Chapter 5: Development of Diverse detectors

5.1 Preamble

The confirmation of leak signal at all sodium temperatures and identification of the leaking SG module requires the development and deployment of diverse methods and the chapter details the research efforts concerning electrochemical hydrogen meter and hydrogen in argon detector.

5.2 Electrochemical hydrogen meter (ECHM)

5.2.1 Principle of ECHM

Hydrogen detection in sodium involves measurement of the hydrogen partial pressure in equilibrium with the dissolved hydrogen in sodium. Hydrogen partial pressure (p_{H2}) is correlated to concentration of hydrogen in sodium (C_H) by Sievert's law [10]:

$$\left(p_{H_2}\right)^{1/2} = \frac{C_H}{k} \tag{5.1}$$

where, k is the Sievert's constant for this system, which is found to be almost independent of temperature.

Electro Chemical Hydrogen Meter (ECHM) is a concentration cell and can be used to measure the hydrogen pressures. The cell is represented as [12]:

$$p_{H_2}(\text{sample}) \, | \, \text{electrolyte} \, | \, p_{H_2}(\text{reference}) \tag{5.2}$$

The electromotive force that develops across the electrolyte is given by Nernst relation [9]:

$$E = \frac{RT_M}{2F} \ln\left(\frac{p_{H_2}(ref)}{p_{H_2}(sample)}\right) \tag{5.3}$$

where, the reference hydrogen partial pressure, p_{H_2}(reference) is known and fixed at the sensor operating temperature, p_{H_2}(sample) is hydrogen partial pressure in sodium, R is universal gas constant, F is Faraday constant and T_M is the temperature of meter operation. A mixture consisting of oxides of calcium and magnesium along with magnesium metal and calcium hydride is used as the reference electrode that fixes the reference hydrogen pressure at the meter operating temperature. Hydrogen activity in sodium fixes the sample hydrogen pressure. The electrolyte used in the above cell should have high conductivity for hydrogen ions (proton or hydride ion) and be thermodynamically stable at typical operating temperatures of $400 - 500$ °C and at the prevailing hydrogen pressures of $0.05 - 5 \times 10^{-5}$ kg/cm^2. Based on the systematic study involving electrical conductivity measurements and phase diagram studies carried out, a hydride ion conducting solid electrolyte based on $CaBr_2$-$CaHBr$ system has been chosen for this application and an electrochemical hydrogen meter has been developed in house [77].

5.2.2 Configuration of the ECHMs and their testing in sodium systems

The sensor produces an emf output which is logarithmically related to the concentration of hydrogen in sodium. The instrumentation which consists of preamplifier assembly and ECHM display unit processes the sensor signal suitably and makes it available for recording. A schematic diagram of the electrochemical hydrogen sensor along with its preamplifier assembly is shown in Fig.5.1 [78].

The meter consists of an iron thimble of 16.5 mm outer diameter, 0.5 mm wall thickness and 40 mm height for housing the electrolyte and another one of 8 mm OD, 0.5 mm wall thickness and 25 mm height for holding the reference electrode materials. Both these components were machined from pure soft iron bars. The electrolyte thimble was then welded to a stainless steel pipe which in turn was welded to a knife-edged flange of 70 mm diameter. The reference

electrode mixture was hermetically weld closed inside the other iron thimble. It was then welded to a stainless steel rod of 3 mm diameter through a connecting sleeve. The electrolyte was cast from its molten state and filled up the annular gap between the two iron thimbles. The preamplifier assembly was housed in a stainless steel cylindrical module and attached on the top of the sensor flange. Output from the preamplifier assembly and display unit were connected through shielded cables.
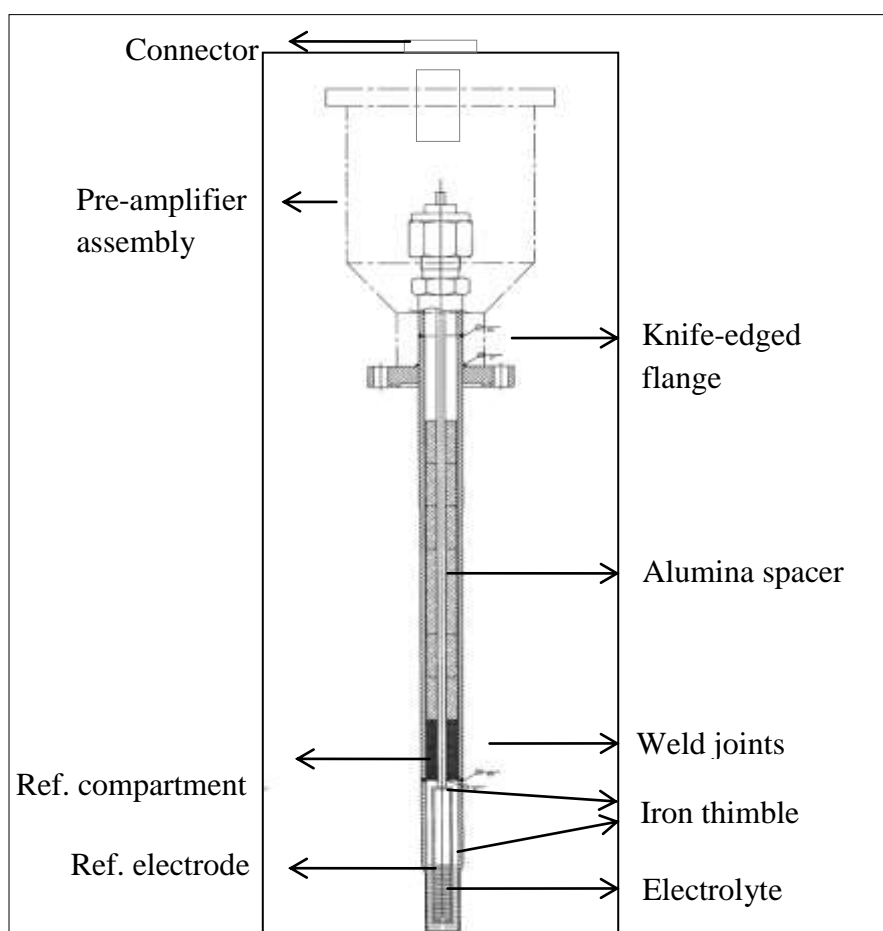
Fig. 5.1: Schematics of electrochemical hydrogen meter cum preamplifier [73]

The meter, after its assembly, was tested and calibrated in mini sodium loops (containing about 2.5 kg of sodium) in the laboratory for a period of three months before incorporating it in the

sodium circuits. The hydrogen level in this sodium loop was maintained at any particular concentration (C_H) by controlling the cold trap temperature, T_{CT} and is related by the following equation [79]:

$$\log(C_H / ppm) = 6.467 - \frac{3023}{T_{CT}}$$

(5.4)

The output of the meter was in the millivolts range. Amplified output from the preamplifier unit was converted into pulses so as to enable the transfer of the signal without any interference over long distances to the power supply cum display unit. In the display unit, the signal in pulses was converted back to analog output, digitized, displayed in volts and was also made available for recording purposes. These sensors along with the instrumentation were then installed in sodium facilities of SGTF, SOWART and FBTR and their performance was evaluated. The typical calibration graph of the sensor as a function of hydrogen concentration in sodium is shown in Fig. 5.2, covering the hydrogen concentration range from ~50 to ~300 ppb in sodium. The ECHM is found to detect about 10ppb increase in hydrogen concentration over a background of 50 ppb [80].
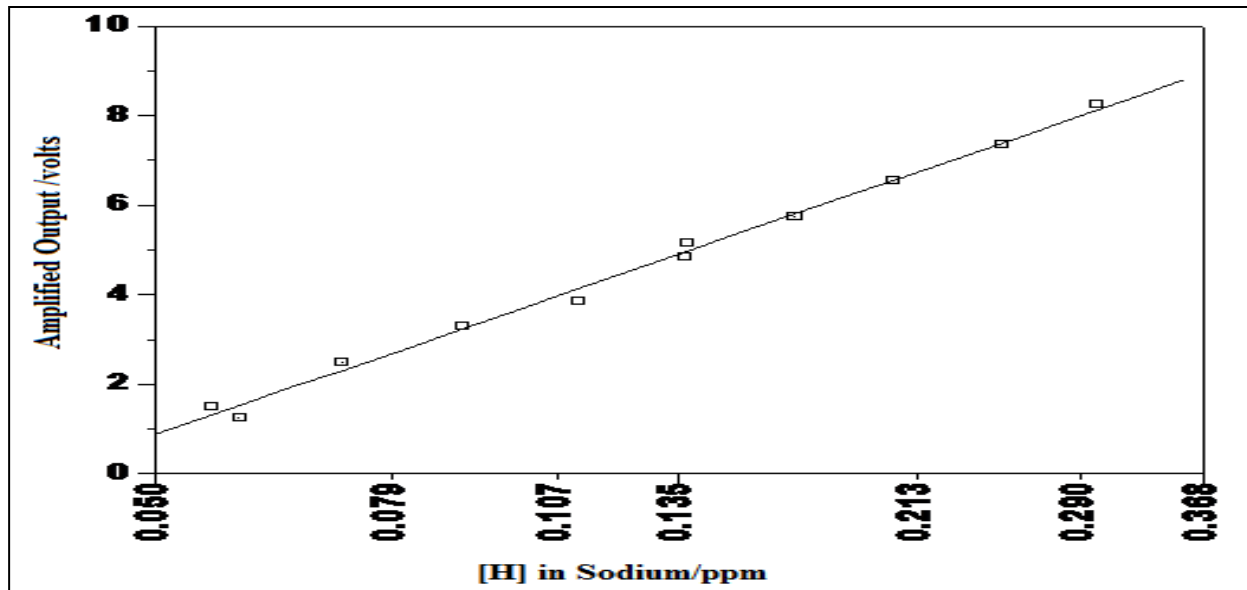
Fig. 5.2: Output of ECHM as a function of hydrogen concentration in liquid sodium

5.2.3 Performance of ECHM in large sodium facilities and FBTR

ECHMs were located in these sodium circuits just upstream of diffusion based hydrogen meters that use sputter ion pump as detector. Both these detectors were periodically calibrated / tested for their performance by injecting a known amount of hydrogen into sodium at temperatures above 350°C after isolating the cold trap from the circuit. Sodium temperature in the sensor section of the sodium circuit was controlled at 450 ± 1°C. Temperature coefficient for the meter is found to be 2% of hydrogen level in sodium per deg.celcius. Thus, when the [H] in sodium is 50 ppb or 100 ppb, the temperature coefficient is 1 ppb/ ^{o}C or 2 ppb/ ^{o}C, respectively. Fig.5.3 shows the ECHM installed at FBTR.
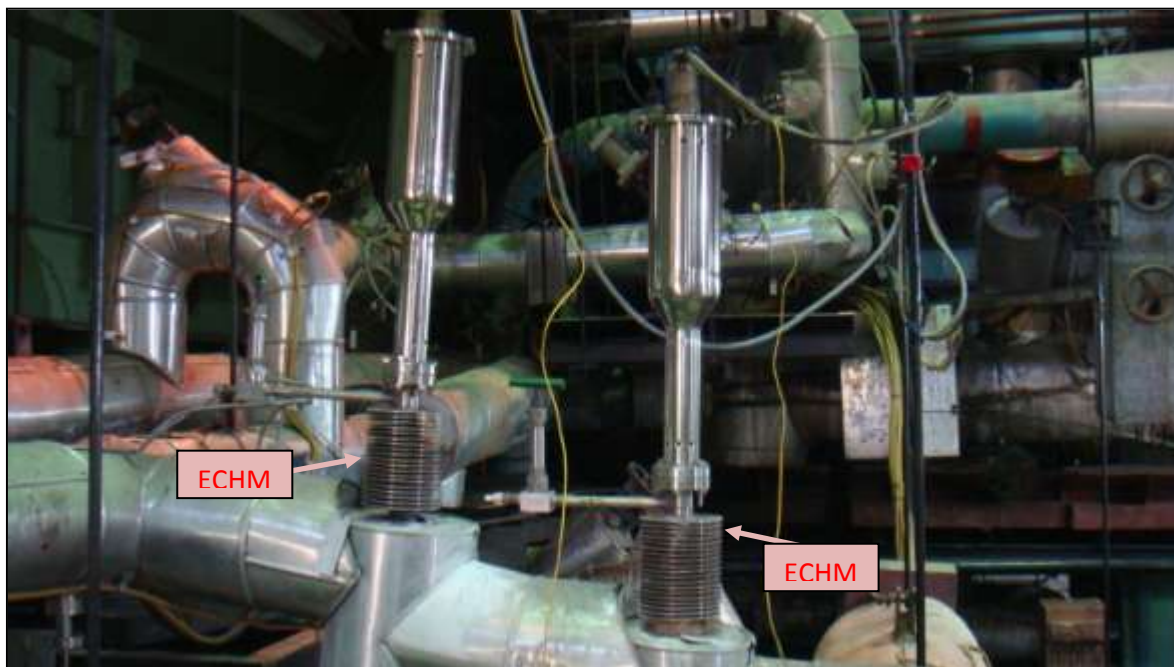
Fig.5.3: Electrochemical hydrogen meters installed at FBTR sodium circuit

Figure 5.4 shows the response of ECHM, SIP and the cover gas hydrogen sensor using thermal conductivity detector (TCD) to hydrogen injection in SGTF. The response was in-phase with the diffusion based sensors for hydrogen detection. Since the sodium temperature was > 400 ^{o}C, the output from Thermal Conductivity Detector (TCD) sensor, which monitored hydrogen levels in argon cover gas remain unaltered.
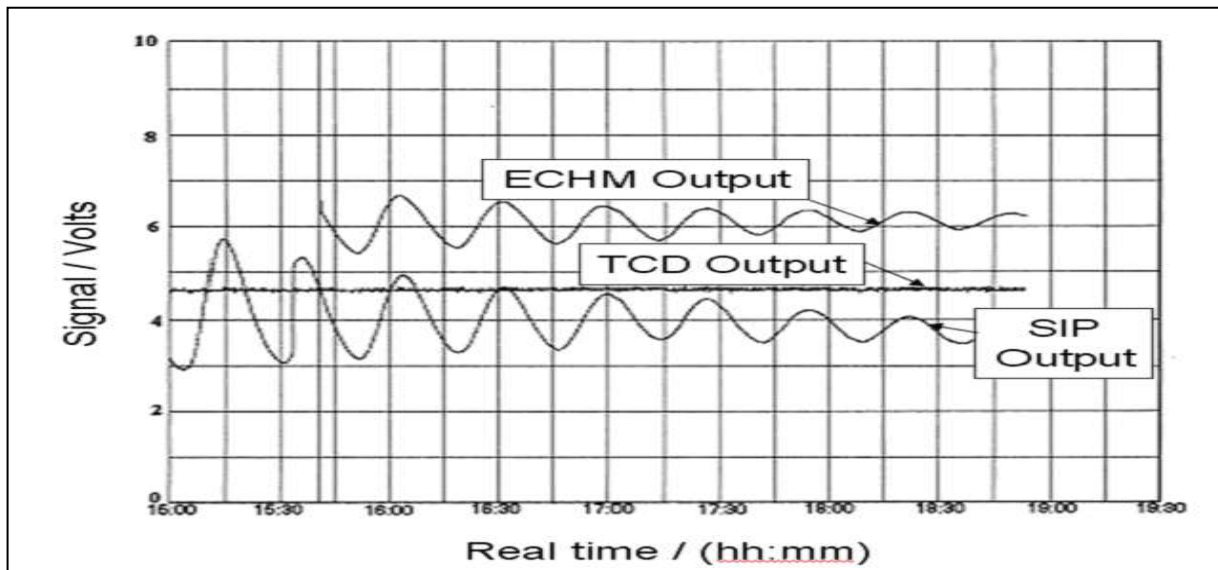
Fig.5.4: Response of the electrochemical sensor to hydrogen injection in sodium at SGTF

Figure 5.5 shows the response of ECHM to steam leak simulation experiment at SOWART, where steam leak at the rate of 55 mg/s was made for 11 minutes. After one to two minutes i.e., time taken for the transport of hydrogen from leak site to meter section, both HSD and ECHM started giving signals. At this leak rate of 55 mg/s, local hydrogen concentration is expected to be high (4-5 ppm).
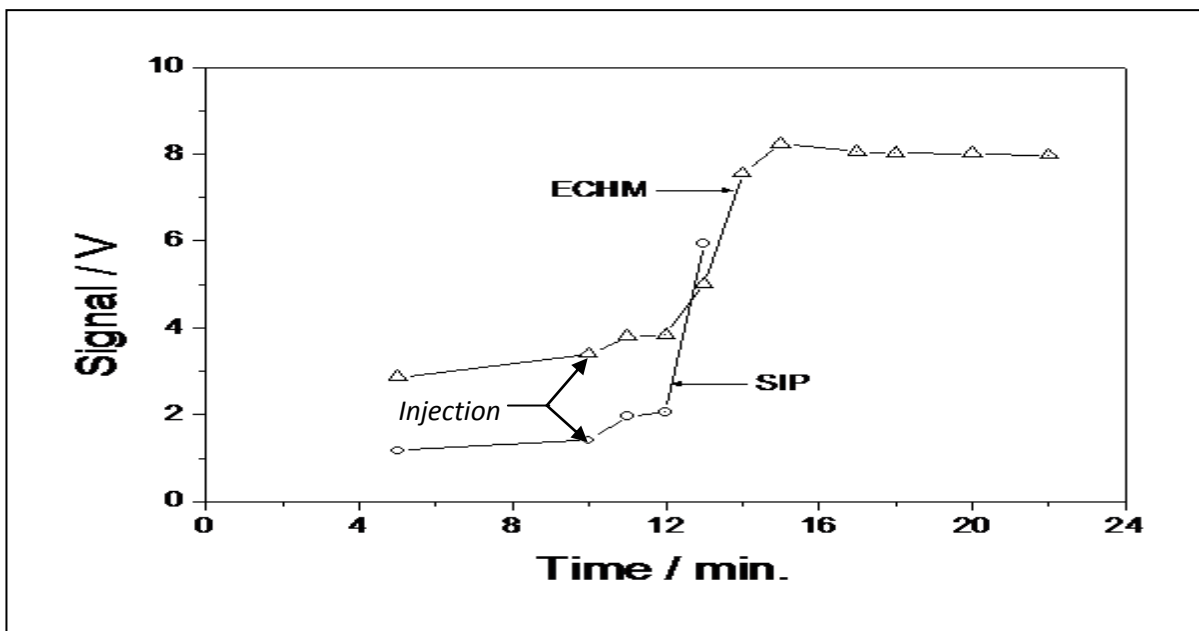
Fig.5.5: Response of ECHM and SIP during steam leak experiments

129

Figure 5.6 shows the response of ECHM and SIP in FBTR where 40 ppb hydrogen was injected into sodium three times successively. ECHM responded instantaneously for all the three injections. Within the framework of IGCAR-CEA collaboration on Sodium-cooled Fast Reactor (SFR) Safety, an ECHM was installed on the intermediate circuit of Phenix reactor, in order to assess its performances in realistic conditions.

The response pattern of ECHM and the diffusion based meter using a quadrupole mass spectrometer (QMS) detector to hydrogen injection at Phenix plant was found to be in the same order of magnitude (to within five seconds). Further, when cold trapping was stopped for 48 h and then reopened to remove the hydrogen in Phenix plant, the response of ECHM was found to be in-tune with three other diffusion based hydrogen detection systems positioned at different locations in the plant [81].
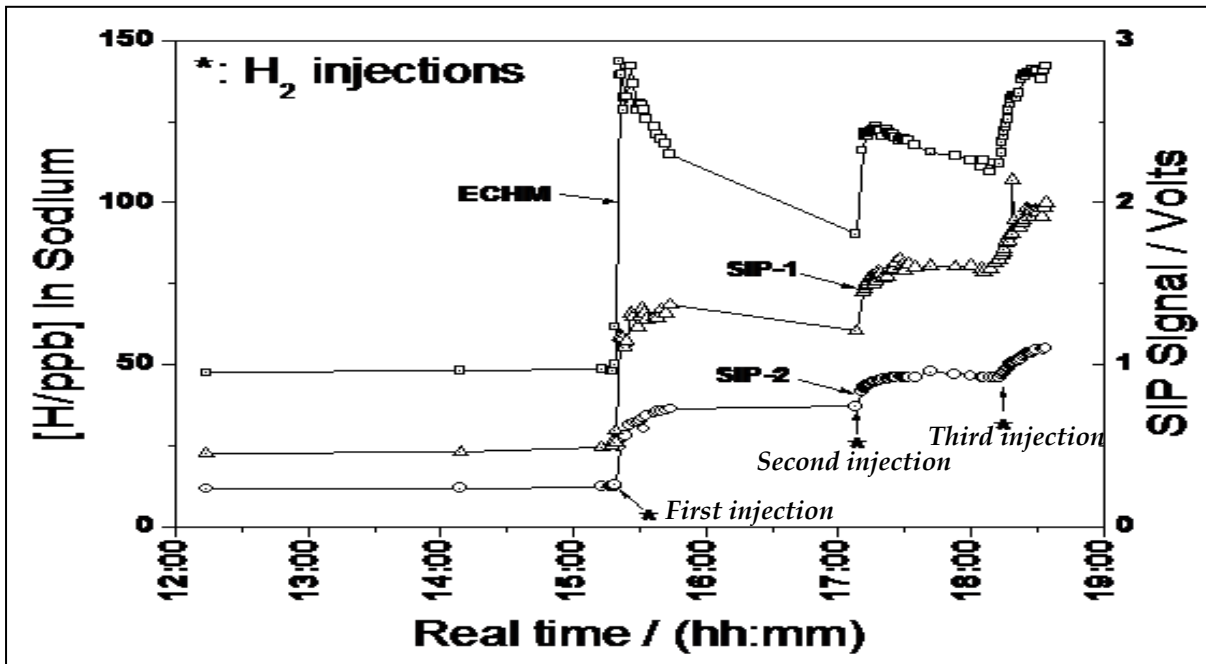
Fig.5.6: Response of ECHM to triple injection of hydrogen in FBTR

The performance of ECHM and SIP were evaluated during the experiments at sodium facilities and in FBTR. The response of both SIP and ECHM during reactor power operation is given in

Fig. 5.7**.** At a higher sodium temp of 400 ^{o}C, the response of the diffusion type meter and Electro Chemical Hydrogen Meter are in agreement with the calculated values. The response time of ECHM is found to be slightly longer than SIP for low hydrogen evolution during power operation.
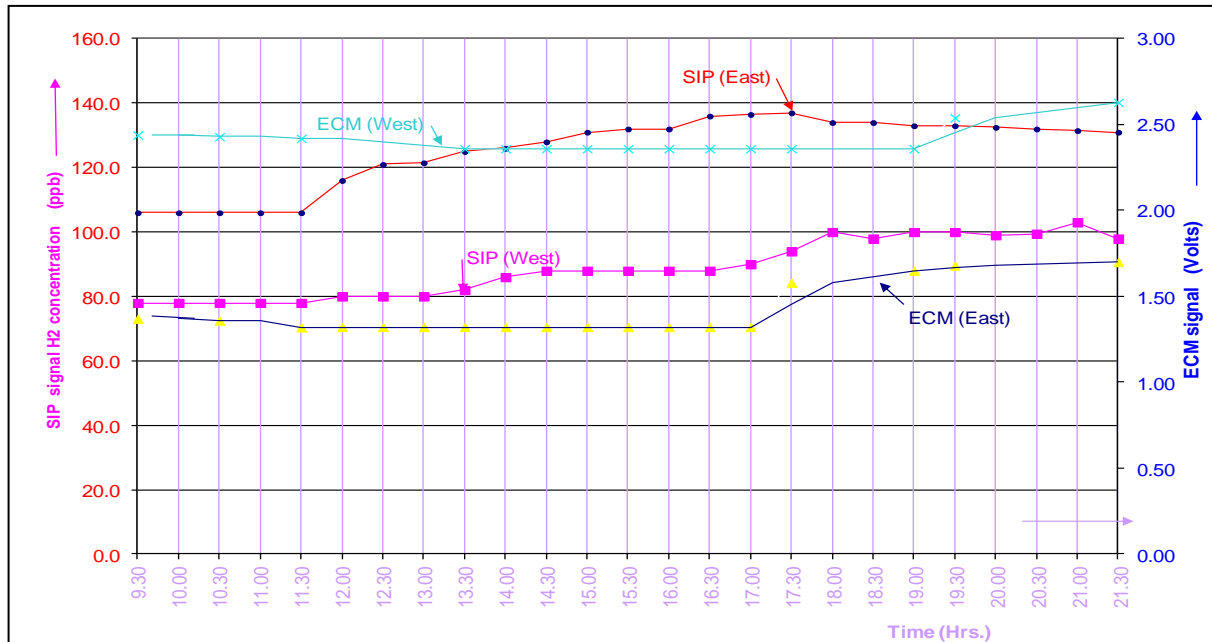
Fig.5.7: Response of detectors during reactor power 13.5MWt

5.3. Hydrogen in argon detection (HAD) system

5.3.1 Hydrogen in argon detector

The hydrogen evolution in sodium during a water / steam leak primarily depends on the size of the leak. Alternatively, an accurate measure of the evolved hydrogen can be translated to the size of the leak. Apportioning of this hydrogen between the amount dissolved in sodium and the amount reaching the cover gas space of the expansion tank is a function of the sodium temperature and it also depends on bubble size and location of leak. The hydrogen produced by Na- H_2O reaction dissolves completely in sodium at T_{Na} > 375 ^{o}C whereas its dissolution is 2% at T_{Na} of 180°C accordingly, the undissloved hydrogen reaches the cover gas space.

The HAD provided in expansion tank is effective in detecting H_2 in the cover gas at lower sodium temperature. The mutually exclusive temperature ranges for good efficiency of HSD & HAD can be combined to achieve good efficiency of leak detection in the total temperature range.

At sodium temperatures below ~250°C, any hydrogen in sodium gets released to the cover gas, whenever it reaches a free sodium capacity. For detection of hydrogen in cover gas, a thermal conductivity based detector was developed in house. It works on the thermal conductivity principle. The meter consists of a nickel tube assembly housed in a stainless steel vessel which forms part of the piping in the cover gas of sodium system. For effective working, this tube needs to be maintained at 500°C and this was achieved by a heater. Pure argon as carrier gas was passed through the nickel tube and was subsequently allowed to pass through the arms of Wheatstone bridge.

Due to the differences in thermal conductivities of the two streams (reference argon gas & argon with sample gas) an unbalance is created in the bridge and the output of the meter varies. The output is proportional to the concentration of hydrogen in the cover gas. Hydrogen in Argon Detector (HAD) is installed over argon balance line above expansion tank. The flow sheet of HAD is shown in Fig.5.8.

The layout is conducive for natural convection flow of cover gas from expansion tank through the detector back to the expansion tank via reaction product discharge line. The argon carrier gas from the supply header was connected to the inlet of the purification tower that contains the catalyst and molecular sieves. The purification step removes impurities such as moisture and oxygen from argon gas stream.

The emerging argon from the purification tower is connected to a 5µ SS filter and then through a line regulator to the SS buffer tank. The line regulator is to be set to control the line pressure at 10 psig.

From the buffer tank (which is meant for taking the pressure fluctuations) the gas is passed through a rotameter where the gas flow can be controlled at desired flow rate. From rotameter the gas is passed through the reference cell of TCD to the inlet of a 2-way-sample - bypass valve. If the valve is in bypass mode, the gas is passed through the sample cell of TCD unit and is made to exit into the atmosphere.

If the valve is in sample mode, the gas is passed through nickel coil assembly. Hydrogen diffusing through walls of the nickel coil is swept by the carrier gas into the sample cell of TCD and then is made to exit to the ambient. Due to the difference in thermal conductivity between Ar-H_2 mixtures in the sample cell with respect to that of the pure argon gas in the reference cell, the TCD produces a DC output. A compact and square type block heater of 100Ω resistance is provided on the TCD block to maintain it at a desired temperature. A thermocouple of 1 mm dia is soldered on to the top surface of TCD block. The temperature of the block is controlled by a PI controller through a 24 V transformer to the heater. The TCD block is to be maintained at 55°C. This detection system based on the thermal conductivity difference existing between argon and hydrogen is utilized to detect hydrogen in the expansion tank cover gas argon [82, 83].

The nickel sensor and TCD block temperature are controlled by dedicated PID temperature controllers at 500 ± 1°C and 150 ± 1°C respectively [84, 85]. In the sample mode, carrier gas after passing over a pair of (reference) resistances goes through nickel tubes and picks up hydrogen, if any and then passes over the remaining pair of (sample) resistances of the bridge. It causes an imbalance in the output voltage, which is directly proportional to the hydrogen

concentration. Periodically the system is to be kept in detector bypass mode for the original set value if there is any drift. The bridge is kept inside a block and the temperature is maintained above the ambient temperature to make the bridge output independent of ambient temperature variations.
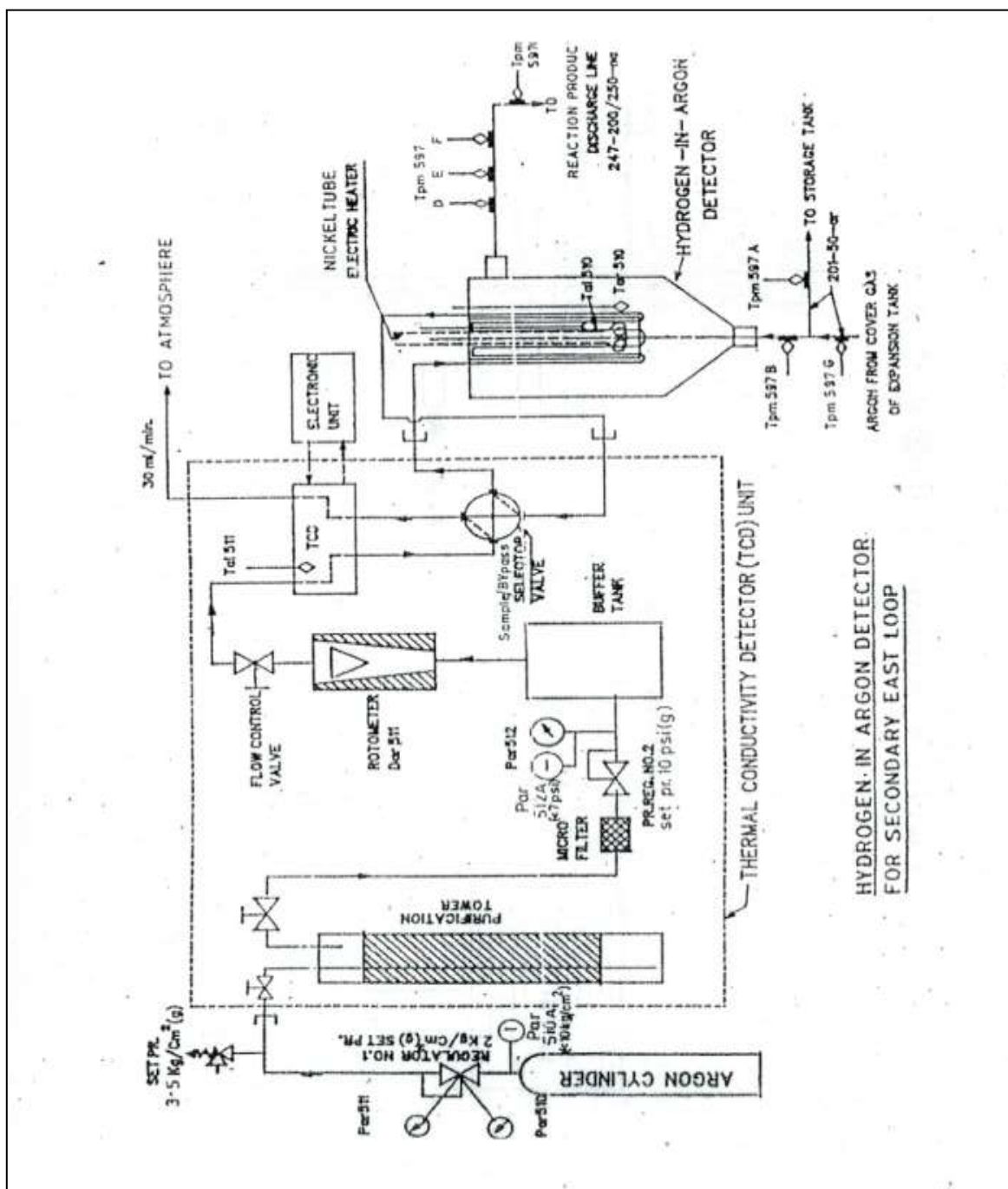
Fig.5.8: Hydrogen in argon detector layout

5.3.2 Principle of thermal conductivity detector (TCD)

Thermal conductivity of hydrogen is many folds higher than that of other gases. Thermal conductivity detector (TCD) makes use of the difference in conductivity of the two gases. Through the thin wall of nickel coil, hydrogen in the cover gas argon diffuses into the nickel tube and is swept away by a flowing carrier gas into a TCD for analyzing the hydrogen concentration in the sample (purified argon at a fixed flow rate from a separate argon manifold is used as the carrier gas). TCD works with Wheatstone's bridge principle. TCD block contains two cells; one is a reference cell and the other one is a sample cell. Each cell contains a pair of filaments arranged in the form of a Wheatstone's bridge. The fresh carrier gas passes through the reference cell to the nickel sensor. As it goes through the nickel sensor, it collects hydrogen diffused from the other side and goes to the sample cell of TCD. Due to the difference in thermal conductivities, the filaments will be subjected to two different temperatures causing a potential difference to develop across the bridge. This voltage is calibrated against hydrogen concentration. Cover gas space of the steam generator or a capacity downstream of the steam generator can be monitored for pick up of hydrogen.

 This method is useful during start up and low power operation since the sodium temperature is normally low under these conditions and there is a possibility that hydrogen evolved by sodium/water reaction is carried by sodium in gaseous form and can escape into the cover gas. Relatively large quantity of hydrogen is available in the cover gas as compared to the fraction that is dissolved in sodium for the HSD to detect.

In this method, a coil of nickel tube is inserted into the cover gas to be monitored. A carrier gas, normally argon, sweeps the hydrogen diffused through the wall of the nickel coil. The carrier gas passes through two chambers of the thermal conductivity detector (TCD) block before entering

the Ni- coil and the gas coming from the nickel coil is passed through the other two chambers of the TCD block. Each chamber of the TCD houses a heated filament and these filaments form a Wheatstone bridge. When there is no hydrogen present in the cover gas, the bridge is balanced and the balance is offset when the carrier gas picks up hydrogen. This method suffers from problems arising from large transport time though the gas phase transport is faster than the transportation of dissolved H_2 in liquid sodium.

The Hydrogen in Argon Detector (HAD) makes use of a thin nickel membrane in the form of coil for hydrogen detection in argon cover gas of expansion tank. Hydrogen which diffuses through the nickel membrane from the cover gas at the operating temperature is carried by pure argon to a thermal conductivity detector (TCD), which gives a DC output signal that is directly proportional to the hydrogen concentration in the gas. The TCD makes use of the difference in thermal conductivity between argon and argon–hydrogen mixture to detect the concentration of hydrogen in Ar-H_2 gas mixture.

This unit maintains a constant current supply to the filaments in the reference and sample compartments of TCD. Also it amplifies the TCD output and the amplified signal output can be fed to a recorder.

The TCD used is of GOW-MAC (USA) type 10-460 [84]. This uses a flow through geometry. The overall size of the block is 3 x 5 x 2 cm. The filament material is gold sheathed tungsten having a cold resistance of 48 Ω at 25°C. The specifications of TCD are given in Table 5.1.

Two of the filaments are used in the reference gas (argon) and the other two in the sample gas section (argon + hydrogen). As the thermal conductivity of hydrogen is greater than that of argon, the bridge produces an imbalance voltage which is proportional to the hydrogen concentration in the cover gas. The TCD uses four closely matched filaments forming the four

arms of a Wheatstone bridge. An interlock is provided for sample flow such that the filament excitation is switched off to avoid the filament burn out when the sample flow is not there.

Table 5.1: Specifications of TCD

Make	GOW-MAC (USA)
Type	10-460
Filament material	Gold sheathed tungsten with a cold resistance of 48Ω at 25^0C
Configuration	Four closely matched resistances of 48 ohms each, two each in reference and reference gas sections in the opposite arms of wheat stone bridge.
Normal bridge	Constant current of 90mA
Normal gas flow	30ml/minute.

The instrumentation system for TCD contains a constant current source for exciting the TCD, a bridge balancing circuit besides many other electronic circuits to cater to the needs of the system such as various dc regulating voltages, amplifier circuits, and current limit circuit to prevent sensor burnout and alarm circuits to annunciate any abnormal process condition [87,88,89,90].

5.3.3. *Calibration of TCD by hydrogen injection in the cover gas*

The setup and procedure for calibrating this detection system by injecting hydrogen in the cover gas space of expansion tank for arriving at the sensitivity of HAD and the results are discussed here. The calibration setup consists of a standard tank `c` of 1550cc volume to store hydrogen for injecting into cover gas space. The HAD and the injection circuit are shown in Fig. 5.9.
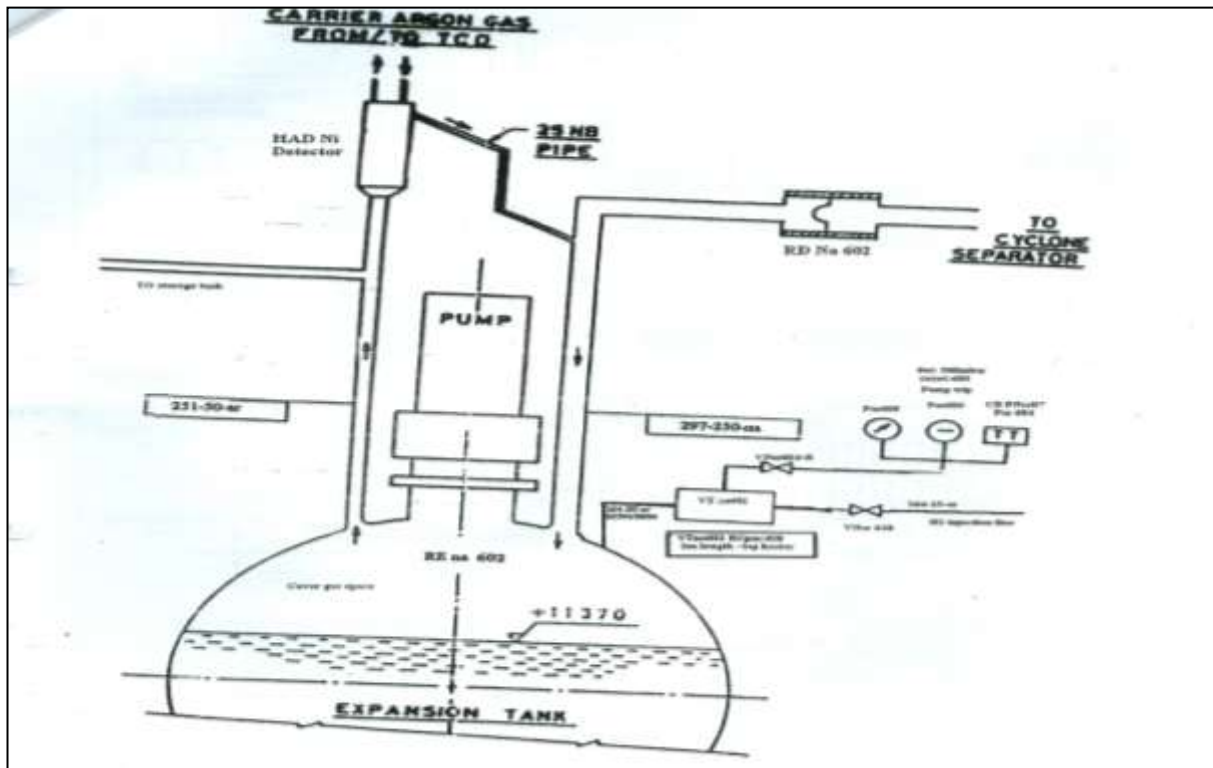
Fig. 5.9: Hydrogen in argon detector and injection circuit

Argon and hydrogen cylinders are fitted with high pressure regulators and gas manifold for pressurizing the tank with hydrogen and argon to the required pressure levels. Additionally, the argon cylinder is used to purge the standard tank C and the injection line from the hydrogen tank to the expansion tank cover gas before actually injecting hydrogen. The required quantity of Hydrogen can be injected into the expansion tank cover gas, by the hydrogen tank pressure drop method as discussed in Appendix-3.

The secondary sodium is maintained at a temperature of 250°C and hydrogen injection is effected isothermally. During this injection process the pressure in the transmitter line goes up to 5 kg/cm^2 which could cause tripping of the secondary sodium pump, so during this calibration process, the secondary sodium pumps are stopped. The expansion tank cover gas space was isolated from the cover gas space of the storage tank to limit the volume of injection.

The carrier argon cover gas flow, TCD output signal and TCD current were maintained steady at 0.5 lps, 1.85 V and 90mA respectively with no discernible fluctuation or drift. The temperature of the Ni membrane was maintained at $500 \pm 1°C$ and that of TCD block temperature was maintained at $55 \pm 0.5\,°C$ through the use of dedicated temperature controllers.

During the calibration operation, the cold trap is bypassed, secondary sodium pump switched off and the water side of the steam generator drained. The static secondary sodium temperature is maintained at 250°C. Hydrogen injection is effected by the following steps:

i)   The standard calibration tank `C` in the injection setup is pressurized with argon to 0.1 kg/cm^2after thorough purging. The pressure is then raised to 1.1 $kg/cm^2$with hydrogen.

ii) The mixture of argon and hydrogen is injected into expansion tank cover gas space from the standard tank till a reduction of pressure from 1.1 to 0.3 kg/cm^2 is reached. The injection line is flushed into the cover gas with argon. This corresponds to a 6mg of H_2. The HAD responds within a period of 420s of injection including the 120s time for flushing. The signal is seen to stabilize after 300s. There was a 0.8 volts rise in HAD output from 1.85 to 2.65V, indicating a sensitivity of 0.33V per 100 ppm(v) of hydrogen. At the end of the calibration the total system is restored by the following steps:

   a)   The cover gas spaces of the expansion tank and the storage tank are communicated

   b)   The secondary sodium pump is started and flow normalized

   c)   The cold trap remains bypassed and the H_2 injection set up is disconnected

The calibration procedure is repeated 4 times with different quantity of hydrogen injection to establish the repeatability of the measurement of the secondary of this meter. The results are tabulated in Table 5.2.

Table 5.2: HAD Calibration

Sl. No.	Qty of H_2 injected(vpm)	HAD signal(V)			Expansion tank pr(mb)			Na Temp(°C)	HAD sensitivity (mV/ppm)
		S_1*	S_2*	S_3*	P_1#	P_2#	P_3#		
1	100	4.21	4.54	0.33	43	49	6	190	3.3
2	200	4.26	4.84	0.58	34	45	11	189	2.9
3	250	4.3	5.15	0.85	37	51	14	189	3.4
4	300	4.36	5.26	0.9	66	84	18	190	3

∗ S_1 and S_2 are the signals before and after H_2 injection into cover gas respectively and S_3

in increase in signal value after injection.

P_1 and P_2 are pressure values of the cover gas before and after H_2 injection respectively

and P3 is increase in pressure value after injection.

Average sensitivity obtained = 3.1 mV/ppm(v)

5.4   Summary

The genuineness of a leak signal can best be judged by confirmation with a diverse system. The

diverse detectors have been developed as given below:

- An electrochemical hydrogen meter has been developed in house and it has been

  evaluated along with SIP during leak simulations and reactor operations. The ECHM can

  detect 10ppb of hydrogen concentration in sodium or 1.25g of water leak in SG in 3

  minutes.

- Thermal conductivity based hydrogen in argon detector has been developed to detect

  small leaks when the sodium temperature is less than 250°C. Performance of HAD

  during hydrogen injection experiments has been studied. It has a sensitivity of

  0.239mV/ppm(v) or 55V/ of water leak in SG.

Chapter 6: Conclusion and future work

6.1   Conclusion

In sodium cooled fast reactors, the availability of SG units is of critical importance as it determines the plant safety and availability. High temperature and high pressure environment in a SG can result in leaks in the system, which ultimately leads to the sodium water reaction. The early detection of incipient mal-function is of paramount importance in the operation of all fast reactors. Monitoring hydrogen in sodium, produced during sodium water reaction of sodium with the leaked water or steam is a convenient way to accomplish this. Nickel diffuser based instrumentation has been developed for real time detection of hydrogen in sodium.

The availability of diffusion based SG leak detection system depends not only on the functioning of the detector but also on the working of other vital components such as nickel diffuser. Any failure of the nickel diffuser results in the liquid sodium entering the high vacuum system. In the open literature, no information is available about any technique for the detection of sodium leak in the event of failure of nickel diffuser used for the SG small leak detection systems. This thesis proposed a non-contact miniature mutual inductance leak detector (MILD). The detector has been modeled, developed and deployed for detection of sodium leak due to failure of a nickel diffuser. The parameters of the detector probe have been optimized by simulation and validation experiments and the important conclusions drawn from the studies are given below:

- FE model optimized the MILD coil parameters, viz. excitation frequency, excitation current and voltage set point as 2.9 kHz, 100 mA and 3.7 mV respectively for detecting sodium leaks independent of the effect of ambient temperature.

- A prototype MILD and its associated electronics unit have been developed for experimental validation of FE model and the model predictions have been successfully

validated through room temperature experiments carried out with an aluminum block simulating sodium, because of identical electrical conductivities.

- A good agreement has been observed between the model predictions and experimental results with a percentage relative error of less than 7%.

- Detection of 1.183g of sodium leak due to the failure of the nickel diffuser in less than 5 seconds has been achieved.

- The MILD along with its electronics has been deployed in the FBTR SG leak detection system to detect any failure of the nickel diffuser membrane to the high vacuum in the diffusion based system.

The quadrupole mass spectrometer was initially installed for detection of small leaks in FBTR SG. But the random failure of the analyzer filament and the large downtime (2-3 weeks) required for normalization of vacuum after filament replacement and the subsequent calibration procedure necessitated alternate detector without the use of QMS. As a solution, this thesis has proposed sputter ion pump (SIP) based SG leak detection and an approach for processing the sputter ion pump current signal for incorporating safety actions. The SIP electronic circuit response has been evaluated and qualified by conducting systematic experiments. Calibration and testing procedures have been developed and safety actions have been formulated and implemented. The main conclusions drawn from the studies on SIP systems are given below:

- The SIP based SG leak detection system can reliably detect 7ppb of hydrogen concentration in sodium.

- With the SIP based system, a small leak of the order of 1g/sec can be reliably detected in 3 minutes.

- The overall availability of the system has been enhanced by triplication i.e. by adding multiple systems, software noise rejection techniques and on-power calibration methods. The average reactor trips from SG leak detection system got reduced from four per year to one in two years.

- The developed SIP based system has shown expected increase in output to leak simulation by hydrogen injection tests and reactor power operation.

For faster detection and safety actions on initiation of small leaks at all sodium temperatures, diverse detectors that do not depend on diffusion have been developed. The acoustic method for leak detection of water into sodium can be considered as an additional system for the development of sodium water steam generator protection to improve the SG operating safety and structural integrity.

- As ECHM can detect 10ppb of hydrogen concentration in sodium, it has been added to the SG leak detection system as a diverse detector for evaluation along with SIP during leak simulations and reactor operation.

- In line with the reported literature, thermal conductivity based hydrogen in argon detector developed has been found to detect small leak when the sodium temperature is less than $250^{o}C$.

- The performance of HAD during hydrogen injection experiments has been studied and experiments have confirmed that it has a sensitivity of 0.239 mV/ppm(v) or 55V/g of water leak in SG.

- The HAD is effective in detecting H_2 in the cover gas at lower sodium temperatures of $<250^{o}C$ while SIP and ECHM are effective at higher sodium temperatures as H_2 remains dissolved in sodium.

To have adequate coverage, redundant detectors are required to accommodate detector malfunctions during operation. A minimum of two operational hydrogen meters are to be installed to ensure leak detection coverage at all times. Intermediate leaks generally continue for 30s and a leak can be identified within 3s by an acoustic detection system after which SG protective actions are initiated. The acoustic system provided leak detection reliability and diversity in the overlapping region. Large leaks generally continue for several seconds and cause a rupture disc to burst. These leaks can be found by detecting the pressure of sodium or the sodium water reaction product in the pipe region between two rupture disks serially installed at the outlet of SG.

The early detection of incipient mal-function is of paramount importance in the operation of all fast reactors. SG presents special threats because of the possible interaction between water and sodium in the event of a leak in any of the tubes in the heat exchanger.

Small leaks are detected by using hydrogen in sodium detector at normal operating temperature, while hydrogen in argon detector is used during start up and shutdown at which time sodium temperatures are low. Intermediate size leak are detected by monitoring increase in secondary sodium circuit cover gas pressure. Large leaks are detected by sodium leak detectors placed downstream of the rupture discs. The performances of the SIP, ECHM and acoustic system have been compared experimentally.

Considering the experience and response of diverse detectors in FBTR and other sodium facilities, in order to detect small leaks, two diverse methods based on SIP and ECHM are essential for real time leak detection of SG leaks in FBRs. An online leak detection using acoustic technique has to be developed for rapid detection of sodium water reaction and identification of leaking module. For intermediate and large leaks, rise in expansion tank cover

gas pressure and rupture discs are adequate. Thermal conductivity detector has to be developed for detection of leaks at sodium temperature $< 250^{o}$C when hydrogen remains more in gaseous form than dissolved in sodium.

Table 6.1: Review of leak detection techniques

Sl. no.	Leak detection techniques	Performance features
1	Hydrogen in sodium-QMS	Responds above 250°C, detects partial pressure of H_2, response time 3min, availability affected due to random failure of filament, nickel diffuser temperature to be precisely controlled
2	Hydrogen in sodium-SIP	Responds above 250°C ,detects total pressure of H_2, response time 3min, nickel diffuser temperature to be precisely controlled, sensitivity is 7ppb of H_2 in sodium
3	Hydrogen in sodium-ECHM	Responds above 250°C, nickel diffuser temperature to be precisely controlled, sensitivity is 10ppb in sodium
4	Hydrogen in Argon	Responds below 250°C, sensitivity is 0.239mV/ppm
5	Acoustic based system	Responds at all temperatures, response time 3sec

The improvements in the system design will be of considerable importance in view of the requirements of increased number of such systems for future fast breeder power reactors. This along with improved surveillance method for validating the calibration on-line without requiring plant shutdown will increase the reliability and availability of the SGLDS, thus increasing plant availability.

6.2   Scientific and technical achievements

- A non-contact miniature mutual inductance leak detector has been developed for FBTR SG and detection of 1.183g of sodium leak due to the failure of nickel diffuser to the high vacuum in a diffusion based SG leak detection system in less than 5 seconds has been demonstrated.

- A novel and robust SIP based instrumentation has been developed and this could reliably detect a small leak of the order of 1g/sec of water/steam in SG in 3 minutes.

- The genuineness of the SG small leak signal annunciation has been made possible with the incorporation of multiple leak detection systems in a secondary sodium circuit.

- The developed electrochemical hydrogen meter has detected 10ppb of hydrogen concentration in sodium. This acts as a diverse detector for confirmation of a leak in SG during the reactor operation.

- Thermal conductivity based hydrogen in Argon detector has been developed and this technique could detect H_2 in cover gas due to a small leak when the sodium temperature is less than 250°C. It has shown a sensitivity of 0.239 mV/ppm(v) or 55V/g of water leak in SG.

The mutually exclusive temperature ranges of hydrogen in sodium detector and hydrogen in argon detector are effectively combined to achieve good efficiency of leak detection in the total temperature range of reactor operation.

6.3   Future directions

The large size of the nickel diffuser in the diffusion dependant systems provides high amplitude signal but it necessitates larger ion pump and offers a large time lag. If the system is made small,

it results in the smaller time constants and becomes suitable to follow time evolution of H_2 more faithfully. It is worth continuing research efforts in this direction.

2D finite element modeling has been adopted in the thesis for the development of the miniature mutual inductance leak detector for early detection of failure of nickel diffuser. Although it has given vital inputs, carrying out 3D modeling is expected to handle the realistic situations and ensure accurate optimization of the operating parameters. More attention has to be paid to the development of automatic detection algorithms and expert systems for possible implementation in an on-line automated detection system. Such a system should satisfy the requirements of detection speed and reliability.

Efforts are to be made to develop a computerized decision making based on the use of expert systems. This task would consider how various inputs can be combined to produce a more reliable decision in identification of a leaking module based on the past information and data. The output from the various analysis techniques tested in the analysis work could be used as inputs. While these are not statistically independent, as truly separate variables might be, they accurately represent the computational problem of a multi parameter input and would allow the benefits of using diverse parameters to be assessed. During this exercise, particular attention should also be paid to the question of the suitability of the method for implementation in an on-line detection system. Studies in the areas of mathematical modeling of the physical processes involved may throw more light and identify new possibilities.

Appendix-1
MILD Sensitivity calculation

Cross-sectional area of collection region in the pocket

$$= \frac{\pi}{4}\{((d_1)^2 - (d_2)^2)\}$$

$$= \frac{\pi}{4}\{((45)^2 - (20)^2)\}$$

$$= \quad 1276.27\text{mm}^2$$

Density of sodium $\quad = \quad$ 0.927 g/cm^3

Volume for 1 mm level of sodium in collection pot $=$ Area x 1 mm

$$= \quad 1276.27\text{mm}^2 \text{ x 1 mm}$$

$$= \quad 1.276\text{c.c}$$

Quantity of sodium for 1 mm level in collection pot $=$ 1.276X 0.927g

$$= \quad 1.183\text{g}$$

Hence sensitivity of MILD $\quad = \quad$ **1.183g**

Alarm is set for 10 mm of sodium level in the active region in the collection pot

Volume for 10mm sodium level in the collection pot$=$ 1276.27mm^2 x 10 mm

$$= \quad 12.76\text{c.c}$$

$\therefore$ Quantity of the sodium for 10mm level $\quad = \quad$ 12.76x 0.927 g

$$= \quad \textbf{11.82g}$$

Alarm is set for a leak of 11.82g of sodium

Appendix - 2

Leak simulation calculations

a) Calculation of amount of H_2 required to raise the H_2 of 13.92 (16 m^3 at 375°C) tonnes of sodium by 40 ppb.

$$\frac{13.92 \times 10^6 \times 40}{10^9} = 0.557g$$

b) Calculation of instantaneous rise in H_2 concentration.

Amount of H_2 injected	=	0.557 g
Duration of injection	=	7 min
Hence rate of injection	=	1.326 mg/s
SG sodium flow	=	33 kg/s

Hence, instantaneous Rise in concentration $= \dfrac{1.326 \times 10^{-6} \times 10^9}{33}$

$$= \quad 40.1 \text{ ppb } = 40 \text{ ppb.}$$

c) Calculation of initial and final pressure values of H_2 tank.

Argon pressure (initial)	=	100 mb (g)
	=	1.1 b (a)
Tank pressure with H_2	=	2.0 b (g) assumed
	=	3.0 b (a)
Partial pressure of H_2	=	1.9 b
Volume of the tank	=	15.6 1
	=	15.6x10^{-3} m^3
Characteristic gas constant for H_2	=	4124.4 J/kg/^{o}K

Mass of H_2 in the tank is calculated using ideal gas equation $pV = mRT$,

where, p = Partial pressure of H_2 in N/m^2 (1 b = 10^5 N/m^2)

V = Volume of the tank in m^3

R = Characteristics gas constant for H_2

T = Temperature of the tank in deg. C

Hence m $= \dfrac{19 \times 10^{-5} \times 15.6 \times 10^{-3}}{4124 \times 303}$

$= 2.372 \times 10^{-3}$ kg

Mass of H_2 (tank) after injection $= (2.372 - 0.557) \times 10^{-3}$ kg

$= 1.815 \times 10^{-3}$

Partial pressure of H_2 after injection $= \dfrac{1.815 \times 10^{-3} \times 4124.4 \times 303}{15.6 \times 10^{-3}}$

$= 1.454 \times 10^5$ N/m^2

$= 1.454$ b (a)

The ratio of partial pressure of hydrogen to the total pressure remains unchanged after injection.

Initial ratio   =   1.9/3.0   =   1.454/x

where x is total pressure

Hence,   x   =   2.296 b (a)

Hence total pressure after injection   =   1.296 = 1.3 b (g)

Initial pressure   =   2.0 b (g)

Appendix-3
HAD sensitivity calculation

Calculation of mass and volume of the injected hydrogen into the expansion tank to calibrate HAD system

V = Volume of the standard hydrogen cylinder = 1550 cc

T = Temperature of hydrogen in the cylinder $\quad$ = 40 ^{o}C

P = Pressure drop after injection $\quad\quad\quad$ = 5kpa= 0.05 N/m^2

R = 4124.4 J / Kg/ K

a) Mass of hydrogen injected in the expansion tank cover gas:
$\quad\quad\quad\quad$ As per ideal gas law, $pv = mRT$

∴ Mass of H_2 injected into cover gas $\quad\quad$ = 0.05x 10^5x1550x10^{-6} / 4124.4 x313
$\quad\quad\quad\quad\quad\quad\quad\quad\quad\quad\quad\quad\quad\quad\quad$ = 6 x 10^{-3} g

b) Volume ration (ppm −v) of the H_2 injected into the expansion tank cover gas:
$\quad$ Expansion tank volume $\quad$ = 0.93 m^3

$\quad$ Cover gas temperature $\quad$ = 140 ^{o}C

$\quad$ Mass of H_2 injected $\quad\quad$ = 6 mg

1 mole of H_2 occupies 22.4 litres (V_1) at a pressure of 1 bar (0.1 Mpa) and temperature of

1°C (T_1), From general gas law,
$\quad$ the volume V_1 occupied by 6 mg hydrogen injected into the expansion tank

$\quad\quad\quad\quad\quad\quad\quad\quad\quad\quad\quad\quad\quad\quad\quad$ = 22.4 x 6x10^{-3} x 413 x 0.1/2 x 273.6 x 0.1503

$\quad\quad\quad\quad\quad\quad\quad\quad\quad\quad\quad\quad\quad\quad\quad$ = 96.768x10^{-3} liter

The volume ratio of H_2 injected = V_2/ V_1 $\quad$ = 96.768 x 10^{-3} /0.93 x 10^3 = 104.05 x 10^{-6}
$\quad\quad\quad\quad\quad\quad\quad\quad\quad\quad\quad\quad\quad\quad\quad$ = 104 ppm(v)

c) Sensitivity of HAD:

$\quad$ The injected hydrogen gas = 104 ppm(v) = 6mg
$\quad$ The recorded signal increase = 0.33V

$\quad$ ∴ Sensitivity = 0.33V / 104 = 3.3 mV / ppm(v)

Hence the sensitivity of HAD can be arrived at as 3.3 mV / ppm(v) or 6.11V/g of H_2 leak or 55V /g of H_2O leak.

References

1. P Rodriguez, S.B Bhoje, The FBR program in India, Elsevier science Ltd. Energy Vol. 23, No. 7/8, 1998, pp 629-636.

2. FBTR Experience book, An Exciting Journey through a new technology, Oct, 2010.

3. V.Ramanathan, B.Babu, B.Rajendran, H.K Sahu, Nickel diffuser based instrumentation for real time detection of hydrogen concentration in liquid sodium in Fast Breeder Test Reactor, Proceedings of the Eight national seminar on physics and technology of sensors, Kalpakkam, India, Feb 27-Mar 1, 2001.

4. J.H.Singleton, Hydrogen pumping speed of sputter ion pump, The Journal of Vacuum, Science and Technology, Vol.8, Feb, 1971.

5. IAEA Techdoc 908, Sodium water interactions in steam generators, sodium fires: Tests and Analyses, pp 149-188, Oct 1996.

6. Desmas.T, Lemoine.P, A study of small leaks of water in sodium heated steam generators: self evolution and wastage, Proceedings of the third international conference on liquid metal engineering and technology, Oxford, Apr 9-13, 1984.

7. B. Babu, Quality assurance during O&M stage of I&C systems, Theme meeting on Robust   I&C systems for FBR programme, Kalpakkam, 2010.

8. Hori.M, Sodium/water reaction in steam generators of liquid metal fast breeder reactors, Atomic Energy Review, 183, 1980.

9. Hans. R and Dumm. K, Leak detection of steam or water into sodium in steam generators of liquid metal fast breeder reactors, Atomic Energy Review 159, 1971

10. T. Gnanasekaran, Thermochemistry of binary Na–NaH and ternary Na–O–H systems and the kinetics of reaction of hydrogen/water with liquid sodium – a review, Journal of Nuclear Materials, Vol. 274, 1999, pp 252-272.

11. P. Lecocq, L. Lannon and J.C. Masson, Nuclear power plant control and instrumentation, Proc. Symp.Praque, IAEA, Vienna, 1973.

12. R.Sridharan, K.H.Mahendran, T.Gnanasekaran, G.Periaswami, U.V. Varadha Raju, C.K.Mathews, On the phase relationships and electrical properties in the $CaCl_2$-CaH_2 system, Journal of Nuclear Materials, Vol.223, 1995, pp 72-79.

13. K.Joseph, K.Sujatha, S.Nagaraj, K.H.Mahendran, R.Sridharan, G.Periaswami, T.Gnanasekaran, Investigations on the phase equilibria of some hydride ion conducting electrolyte systems and their application for hydrogen monitoring in sodium coolant, Journal of Nuclear Materials, Vol.344, 2005, pp 285-290.

14. S.C.Chetal, Safety aspects of Intermediate heat transport and decay heat removal systems of Sodium- cooled Fast Reactors,Nuclear Engineering and Technology, Vol.47,Jan 2015,pp 260-266.

15. H. Kim1, S. H. Seong1 S. O. Kim,Seop HurKey Engineering Materials, Measurement Strategy of the Water Leakage into a Low Pressure Sodium Boundary for a Liquid Metal Reactor Seop Hur1, Vol. 270-273, 2004, pp 518-524.

16. Choi, Jong Hyun, Hwang, S. T. Nam, H. Y., Liquid metal reactor design technology development: Development of sodium technology for LMR, KAERI/RR-2203, 2002.

17. X. Elie, J.M. Chaumont, Operation experience with the Phenix prototype fast reactor, Atomic Energy Society of Japan, Tokyo, Vol.24, 1991.

18. Hori.M., Sato.M., Nei.H., Harasaki.T., Hishida.M., Saito.T, Sodium-water reaction studies for MONJU steam generators, IWGFR-1,1975, pp 81-91.

19. Summary of The Coordinated research program, IAEA-TECDOC-946, 1997.

20. T. J. Kim, V. S. Yugay, S. T. Hwang, Noise Generation by Water-Sodium Reaction and its absorption on Hydrogen bubbles for KALMER Steam Generator, Proceeding of Noise and Vibration, Rep.of Korea, 2000, pp 1829-1835.

21. Tae-Joon kim, Valeriy S.Yugay, JI-Young jeong, Jong-Man kim, Byenug-Ho kim, Tae-Ho lee, Yong-Bum lee, Yeong-Il kim, Dohee Hahn, Acoustic leak detection technology for water/   steam small leaks and micro leaks into sodium to protect an SFR steam generator, Nuclear Technology, Vol.170, May, 2010.

22. Joel Gudez phenix, The Experience feedback book-CEA, 2013.

23. N Kong , M Brunet, P Garnaud, D Ghaleb, Water leak detection in steam generators of Super Phenix (IWGFR-79), Oct, 1990.

24. P.R. Bolt, Some conditions affecting the definition of design basis accidents relating to sodium/ water reactions, IWGFR-50, Vol.64, 1984.

25. Desmas.T, Le Bris, A., Running of Super phenix hydrogen detectors vacuum circuits (Translated from French), Vol.21, 1989, pp 33-44.

26. F .A. Kozlov, V. A. Egorov, P. S. Kozub,R. F. Masagutov.V. I. Bolgarin,A. A. Samarkin, Yu. A. Tsoi,É. P. Kozubov,P. G. Chernykh,V. L. Novak, Operating detectors for hydrogen in sodium on the BN-350 and BN-600 reactors. Translated from Atomnaya Energiya, Vol.64, No.3, Mar, 1988, pp 227-229.

27. Y.M.Ashurko, R.P.Baklushin, Y.I.Zagorulko, V.N.Ivanenko, V.P.Matveyev, B.A.Vasilyev, Fast Reactor operating experience gained in Russia: Analysis of anomalies and abnormal operation cases, Xa0056255, pp 117-144.

28. R. Hans, K. Dumm, Leak detection of steam or water into sodium in steam generators of liquid metal fast breeder reactors, Atomic Energy Review,Vol.15(4), 1977, pp 611-699.

29. T Saito and T. Kosugi, Leak detection and location in Monju steam generators, IWGFR-25, Nov, 1978, pp 41-70.

30. M. Kuroho and M.Sato, PNC status report on leak detector development for LMFBR steam generators, IWGFR-50, 1984, pp 84-97.

31. K. Dumm, The SNR-300 Steam Generator Small Leak Detection system, IWGFR-25,Interatom GmbH, Bergisch Gladbach, Federal Republic of Germany, 1984, pp 102-114.

32. G.B.Kruger, K.Y.Eng, W.L.Kelly, Leak detection system design and operating considerations for the US – CRBRP, Seminar on the development of sodium –cooled fast breeder steam generators,USSR, Jul,1976, pp 1-8.

33. D.Greene, R.Greene, Case histories and lessons learned from the design, Development, planning and implementation of new I&C systems, including effective integration with existing systems and processes, IAEA – CN- 155-076.

34. K.V.Suresh Kumar, A.Babu, B. Anandapadmanaban, G.Srinivasan, Twenty five years of operating experience with the Fast Breeder Test Reactor, Energy procedia 7, Asian nuclear prospects, 2010, pp 323-332.

35. Vaidyanathan.G, Kalyanasundaram.P, Sylvia J.I, Rajan K.K, Veerasamy.R, Krishnakumar.B, Sensors in sodium cooled Fast Breeder Reactors, National journal on electronic sciences & systems, Vol. 3, No.2, Oct, 2012, pp 78-87.

36. William Hayt,John buck, Engineering electromagnetic, Seventh edition, Tata McGraw-Hill,17 Jan, 2011.

37. Jian-ming Jin, The Finite element method in electromagnetic, second edition, Wiley Interscience publications, 2002.

38. R.W. Freund, Conjugate gradient-type methods for linear systems with complex symmetric coefficient matrices, SIAM Journal of Scientific and Statistical Computing, Vol.13, No.1, 1992, pp 425-448.

39. David Meeker, Finite Element Method Magnetics version 4.2 – User manual, 2015.

40. Douglas C. Giancoli, Physics Principles with Applications, Sixth edition, Pearson prentice hall, 2005.

41. R.A.Matula, Electrical resistivity of copper, gold, palladium and silver, Journal of Physical and Chemical Reference Data, 1147, 1979.

42. Sodium technology handbook, Fast Reactor Technology, IGCAR, 2015.

43. Babu, B.; Ramanathan, V., Real time steam generator leak detection system for FBTR, Proceedings of the second national symposium on advances in control and instrumentation, INIS Vol. 36, 2005.

44. B. Babu, Real time Steam Generator Leak Detection system for FBTR. CEA-IGCAR (Indo-French) Technical Seminar, 2007.

45. V.Ramanathan, B. Babu and C.P. Pillai, Online hydrogen partial pressure measurement in industrial environments, Sixth National symposium on QMS, Indian institute of petroleum, Dehradun, India, Oct 11-13, 1994.

46. Yang Xianyong and Wang Zhou, The analysis and design of hydrogen meter system in sodium, International Fast Reactor Safety meeting, Vol. 4, 1990, pp 341-350.

47. Smith C.A, Wittingham A.C, Proceedings of the conference on material behaviour and physical chemistry in liquid metal systems, Karlsruche, Germany, Mar 24-26, 1981, pp 365.

48. Desmas.T, Le Bris.A, Running of Super phenix hydrogen detectors vacuum circuits (translated from French- Functionment des circuits de vide des detecteurs d` hydrogen installe`s a`super phenix, EDF bulletin de la direction Des Etudes et Rechachesserie A, Nuclear, Hydraulic, Thermique No.2), 1989, pp 33-44.

49. Roth A., Vacuum Technology, North Holland Publishing Co. Amsterdam, 1982.

50. G.Yevick., Fast reactor technology, plant design, MIT, Massachusetts, 1966, pp 224-227.

51. V.Ramanath elean, B.Babu and C.P. Pillai, Design and experience on instrumentation and control system of Fast Breeder Test Reactor, Indo-Kazakastan International seminar on operating experience of Fast Reactors, Indira Gandhi Centre for Atomic Research, Kalpakkam, India, Aug.5-9, 1996.

52. Varicak .M, Review of Scientific Instruments, Vol.27, 1956, pp 655.

53. Vijendran.P, CVG Nair, Vacuum, Vol.21, 1971, pp 159.

54. D.J. Litler, F.Kirkby, H. E. Johnson, P. B. Myerscough, W. Wright, Modern power station practice, Vol.12, Control and Instrumentation, Pergamon press, British Electricity International, 1990.

55. P.Brakaw, Jeff Barrow, Grounding for low and high frequency circuits, Analog dialogue, 1989.

56. V.Ramanathan, Ph.D Thesis, University of Madras, 2000.

57. W.Ott. Hay, AT & T Laboratories, Noise reduction techniques in electronics systems, John wiley and sons publication, USA, 1988.

58. V.Ramanathan, B.Babu and J.Joseph, Real time steam generator leak detection system for FBTR based on quadrupole QMS residual gas analysis technique, International conference on vacuum science and technology, Centre for Advanced Technology, Indore, India, Jan 30-Feb 02, 1995.

59. V. Ramanathan, B. Babu, B. Rajendran, H.K. Sahu, Nickel Diffuser Based Instrumentation for Real Time Detection of Hydrogen concentration in liquid sodium in Fast Breeder Test Reactor, Proceedings of the Eighth National Seminar on Physics and Technology of Sensors, Kalpakkam, India, Feb 27-Mar 1, 2001, C-11.1-3, 2001.

60. Prodyot Roy, Douglas N.Rodgers, Hydrogen burden from the steam side corrosion in sodium-heated steam generators, Nuclear Technology, Vol.39, Jul, 1978, pp 213-215.

61. L.V. Hampton, G.J. Licina, P.Roy,Water side corrosion correlations for 2.25 Cr-1Mo steel in liquid metal fast breeder reactor steam generators, Nuclear Technology, Vol.52, Mar, 1981, pp 431-434.

62. P.Kalyanasundaram, Baldev Raj, V.Prakash, Ramakrishna Ranga, Detection of simulated steam leak into sodium in steam generator of PFBR by argon injection using signal analysis techniques, Nuclear Technology, Vol.182, Jun, 2013, pp 249-258.

63. IAEA TECHDOC1083, Some aspects of instrumentation and inspection of main LMFR components, Status of liquid metal cooled fast reactor technology, April, 1999, pp 225-270.

64. G.S. Srinivasan, Investigations on sodium boiling and leak noise detection in liquid metal fast breeder reactors, PhD thesis, Madras University, 1996.

65. Acoustic signal processing for detection of sodium boiling or sodium-water reaction in LMFRs, IAEA-TECDOC-946, 1997.

66. FRTG internal report, acoustic leak detection system for SGTF, FRTG/VNAS/99221/EX/ 3096/Rev-A, Feb, 2012

67. Kim Tae-Joon, Valery S.Yughay, Hwang Sung-Tai, Jeong Kyung-Chai and Choi Jong-Hyeyn, Advantages of acoustic leak detection system development for KALIMER steam generators, Journal of the Korean nuclear society,Vol-33, No-4, Aug, 2001, pp 423-440.

68. Ji-Yong jeong, Tae- Joon kim. Jong-Man kim, Byoung-Ho kim, Nam-Cook park, Analysis of micro-leak sodium-water reaction phenomena in a sodium-cooled fast reactor steam generator, Korean Journal of Chemical Engineering, Vol.26, No.4, 2009, pp 1004-1008.

69. Yoshitaka Chikazawa, Acoustic leak detection system for sodium-cooled reactor steam generators using delay-and-sum beam former, Nuclear Science and Technolgy,Vol.47.No.1, 2010, pp 103-110.

70. R.Prabhakar, R.K.Vyjayanthi and R.D.Kale, Detection of Steam Leaks into Sodium in Fast Reactor Steam Generators by Acoustic Techniques -An overview of Indian programme, IWGFR/79 (ed.JPh.Girard), IAEA, Oct, 1990.

71. Seop Hur, D.H. Kim, S.H. Seong and S.O.Kim, Measurement Strategy of the Water leakage into a low pressure sodium boundary for a Liquid Metal reactor, Key Engineering Materials, ISSN: 1662-9795,Vols 270-273, pp 518-524, 2004.

72. M. Hori, Sodium water reactions in steam generators of liquid metal fast breeder reactors. Atomic Energy Review, Vol.18, 3, 1980, pp 707-778.

73. R. Anderson, Analysis of experimental data on material wastage by sodium water reaction jets, Nuclear Energy 18, 1979, pp 333-342.

74. Kishore,A. Ashok Kumar, S. Chandramouli, B.K. Nashine, K.K. Rajan, P. Kalyanasundaram, S.C. Chetal, An experimental study on impingement wastage of Mod 9Cr 1Mo steel due to sodium water reaction, Nuclear Engineering and Design, Vol. 243, Feb, 2012.

75. FRTG internal report, IGCAR-CEA experiment SW7 on impingement wastage, 99120/EX/5001/R-A, Oct, 2012

76. FRTG internal report, Experimental studies and code calculations on impingement wastage for 9CR-1Mo SG tubes, IGC/FRTG/99120/EX/5008, 2014.

77. R. Sridharan, IIT, Madras, Ph.D Thesis, 1994.

78. Sridharan. R, Mahendran. K. H, Nagaraj. S, Gnanasekaran.T, Periaswami. G, An electro chemical hydrogen meter for measuring hydrogen in sodium using a ternary electrolyte mixture, Journal of Nuclear Materials, Vol.312, 2003, Issue 1, pp 10-15.

79. A.C. Whittingham, An equilibrium and kinetic study of the liquid sodium-hydrogen reaction and its relevance to sodium-water leak detection in LMFBR systems, Journal of

Nuclear Materials, 60, 1976, pp 119-131.

80. T. Gnanasekharan, K.H. Mahendran, R. Sridharan, V. Ganesan, G. Periaswami, C. K. Mathews, An electrochemical hydrogen meter for the measurement of dissolved hydrogen in liquid sodium, Nuclear Technology, Vol. 90, Jun, 1990, pp 408-416.

81. J.Ph. Jeannot, T. Gnanasekaran, R. Sridharan, R. Ganesan, J.M. Augem, C. Latge, G. Gobillot, K. Paumel, J.L. Courouau, In-Sodium Hydrogen Detection in the Steam Generator of Phenix Fast Reactor: a Comparison Between Two Detection Method, ANIMMA International Conference, Marseille, France, 7-10 Jun, 2009.

82. Leck J.H., Total and partial pressure measurement in vacuum system, University of liver pool, Blakie & Son Ltd., London, 1989.

83. K. H. Mahendran , R. Sridharan , T. Gnanasekaran , and G. Periaswami., A Meter for measuring hydrogen concentration in argon cover gas of sodium circuits, Design and Development , Industrial engineering and chemical research, 37, 1998, pp 1398-1403.

84. Toshio Funada, Isao Nihei, Shunichi Yuhara, Takashi Nakasuji., Measurement of hydrogen concentration in liquid sodium by using in inert gas carrier method, Nuclear Technology, Vol. 45, Sep, 1979, pp 158-165.

85. Nei H, Development of sodium/ water leak detectors in dynamic sodium system and in cover gas: Meeting of experts on the measurement and control of impurities in sodium, Cadarache, Nov, 1972.

86. Hermingway T.K., Electronic designers hand book, Business books publication, London, 1970.

87. Gray P.R. and Meyer R.G., Analysis and design with analogue integrated circuits, John wiley publication, Newyork, 1977.

88. Web R.E., Electronics for scientists, Ellis wood publishers, Newyork, 1990.

89. Helms H.I., Master guide to Electronics circuits, Obl.Cliffs – Publilshers, Practice Hall Englwo, 1988.

90. Gow-Mac Instrument Co., Instrument manual on Gow-Mac model 40-001 DC power supply and bridge control, NJ 08805, USA.